Plant hydration dynamics:

measurement and uptake pathways

Tomás Ignacio Fuenzalida Gasman

Research School of Biology

A thesis submitted for the degree of Doctor of Philosophy of

The Australian National University

July 2022

© Copyright by Tomás Ignacio Fuenzalida Gasman (2022). All rights reserved.

TABLE OF CONTENTS

LIST OF TABLES

LIST OF FIGURES

DECLARATION

This thesis was compiled by myself, that the work it contains is my own except where explicitly stated otherwise. This work has not been submitted for any other degree or professional qualification.

Chapter 2 was published in 2019 in *New Phytologist* (224 (4), 1504-1511) by myself as the first author and C. J. Bryant, L. I. Ovington, H-J. Yoon, R. S. Oliveira, L. Sack and M. C. Ball as co-authors. I conceived the study with M. C. Ball; performed the experimental work with the help from C. J. Bryant and L. I. Ovington; analysed the data with suggestions by H-J. Yoon, L. Sack and M. C. Ball; and wrote the manuscript with input from all co-authors.

Chapter 3 was reviewed once in 2021 in *New Phytologist* and rejected with resubmission encouraged, with myself as the first author and M. J. Blacker, M. Tuner, A. Sheppard and M. C. Ball as co-authors. M. C. Ball, A. Sheppard and I conceived the study. I performed the pneumatic measurements for stem air discharge. M. C. Ball and I collected and processed the micro-CT samples. M. Turner performed the micro-CT imaging. A. Sheppard, M. J. Blacker and I analysed the data. I drafted the manuscript with suggestions from M. C. Ball. and A. Sheppard.

Chapter 4 was published in 2022 in *Plant, Cell & Environment* by myself as first author and O. Binks, C. J. Bryant, J. Wolfe and M. C. Ball as co-authors. I conceived the hypotheses and designed the instrument; I designed and planned the experiments with suggestions from O. Binks, C. J. Bryant and M. C. Ball; I performed the experiments; I analysed the data and wrote the manuscript with suggestions from J. Wolfe, O. Binks, C. J. Bryant and M. C. Ball.

Chapters 2, 3 and 4 have been the product of collaborative work and I have thus retained the pronoun ‘we’ in these chapters; in Chapters 1 and 5, I use the pronoun ‘I’, as these represent work of my own. The copyright of published work resides with the copyright holders of the publication.

Tomás I. Fuenzalida

ACKNOWLEDGEMENTS

A PhD is a personal project but is by no means pursued alone. In the course of my degree, I received guidance, support and critiques which greatly contributed to the form and content of the present work. But most fundamentally, the people who provided them have shaped to my way of thinking about science. For this reason, I feel sincerely grateful and fortunate.

I thank Marilyn Ball for inviting me to take this journey and for sharing the keen and joyful interest with which she interrogates plant science. Marilyn's enthusiasm for new ideas captivated me and proved contagious over the years; perhaps predictably, this resulted in me chasing my own. The opportunity and the encouragement to think divergently is what made my experience challenging and fascinating. I also thank Joe Wolfe, who took upon an unexpected but natural mentoring role during my PhD, guiding my sometimes-messy thinking about plants through the exact language of physics, and dousing my naïve excitement with cautious scholarliness. I thank Lawren Sack for his patience and dedication in revising and contributing to my work. I thank my supervisory panel, John Evans, Patrick Meir and Graham Farquhar for their recurrent and interested observations about my thesis, and John Passioura for his advice and experimental support. I thank Adrian Sheppard, Levi Beeching and Michael Turner for their support in approaching the world of micro-CT imaging.

I thank Oliver Binks for introducing me to the world of sensors and Arduinos, and for his incisive scrutiny about my work. I thank Cal Bryant for his companionship in the field and the lab, and for the many fruitful discussions and ideas that we shared over these four years. I thank Helen Holmlund for flooding us with her fundamentally positive way of doing science, Alonso Zavafer for his insights about building scientific instruments, and Leuwin Ovington for his support in the field. I thank Nigel Brothers and Catherine Bone for their outstanding support and patience while having us bombing leaves for weeks over at their place.

I thank Javier Merrill for his always grounding advice on life and science, Aria Carroll for her loving care and support, and Kathleen Rutherford for being my unconditional friend and family in Canberra. I thank my friends Damien, Vero and Juan for the often-needed escape to our South American idiosyncrasies. I thank my family and friends for supporting me from my distant home, which is not a place but a group of people.

I thank the Chilean State through the Agencia Nacional de Investigación y Desarrollo (scholarship 72180256) for providing financial support during these four years, and the Australian Research Council (grant DP180102969) for supporting my research. I thank Marilyn Ball for additional funding via the ANU top-ups, and Luis Corcuera and Ana María Vliegenthart for giving me the opportunity to attend so many wonderful courses and colloquiums in Katalapi. None of this would have been possible without Katalapi.

ABSTRACT

Transpiration accounts for most terrestrial water fluxes, and agriculture uses most of the water managed by humans. Transpiration is tightly regulated by plants, so climate models and irrigation water use efficiency could be improved by understanding how plants regulate water status. In this work, I address questions that are relevant to our understanding of plant hydration dynamics: (1) Can foliar water uptake (FWU) restore leaf hydraulic conductance (K_{leaf}) lost due to dehydration? (2) Is embolism refilling involved in FWU-induced hydraulic recovery? (3) Can plant water status be measured by uniaxial compression of the leaf lamina?

Many plants are able to access atmospheric water through FWU; however, the physiological consequences of FWU are unclear. While FWU represents a small water flux, it may play a role in restoring hydraulic conductivity lost during dehydration. My results showed that FWU can restore K_{leaf} in *Avicennia marina* lost during dehydration. While hydraulic recovery retraced the same path observed during dehydration-dependent loss of K_{leaf}, a reduced ability for FWU impaired K_{leaf} recovery under severe dehydration. Most of the resistance to FWU was located in the leaf surface. I conclude that FWU may play a role in the maintenance of shoot hydraulic function during changing water status.

Plants living in saline environments experience constant xylem tension. Under these conditions, it is unclear how embolism refilling can take place. Using micro-CT imaging, I imaged *Avicennia marina* twigs in a dehydrated state and 4-48 h after wetting the twig surface. Emboli were present in the stem and leaves in the dehydrated state. Stem emboli were likely caused by cutting, while leaf emboli were likely caused by dehydration. Emboli in stems and leaves refilled with water after wetting, taking up to 48 h in the process, which is slower than the documented FWU rehydration kinetics. Possibly, refilling was facilitated by a vascular constriction at the stem-petiole junction and/or by loading of inorganic solutes into xylem vessels. My results substantiate that FWU is an important source of water for this widespread mangrove species; however, differences between field and experimental conditions currently preclude extrapolating these results to natural settings.

Turgor is an essential indicator of plant water status; however, turgor measurements are not routine. Turgor can be measured by localised compression of cells or tissues, but an accessible method to perform these measurements is lacking. I hypothesized that leaf turgor pressure can be monitored by uniaxially compressing the leaf lamina and by measuring the stress under a constrained thickness (‘stress relaxation’, SR); and that leaf water content can be monitoring by measuring the thickness of leaves compressed under a constant force (‘constant stress’, CS). Using a c. US$300 leaf squeeze-flow rheometer, I showed that uniaxial compression provides accurate measurement of plant water status with high temporal

resolution at low cost. Experimental results and a simple hydrostatic equilibrium model indicate that the stationary bulk modulus during compression is largely determined by the bulk osmotic pressure. Leaf squeeze-flow rheometry is presented as a novel, automatable and potentially standard method to quantify plant water status.

CHAPTER 1: INTRODUCTION

Plants move vast amounts of water. In fact, more water moves through plants than through rivers (Jasechko et al., 2013), and agricultural irrigation consumes about 70% of the water managed by human society (Pimentel et al., 2004). The process driving plant water transport, transpiration, has attracted interest from scientists for centuries (Brown, 2013). Without pumps or muscles, plants are able to extract and lift large volumes of water from the soil into the canopy. Transpiration is possible thanks to the vapour pressure deficit that usually exists between leaves and the atmosphere, which generates a negative hydrostatic pressure in the evaporating surfaces of leaves and allows plants to extract water from the soil (Philip, 1966), even when it is visibly dry. This water transport system is efficient, but unstable, as the conduits transporting the water can become embolised under severe dehydration (Milburn and Johnson, 1966, Tyree and Dixon, 1986), threatening the life of plants. Indeed, the interactions between water, vegetation and climate are now at the forefront of forest conservation and environmental plant physiology (Choat et al., 2018, Allen et al., 2010, Brodribb et al., 2020), and as we meander into imminent climate change, understanding the relations between plants and water may become vital for human existence.

This thesis is broadly concerned with the study of water motion in plants in relation to their driving forces, which I refer to as 'plant hydration dynamics'. Traditionally, plant physiologists have referred to the study of water in plants as 'plant-water relations' (Kramer, 1974), although more recently, the term 'plant hydraulics' has been used to refer to the study of water movement in plants (Tyree, 2003, Sack et al., 2016). 'Water relations' is loosely used to refer to study of the interactions between plants and water (Philip, 1966, Kramer, 1974, Kramer and Currier, 1950), although it commonly refers to plant-water interactions under hydrostatic equilibrium (*e.g.*, in the description of plant water status by the terms of osmotic and turgor pressure) (Meinzer et al., 2014, Xiong and Nadal, 2020, Sobrado, 1986, Meyer, 1938). 'Plant hydraulics' is used to refer to plant water movement, particularly to the study of water flow within the xylem tissue (Tyree, 2003); while the term is appropriate for describing water movement within the xylem vessels, 'hydraulics' is also used including water movement outside the xylem (Sack and Holbrook, 2006), where water transport occurs primarily via diffusion. As a goal of this thesis is to capture static and dynamical aspects of plant-water interactions, *plant hydration dynamics* seems suitable and warranted.

1. Plant hydration dynamics: a brief historical account

The fact that plants need water has been recognised for a long time. As in many subjects, Aristotle commented on the importance of water for plant life, saying that "*it might be thought*

that [plants] are fed by one substance only, by water" (Sprague, 1991). In fact, it was not until the discovery of photosynthesis in the late 18th century that carbon dioxide was identified as the main source of plant biomass. (The discovery of photosynthesis was a collective effort closely related to the early studies of plant water movement; however, it is not of primary interest in the present work and the topic has been recently reviewed by Hill (2012).) At around the same time photosynthesis was discovered, the first observations of stomata (Hedwig, 1793) gave rise to questions regarding their role in water transport. For example, Joseph Banks thought that stomata may serve as a pathway for water absorption (Banks, 1806):

> "*A plant cannot when thirsty go to the brook and drink, but it can open innumerable orifices for the reception of every degree of moisture, which either falls in the shape of rain and of dew, or is separated from the mass of water always held in solution in the atmosphere*"

Banks' is one of, but not the first scholarly description of foliar water uptake (FWU) (Hales, 1727). In the decades that followed their discovery, Moldenhauer (1812) described the opening and closing of stomata in response to light and humidity, Dutrochet (1826) described the process of osmosis, and Von Mohl (1856) suggested that stomatal movements were driven by turgor pressure inside the guard cells. The role of stomata in photosynthesis and transpiration was established, but the mechanism by which the water reached the canopy remained unresolved.

In parallel to the first research about stomata, and understandably after Banks' idea of plants 'separating' water from the atmosphere, Fick (1855) derived the mathematical formulation of molecular diffusion. Forty years later, Dixon and Joly (1895) proposed the now famous cohesion-tension theory for the ascent of sap. The cohesion-tension theory proposed that plant water was extracted from the soil and lifted by transpiration, driven by the turbulent diffusion of water vapour out of leaves and into the atmosphere. Francis Darwin manifested scepticism about Dixon and Joly's idea:

> "*To believe that columns of water should hang in the tracheals like solid bodies, and should, like them, transmit downwards the pull exerted on them at their upper ends by the transpiring leaves, is to some of us equivalent to believing in ropes of sand*"

Darwin's scepticism was warranted, for if water is lifted above 10 m, the gravitational pull alone would make the liquid metastable, possibly interrupting the continuity of the water columns inside the plant by cavitation. The presence and spread of gas within xylem conduits, embolism, is now widely documented in plants and is thought to be the main cause behind current increasing trends in tree mortality around the globe (Choat et al., 2018).

The scientific understanding of water movement in plants has advanced significantly since the introduction of the cohesion-tension theory, which has now wide acceptance (Angeles et al., 2004, Scholander et al., 1965, Schenk et al., 2017), and the concepts from the cohesion-tension theory have been unified in the 'soil-plant-atmosphere continuum' (SPAC) (Philip, 1966). What is notable about the SPAC is that it treats plant water movement as a process governed by the same transport phenomena applicable to inert physical systems: water in plants moves via flow and diffusion in response to pressure and concentration gradients. While flow and diffusion are distinct transport phenomena, they share a similar mathematical formulation and thus plant water transport can be well approximated by an electrical circuit analogy (van den Honert, 1948, Sack and Holbrook, 2006); at the same time, the forces that drive plant water movement can be quantified by a single metric, water potential (Meyer, 1938, Owen, 1952). The SPAC also highlights an important feature of plant water transport: long-distance water movement requires a continuous liquid path.

2. Thesis outline

This thesis deals with two distinct topics within the study of plant hydration dynamics. First, I investigated the role of foliar water uptake in the recovery of shoot hydraulic function; and second, I explored the measurement of plant hydration dynamics via static uniaxial compression. Although the ideal order would have been the opposite, serendipity played a role in this work and the chapters are presented chronologically.

Foliar water uptake refers to the absorption of water by above-ground organs. (While in strict sense FWU only refers to the uptake of water by leaves, the term is commonly used including water uptake via other aerial anatomical structures.) Historically, FWU has been recognised but deemed insignificant to the water economy of plants (Paul, 1895, Williams, 1932, Hales, 1727). Although the contribution of FWU to the mass balance of a plant may be small, FWU may have functional roles that have been scarcely tested (Schreel and Steppe, 2020). In this context, I hypothesized that the absorption of water by leaves may enable plants to recover from losses in hydraulic conductivity caused by dehydration. This question was addressed in two parts: in Chapter 2, I characterised the rate and conductance of FWU in the grey mangrove (*Avicennia marina*) and evaluated the effect of FWU in the recovery of leaf hydraulic conductance; in Chapter 3, I evaluated the effect of FWU in the refilling of embolised vessels of the same species.

The fluxes that occur along the SPAC are highly regulated by, and depend on, plant water status; however, measurements of plant water status are time-consuming and hard to automate. Potentially, better knowledge of plant water status could inform irrigation practices in agriculture and climate modelling (Jasechko et al., 2013). Plant water status is

fundamentally described by two quantities, water content and water potential (Turner, 1988). In Chapter 4, I present a method to study plant hydration dynamics via static uniaxial compression of laminar leaves. In a multidisciplinary approach, I draw on two basic measurement paradigms from rheology (constant stress and stress relaxation) to develop a procedure to monitor leaf water content and leaf water potential. The chapter introduces: (i) a simple hydrostatic equilibrium model used to infer the changes in leaf turgor pressure brought by uniaxial compression; (ii) the development of a low cost, custom-built leaf squeeze-flow rheometer; and (iii) the empirical relations between leaf pressure-volume parameters and leaf squeeze-flow parameters.

Foreword

The next chapter presents a study of the kinetics of FWU and its effects on leaf hydraulic conductance. Due to journal and co-author suggestions, the term used in the paper was ‘shoot surface water uptake’ (SSWU). Throughout the thesis, FWU and SSWU are used equivalently and both refer to the uptake of atmospheric water via the surface of aerial plant organs.

CHAPTER 2: SHOOT SURFACE WATER UPTAKE ENABLES LEAF HYDRAULIC RECOVERY IN *AVICENNIA MARINA*

1. Abstract

- The significance of shoot surface water uptake (SSWU) has been debated, and it would depend on the range of conditions under which it occurs. We hypothesized that the decline of leaf hydraulic conductance (K_{leaf}) in response to dehydration may be recovered through SSWU, and that the hydraulic conductance to SSWU (K_{surf}) declines with dehydration.
- We quantified effects of leaf dehydration on K_{surf} and effects of SSWU on recovery of K_{leaf} in dehydrated leaves of *Avicennia marina*.
- SSWU led to overnight recovery of K_{leaf}, with recovery retracing the same path as loss of K_{leaf} in response to dehydration. SSWU declined with dehydration. In contrast, K_{surf} declined with rehydration time but not with dehydration.
- Our results showed a role of SSWU in the recovery of leaf hydraulic conductance and revealed that SSWU is sensitive to leaf hydration status. The prevalence of SSWU in vegetation suggests an important role for atmospheric water sources in maintenance of leaf hydraulic function, with implications for plant responses to changing environments.

2. Introduction

There is a pressing need to understand the dynamics of loss and recovery of leaf hydraulic function in plants. Leaves represent a major (>30%) fraction of the resistance to liquid water movement through entire plants (Sack and Holbrook, 2006). The efficiency of water transport through leaves, leaf hydraulic conductance (K_{leaf}), has indirect effects constraining gas exchange through its effects on stomatal conductance (Blackman et al., 2009, Xiong et al., 2017, Flexas et al., 2018, Wang et al., 2018, Sack and Holbrook, 2006), and is a critical determinant of plant productivity (Scoffoni et al., 2016). Yet, K_{leaf} is strongly affected by plant hydration. As plants dehydrate, K_{leaf} declines due to changes in conductance within and outside the xylem tissue (Scoffoni et al., 2017b), with the latter occurring at mild levels of water stress in association with decline in turgor. Because decline of K_{leaf} occurs at mild water stress, many plants experience diel cycles of loss and recovery of K_{leaf} (Bucci et al., 2003, Lo Gullo et al., 2003, Brodribb and Holbrook, 2004, Hao et al., 2008, Johnson et al., 2009, Yang et al., 2012), and that recovery depends on the extent of dehydration (Blackman et al., 2009, Brodribb and Cochard, 2009).

Many plants live in arid or saline environments in which low soil water potential may limit the extent of overnight K_{leaf} recovery, or where rehydration may be delayed by loss of conductance itself (i.e. a negative feedback response). In these cases, alternative water sources might enable rehydration leading to K_{leaf} recovery. Absorption of liquid water from the

surface of above-ground organs, herein referred to as shoot surface water uptake (SSWU), is a water acquisition mechanism found in nearly all plant families (Dawson and Goldsmith, 2018). Despite its common occurrence, there are important knowledge gaps regarding the mechanisms and physiological consequences of SSWU (Berry et al., 2018), and how these influence tree fitness. For example, recent evidence indicates that anisohydric species that rely strongly on SSWU are more vulnerable to drought and climate change than isohydric species with lower SSWU capacity (Eller et al., 2016), suggesting a role for SSWU in maintenance of hydraulic function. While stem embolism refilling through SSWU has been observed in two conifer species (Mayr et al., 2014a, Earles et al., 2016), there are no experimental data on whether SSWU affects K_{leaf}.

To better understand the implications of SSWU to plant function, we need to understand how water moves across the leaf surface and whether this process is affected by leaf hydration. The hydration status of the leaf surface can affect its permeability to water (Fernandez et al., 2017), and thus affect the conductance of the leaf surface to SSWU (K_{surf}), which may occur in liquid or gaseous form. Although Guzman-Delgado et al. (2018) documented temporal changes in K_{surf} during leaf rehydration, whether K_{surf} depends on leaf hydration status, as does K_{leaf}, remains untested.

We tested two novel hypotheses in *Avicennia marina*, a mangrove species that exhibits SSWU (Schreel et al., 2019, Nguyen et al., 2017b): that (i) K_{surf} declines with decreasing leaf water potential and (ii) K_{leaf} recovers overnight through SSWU.

3. Materials and methods

Sampling and processing

During two field campaigns in May and August 2018, one sun-exposed branch per tree, *c*. 20 mm diameter, was collected from eight individuals of *Avicennia marina* ssp. *eucalyptifolia* (Zipp. ex Moldenke) J. Everett growing on the south arm of the Daintree River (16° 17’ 20’’ S, 145° 24’ 59’’ E) for measurements of K_{leaf}; five individuals from the same populations were used to build pressure-volume curves and to estimate K_{surf}. Branches were collected at *c*. 1 m above the maximum tide level from trees *c*. 6 m tall. Soil water (collected at a depth of 30 cm) and surface water salinity at the sampling site were determined in August using a refractometer (AST, Japan). Soil water salinity (at a depth of 30 cm) averaged 25 ppt (n = 2), and surface water salinity was 24.3 ± 0.2 ppt (n = 5, Table 2.1), equivalent to osmotic potentials of -1.71 MPa and -1.66 ± 0.1 MPa, respectively. The climate in the study site is classified as a tropical monsoon climate (Am) under the definition of Koppen (1936).

Sampling of branches took place between 16:00 and 18:00 h. Immediately after cutting, branches were placed in black plastic bags and brought to the laboratory within 30 min, where they were recut under a solution of 5% seawater and left to rehydrate overnight; the solution salinity was based on measured xylem sap concentrations in this species (Ball, 1988, Stuart et al., 2007a). Suspended matter was allowed to settle from fresh seawater before the desired amount was decanted into fresh water to prepare the 5% seawater solution. The day after collection, the branches were recut into twigs bearing *c*. 10-20 leaves and maintained with the cut ends in the solution under dark, non-transpiring conditions.

Pressure-volume curves

One leaf from each of five trees was used to construct a pressure volume curve (PV curve) (Tyree and Richter, 1981). Measurements of leaf weight and leaf water potential (Ψ_{leaf}) were made at intervals corresponding to a decrease of 10-20 mg in fresh weight using a 1 mg resolution balance (ML303E, Mettler-Toledo GmbH, Switzerland) and a pressure chamber (1505D, PMS Instruments, OR, USA). All leaves were scanned with a CanoScan LiDe 110 (Canon Inc., Tokyo, Japan) for measurement of leaf area (Adobe Photoshop CC, Adobe Systems, CA, USA). Leaf dry weight was determined after oven-drying at 70°C for 48 h using a 0.1 mg resolution balance (AX205, Mettler-Toledo GmbH, Switzerland). Relative water content (*RWC*) was calculated as

$$RWC = \frac{FW - DW}{SW - DW} \times 100 \qquad Eqn\ 2.1$$

where *FW* is the leaf fresh weight (g), *DW* is the leaf dry weight (g) and *SW* is the leaf saturated weight (g) (i.e., the maximum fresh weight measured for each leaf after rehydrating). The water potential at the turgor loss point (Ψ_{TLP}) was determined as the highest Ψ_{leaf} value on the linear domain of the plot between the inverse of leaf water potential ($1/\Psi_{leaf}$) and relative water deficit (100-RWC). For determination of the osmotic potential at full turgor (Π_{ft}), we excluded the apoplastic water fraction for the first domain of the PV curve, as in Nguyen *et al.* (2017b) (Fig. 2.S1).

Because *Avicennia marina* leaves exhibit a three-domain PV curve (Nguyen et al., 2017b, Nguyen et al., 2017a), leaf capacitance between full hydration and the Ψ_{TLP} was determined as the first derivative of a third-order polynomial function fitted to the values of RWC and Ψ_{leaf} from all curves ($RWC = 102.17 - 18.22 \times \Psi_{leaf} + 8.01 \times \Psi_{leaf}^2 - 1.3 \times \Psi_{leaf}^3$; $r^2 = 0.91$; $P < 0.0001$). As the solution used for plant tissue hydration was always 5% seawater (equivalent to a water potential of -0.12 MPa), the curve fitting was made with the constraint that it must pass through (0.12, 100). At values of $\Psi_{leaf} < \Psi_{TLP}$, capacitance was obtained from

a straight line fitted to the values of RWC and Ψ_{leaf} (RWC = 111.82 - 8.88 × Ψ_{leaf}; r^2 = 0.5; P < 0.0001) with the constraint that it must intersect the value of the polynomial fit at the Ψ_{TLP}.

Shoot surface water uptake kinetics

The rates of SSWU were determined by placing excised branches in a plastic chamber kept at saturating humidity (see *Rehydration kinetics* for details) and by tracking changes in Ψ_{leaf}, using the same principle as the RKM method (Brodribb & Holbrook, 2003), i.e., estimating changes in mass through PV-curve derived capacitance values and relaxation of Ψ_{leaf}. Working with attached leaves enabled us to study the rates of SSWU in branches which were treated in the same way as for the RKM measurements (see *Rehydration kinetics*). However, our experimental design does not distinguish the organ taking up the water, and thus SSWU may also involve water absorbed by bark (Earles et al., 2016). Five branches (one per tree) were cut into three branchlets and randomly assigned to each of three different dehydration levels corresponding to water potentials of -3.2 ± 0.1, -3.9 ± 0.1 and -4.9 ± 0.1 MPa (mean ± SE), after which they were sprayed with rainwater until dripping and placed in the chambers. Ψ_{leaf} measurements were made on two leaves per branch after 30 min and then every hour for the next four hours. Most branches were equilibrated prior to the start of the experiment, as the difference in Ψ_{leaf} within branches was lower than 0.1 MPa in all but two branches (in which $\Delta\Psi_{leaf}$ was 0.24 and 0.26 MPa). After each measurement, branches were sprayed until dripping and placed back into the chambers. The last measurement was made 12 h from the start. All measurements were started at night (*c.* 20:00 h).

In one of the treatments (-3.2 MPa starting Ψ_{leaf}), the salinity of the water on the leaf surface was determined for each of the five replicate branches at each time point by gently rubbing 3-5 leaves on a refractometer (AST, Japan), until a continuous film of water was collected. The measured salinity values were then converted to osmotic potentials and used for calculating the gradient driving water movement into the leaf. Time-dependent variation in Ψ_{leaf} and in osmotic potential of leaf surface water were fitted with an exponential decay function of the form

$$\Psi = \Psi_f + A \times e^{-\frac{t}{\tau}} \qquad Eqn\ 2.2$$

where Ψ_f is the final Ψ_{leaf}, A is the function amplitude constant, τ is the function time constant and t is the time since the start of the experiment (h).

The cumulative amount of water taken up per unit leaf area (SSWU, mol H_2O m^{-2}) in response to SSWU was estimated using the functions fitted to the PV curves, and corrected for the water content per unit area as:

$$SSWU = \left(RWC\left(\Psi_{leaf}\right)_t - RWC\left(\Psi_{leaf}\right)_0 \right) \times \frac{1}{100} \times WCA_{sat} \times \frac{1}{M} \qquad Eqn\ 2.3$$

Where $RWC(\Psi_{leaf})_t$ is the value of the function fitted to the data from PV curves evaluated at the Ψ_{leaf} measured at times t=0.5, 1.5, 2.5, 3.5, 4.5 and 12 h and WCA_{sat} is the saturated leaf water content per unit area (g m^{-2}). The change in moles of water was thus calculated between each measurement of Ψ_{leaf}. Conductance to SSWU (K_{surf}, μmol H_2O m^{-2} s^{-1} MPa^{-1}) was calculated between each time point as:

$$K_{surf} = \frac{SSWU_t - SSWU_{t-1}}{S_t - \Psi_{leaf_t}} \times \frac{1}{\Delta t} \qquad Eqn\ 2.4$$

Where S_t (MPa) was the estimated value for the osmotic potential of the leaf surface water obtained from the exponential decay function fitted to the data of one of the SSWU treatments (-3.2 MPa; $S_t = 1.02 \times e^{(-t/1.82)} + 0.37$; $r^2 = 0.88$; $P = 0.003$) evaluated at each time point, and Δt is the time between each pair of measurements (s).

Rehydration kinetics

K_{leaf} was determined with a modified version of the rehydration kinetics method (RKM) (Brodribb and Holbrook, 2003), which estimates water fluxes based on Ψ_{leaf} relaxation kinetics in response to rehydration and leaf capacitance values derived from the PV curve.

To construct leaf vulnerability curves, branches were bench dried to different levels of Ψ_{leaf} and left to equilibrate in black plastic bags for 30 min, after which the initial Ψ_{leaf} was measured. Subsequently, six leaves from the same branch were cut with the petiole submerged under a 5% seawater solution and left to rehydrate for periods of 30, 60, 120, 240, 300 and 480 s. Following these time periods, leaves were equilibrated in bags in the dark for *c*. 10 min, after which Ψ_{leaf} was measured and K_{leaf} calculated as

$$K_{leaf} = \frac{C_{leaf} Log_e \left(\frac{\Psi_0}{\Psi_t - \Psi_s} \right)}{t} \qquad Eqn\ 2.5$$

where C_{leaf} is leaf area normalised capacitance calculated from the PV curve function evaluated at Ψ_t (mol H_2O m^{-2} $MPa^{-}1$, see below), t is the duration of rehydration (s), Ψ_0 is the leaf water potential before rehydration (MPa), Ψ_t is the leaf water potential at time t (MPa) and Ψ_s is the osmotic potential of the water source (-0.12 MPa). The last term corrects for the fact that $\Psi_t < \Psi_s$ (Notes 2.S1). C_{leaf} was calculated for each value of Ψ_t as

$$C_{leaf} = \frac{dRWC}{d\Psi_{leaf}} \times \frac{1}{100} \times WCA_{sat} \times \frac{1}{M} \qquad Eqn\ 2.6$$

where $dRWC/d\Psi_{leaf}$ is the derivative of the PV function evaluated at Ψ_t and M is the molar mass of water (g mol^{-1}). As K_{leaf} is a function of C_{leaf}, the relaxation time constant of Ψ_{leaf} (k) was calculated as

$$k = \frac{Log_e\left(\frac{\Psi_0}{\Psi_t - \Psi_s}\right)}{t} \qquad Eqn\ 2.7$$

to test if leaf hydraulic recovery was dependent on the different values of C_{leaf}.

The same method described for constructing vulnerability curves was used for measuring changes in K_{leaf} in response to SSWU. After reaching a value of Ψ_{leaf} at which considerable K_{leaf} was lost (-3.8 ± 0.1 MPa), each of eight equilibrated branches was cut in two using pruning clippers. Half of these branches were used for measuring K_{leaf} in this partially dehydrated state, and the other half were placed in a 50 L polypropylene container at saturating humidity, sprayed once with water and left to rehydrate through SSWU overnight. The container was kept humid by a c. 5 cm film of water in the bottom with semi-submerged wads of sponge to increase evaporative surface area. Branches were kept suspended inside the box so that the cut ends were not in contact with free water. Leaves were visibly wet the next morning. K_{leaf} was then measured for these half-branches as described above. The procedure was repeated for eight branches at a more severely dehydrated state (-4.9 ± 0.1 MPa), with the addition of an unsprayed control treatment. To account for the possibility of leaves taking up water from stem tissues in the -3.8 MPa treatment, an unsprayed control treatment was added (April 2019) for a set of eight branches at a similar starting water potential (-3.9 ± 0.1 MPa) ($F_{1,14}$ = 1.62, P = 0.23, one-way ANOVA). Unsprayed controls were kept in plastic bags with no addition of water.

The vulnerability curve obtained from the RKM measurements during dehydration was fitted with a sigmoidal function (Pammenter and Van der Willigen, 1998) of the form

$$K_{leaf} = \frac{K_{max}}{1 + e^{a(\Psi_{leaf} - \Psi_{50})}} \qquad Eqn\ 2.8$$

where K_{max} is the estimated maximum value of K_{leaf}, a is the function rate constant and Ψ_{50} is the water potential at which 50% K_{leaf} has been lost.

Data analyses

The differences in k, K_{leaf} and Ψ_{leaf} between before and after SSWU were analysed using paired t-tests using Genstat 18.2 (VSN International, UK) under the null hypothesis that there were no differences before and after SSWU. All plots and non-linear models were generated using OriginPro 2017 (OriginLab, MA, USA) and stylised in Adobe Illustrator CC (Adobe

Systems, CA, USA). Models were fitted using the Levenberg-Marquardt algorithm and validated via normal distribution of the residuals. The effects of time and starting Ψ_{leaf} on SSWU and K_{surf} were analysed using linear mixed-effects models in R (v. 3.5.1, the R Foundation for Statistical Computing, Vienna, Austria) using the *lme4* and *lmertest* packages. The standard error of WCA_{sat} and the 95% confidence interval of the function fitted to PV curve data (PV.CI) were propagated throughout the calculations of SSWU and K_{surf}. To test if the sources of error had any effects on the results, the models were also run using the higher and lower bounds of the estimates of SSWU and K_{surf} based on the error terms derived from PV.CI and WCA_{sat}. The model used for SSWU and K_{surf} was initial Ψ_{leaf} × rehydration time; plant individual was considered as a random effect. Models for SSWU and K_{surf} were run using all time points (0-12 h) or the time points from 0 to 4.5 h, as SSWU ceased after 4.5 h in all treatments. Results of K_{surf} are discussed excluding the last time point, but the results of both analyses are presented in Fig. 2.2. Results of these models are included in Tables 2.S1-S2.

4. Results

Continuous variation in leaf capacitance

Leaf capacitance varied 10-fold from 3.15 mol H_2O m^{-2} MPa^{-1} at full hydration to 0.31 mol H_2O m^{-2} MPa^{-1} at the capacitance function inflection point (-2.05 MPa; Fig. 2.1A). Fitting a polynomial function for points in domains 1 and 2 resulted in a lower goodness of fit than those obtained by fitting linear functions for each domain (Root Mean Square Error = 1.59 from linear functions, Fig. 2.S2; RMSE = 1.67 from polynomial function, Fig. 2.1A). However, because C_{leaf} was derived from the PV curve function, variation in C_{leaf} was continuous with no disjunction in C_{leaf} at the Ψ_{TLP} or at the transition between domain 1 and 2 (Fig. 2.1A, Fig. 2.S2).

Table 2.1 Water salinity at the sampling site and physical properties of leaves of *Avicennia marina* ssp. *eucalyptifolia* used for constructing PV curves. n = 5 for all measurements except soil water salinity (n = 2).

Variable	Symbol	Units	Mean	SE
Surface water salinity	-	ppt	24.3	0.2
Soil water salinity	-	ppt	25	-
Leaf area	LA	cm^2	19.8	1.21
Saturated weight	SW	g	0.89	0.06
Dry weight	DW	g	0.28	0.02
Leaf dry mass per area	LMA	$g\ m^{-2}$	139	1.86
Saturated leaf water content per area	WCA_{sat}	$g\ m^{-2}$	312	7.44
Saturated leaf water content per dry mass	WCD_{sat}	$g\ g^{-1}$	2.25	0.05
Water potential at the turgor loss point	Ψ_{TLP}	MPa	-3.44	0.1
Osmotic potential at full turgor	Π_{ft}	MPa	-2.89	0.09

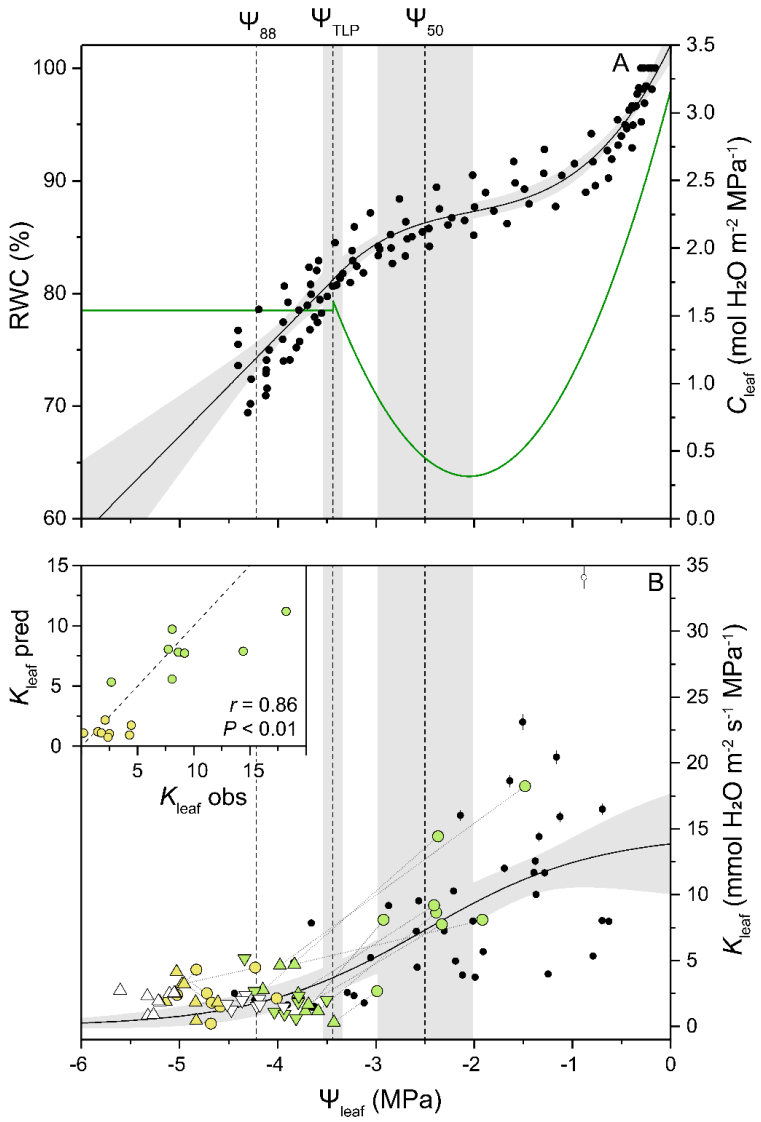

Figure 2.1. A: Pressure-volume curves from *Avicennia marina* ssp. *eucalyptifolia* and capacitance (C_{leaf}) values used for calculation of leaf hydraulic conductance (K_{leaf}) and conductance to shoot surface water uptake. Black dots correspond to values from 5 plants. The black curve corresponds to the polynomial and linear models fitted to the PV curve data at leaf water potential (Ψ_{leaf}) higher than the leaf water potential at the turgor-loss point (Ψ_{TLP}) and $\Psi_{leaf} < \Psi_{TLP}$, respectively. The green curve corresponds to the leaf area standardised capacitance values derived from the PV cu rve fit (i.e. the slope of the estimated leaf relative water content versus Ψ_{leaf}). B: Loss and recovery of K_{leaf} in response to dehydration and shoot surface water uptake (SSWU). Black dots and triangles correspond to data points measured during dehydration; circles correspond to measurements performed after SSWU. Filling colour indicates starting Ψ_{leaf} at -3.8 MPa or -3.9 MPa (light green) and -4.9 MPa (yellow). Open triangles correspond to controls (i.e. no spraying) treatments. Error bars correspond to the uncertainty term propagated from the saturated leaf water content per unit area

measurements. Dotted lines indicate the change in Ψ_{leaf} and K_{leaf} for each individual. Dashed lines indicate the water potential at 50% loss of K_{leaf} (Ψ_{50}), Ψ_{TLP} and the water potential at 88% loss of K_{leaf} (Ψ_{88}). Grey areas indicate the 95% confidence interval for the model and the SE of the Ψ_{50} and Ψ_{TLP}. The open circle corresponds to an outlier measured during dehydration (Grubb's test, $P < 0.05$) and was not included in the model. Inset: correlation between observed and predicted K_{leaf} values measured after the SSWU treatment; the dashed line depicts the 1:1 relation between observed and predicted values.

Table 2.2 Changes in Ψ_{leaf} and K_{leaf} measured overnight under conditions of spraying (+) and no spraying (-). Values correspond to the mean ± SE difference between the initial and final measurements. *P*-values correspond to contrasts obtained from paired t-tests. n = 8.

Ψ_{leaf} (MPa)	SSWU	Δ Ψ_{leaf} (MPa)	*P*-value	ΔK_{leaf} (mmol m^{-2} s^{-1} MPa^{-1})	*P*-value
-3.8	+	1.42 ± 0.1	<0.001	7.23 ± 1.25	0.001
-3.9	-	-0.22 ± 0.08	0.021	-0.13 ± 0.54	0.826
-4.9	+	0.33 ± 0.06	0.001	0.03 ± 0.4	0.954
-4.9	-	-0.34 ± 0.03	<0.001	-0.63 ± 0.45	0.231

Kinetics of SSWU

As expected from SSWU, Ψ_{leaf} increased through time in all treatments (Fig. 2.2A; Table 2.S3). Leaf surface salinity decreased with time, presumably due to salts being washed off with spraying. However, none of the leaves achieved full hydration via SSWU, and Ψ_{leaf} values were always more negative than the osmotic potential in the leaf surface (i.e. the maximum achievable Ψ_{leaf}).

The recovery of Ψ_{leaf} corresponded to increases in leaf mass through time in all treatments ($F_{81.98} = 6.13$, $P = 0.02$) (Fig. 2.2B). Leaves absorbed 0.5-1.2 mol H_2O m^{-2} over a period of 12 h; in all cases, more than 98% of the total water uptake occurred within the first 4.5 h. The effect of Ψ_{leaf} on SSWU was not significant between 0 and 4.5 h ($F_{82.37} = 3.07$, $P = 0.08$); however, when considering all time points (0-12 h), Ψ_{leaf} had a significant effect on SSWU ($F_{96.66} = 7.42$, $P = 0.01$) (Fig. 2.2B, Table 2.S1). The significant effect of Ψ_{leaf} on SSWU was consistent across all analyses, independent of the bounds of the sources of error used in calculations (Table 2.S2).

K_{surf} declined with time ($F_{71} = 4.66$, $P = 0.03$), reaching negligible values after three hours (Fig. 2.2C). The initial Ψ_{leaf} had no significant effect on K_{surf} over the first 4.5 h ($F_{71} = 2.96$, $P = 0.09$) (Fig. 2.2C, inset), and the effect was also non-significant at 0.5 h (i.e., initial

K_{surf}) ($F_{9.33}$ = 2.56, P = 0.14). However, the significance of the effect of Ψ_{leaf} on K_{surf} was dependent on the bounds of the sources of error used in calculations (Table 2.S2). On average, K_{surf} in the -4.9 MPa treatment was less than 50% of that in the -3.2 and -3.9 MPa treatments during the first two hours (Fig. 2.2C). There was no significant interaction between initial Ψ_{leaf} and rehydration time over the first 4.5 h (F_{71} = 1.72, P = 0.19; Fig. 2.2C).

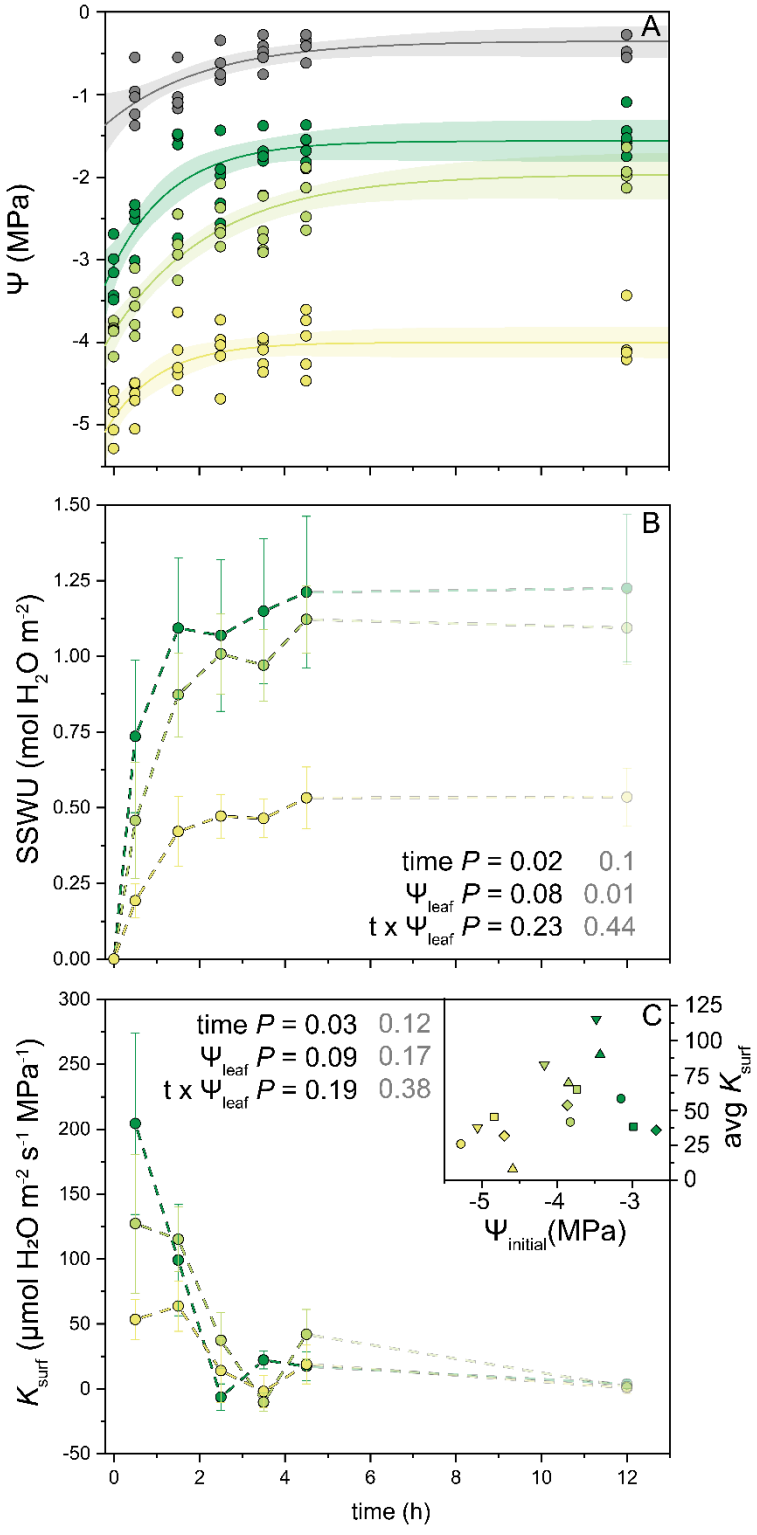

Figure 2.2. Measured changes in leaf water potential (Ψ_{leaf}, coloured symbols) and leaf surface osmotic potential (grey symbols) (A), and estimated changes in fresh mass (B) and conductance to shoot surface water uptake (K_{surf}; C) during a 12-hour period of intermittent spraying. All models in (A) correspond to exponential decay functions (Eqn 2.2) and the parameters fitted by each model are presented in Table S4. For panel (B), shoot surface water uptake (SSWU) was calculated according to Eqn 2.3, and for panel (C) K_{surf} was calculated according to Eqn 2.4. The inset in C corresponds to the average K_{surf} values between 0-4.5 h for each individual (represented by different symbols). Colour depicts the starting leaf water potential of each treatment at -3.2 MPa (dark green), -3.9 MPa (light green) and -4.9 MPa (yellow). Error bars correspond to SE. *P* values shown are from linear mixed models considering all time points (grey) or excluding the data at t = 12 h (black). n = 5.

Effects of dehydration and SSWU on K_{leaf}

K_{leaf} of *Avicennia marina* declined with decreasing Ψ_{leaf} during branch dehydration (Fig. 2.1B). When dehydrated branches were sprayed with water, SSWU led to a significant increase in Ψ_{leaf} overnight (Table 2.2); when unsprayed, all branches dehydrated overnight, as evidenced by a significant decrease in Ψ_{leaf} (Table 2.2). For branches dehydrated to an initial state of -3.8 MPa, SSWU led to an increase in K_{leaf} from 2.36 to 9.63 mmol H_2O m^{-2} s^{-1} MPa^{-1} (i.e., from 16% to 66% of the estimated K_{max}; Table 2.2, Table 2.S3). However, in branches dehydrated to -4.9 MPa, K_{leaf} did not increase significantly whether sprayed or unsprayed (Table 2.2). These results were not due to differences in C_{leaf} (Fig. 2.1A); when calculated independent of C_{leaf}, the changes in the rehydration time constant exhibited a similar pattern to those of K_{leaf} (Figure 2.S3).

While we observed more recovery of Ψ_{leaf} than K_{leaf} in response to SSWU, the values of K_{leaf} observed before and after spraying treatments accorded with those predicted by the model based on Ψ_{leaf} ($r = 0.86$, $P < 0.01$; Fig. 2.1B, inset). Thus, the non-significant changes in K_{leaf} in the -4.9 MPa dehydration treatment were consistent with insufficient rehydration through SSWU.

5. Discussion

A functional significance of SSWU was demonstrated by recovery of K_{leaf} in *Avicennia marina*. Notably, SSWU was dependent on leaf hydration, although the response of K_{surf} to Ψ_{leaf} was not significant. These results provide evidence to guide future research into the role of SSWU in diel K_{leaf} recovery in plants subject to regular leaf wetting events.

Kinetics of SSWU

Our results revealed that K_{surf} varied with time, consistent with Guzman-Delgado et al. (2018), and there was no effect of the initial Ψ_{leaf} on K_{surf}, despite significant effects of initial Ψ_{leaf} on SSWU. For the purposes of discussion, we assume that most surface water is absorbed through leaves. Because the maximum K_{leaf} was *c*. 72 times higher than the maximum K_{surf} (Fig. 2.2C, Fig. 2.1B), SSWU is likely dominated by the permeability of the leaf surface, and not by the hydraulic conductance within the mesophyll. Assuming that the resistances to water movement through the mesophyll during SSWU correspond to those outside the xylem pathway, and that they correspond to approximately $0.5/K_{leaf}$ (Scoffoni et al., 2017b), we calculate that the resistance of water movement across the leaf surface would be c. 26-40 times greater than that through the mesophyll; if the resistances within the xylem were incorporated, then leaf surface resistance would be *c*. 13-19 times greater than that of the mesophyll, depending on leaf hydration status (Notes 2.S2). These values agree with those found by Guzmán-Delgado et al. (2018) in detached leaves of *Prunus dulcis* and *Quercus lobata*, in which the leaf surface resistance was 21-30 times greater than that of the petiole. Thus, SSWU is mainly determined by leaf surface permeability.

Although the permeability of the cuticle may be affected by its hydration status (Fernandez et al., 2017), we observed no effect of Ψ_{leaf} on K_{surf}. Dehydration-dependent changes in the hydraulic conductance within the mesophyll (Fig. 2.1B) may not be reflected in changes in K_{surf}, as the latter largely depends on leaf surface permeability. While the effects of Ψ_{leaf} on K_{surf} were dependent on the sources of error used in calculations, the decline of K_{surf} with time is also inconsistent with hydration status determining cuticle permeability because all plants rehydrated during leaf wetting. It is possible that K_{surf} in *Avicennia* is not governed cuticle permeability, but regulated by epidermal features such as stomata (Eichert et al., 2008), trichomes (Nguyen et al., 2017b) or salt glands (Tan et al., 2013), whose contribution to K_{surf} may vary with time. The decline in K_{surf} with rehydration time was consistent with Guzman-Delgado et al. (2018), who reported a decreasing K_{surf} with time due to incomplete relaxation of Ψ_{leaf} in *Prunus dulcis* and *Quercus lobata*. While salt glands have been shown to take up water in *Avicenna officinalis* (Tan et al., 2013), the lack of salt glands in *Prunus dulcis* and *Quercus lobata* suggests the temporal decline in K_{surf} is regulated via a common mechanism. Further work needs to determine the pathways of SSWU, with particular attention to stomata, and quantify how these are related to the temporal changes in K_{surf} during rehydration.

Our data were comparable to those reported for detached leaves of *Prunus dulcis*, for which the estimated maximum K_{surf} was *c*. 90 μmol m^{-2} s^{-1} MPa^{-1} (Guzman-Delgado et al., 2018), while our values for *Avicennia marina* ranged from *c*. 60 to 200 μmol m^{-2} s^{-1} MPa^{-1} depending on the initial Ψ_{leaf} (Fig. 2.2C); the time required until SSWU ceased and the amount

of water taken up by the leaves were also similar. In contrast to Guzmán-Delgado et al. (2018), *A. marina* leaves were rehydrated while attached to stems and K_{surf} estimated based on changes in Ψ_{leaf}. Consequently, because estimates of C_{leaf} come from detached leaves, K_{surf} values were potentially underestimated because the relaxation kinetics of Ψ_{leaf} may have been quenched by water moving from leaves into stems.

Effects of dehydration and SSWU on K_{leaf}

Our results showed that K_{leaf} can recover through SSWU. After spraying with water, K_{leaf} increased with Ψ_{leaf} along the same plotted path as observed during dehydration (Fig. 2.1B, inset). These results contrast with data available from other studies in which rehydration occurred via the roots. Several studies reported that recovery of K_{leaf} depends on the extent of leaf dehydration (Bucci et al., 2003, Lo Gullo et al., 2003, Brodribb and Holbrook, 2004, Hao et al., 2008, Johnson et al., 2009, Yang et al., 2012). Some studies found that loss of K_{leaf} occurs mainly through reversible loss of conductance outside the xylem, and that embolism in leaves is rare until extreme dehydration (Scoffoni et al., 2017a) and studies with more severe water stress found evidence of irreparable xylem embolism associated with the loss of K_{leaf} (Brodribb et al., 2016, Johnson et al., 2018). Loss of conductance in other organs such as roots and stems might also affect the recovery of K_{leaf}. Creek et al. (2018) found lower K_{leaf} recovery than that expected from Ψ_{leaf} recovery (i.e. irreversible loss) in plants in which losses of hydraulic conductance also took place in roots and stems. It is possible that rehydration through the leaf surface may enable plants to bypass the limitations imposed by embolised conduits in root and stem xylem, thereby enabling K_{leaf} recovery. Thus, SSWU may play an important role in K_{leaf} recovery when rehydration from the soil is limited by the availability of soil water or the capacity for water transport. Further research is needed to extend the role of SSWU in leaf hydraulic recovery to the wide range of conditions in which SSWU has been documented (reviewed in Berry et al., 2018). Our findings suggest that the dependence of SSWU on leaf hydration status would limit the range of conditions under which SSWU is functionally significant for hydraulic recovery. Future studies should determine the mechanisms by which hydraulic conductance can recover via SSWU in leaves and whether leaf xylem refilling is involved.

6. Conclusion

We found two results in the mangrove species *Avicennia marina* that advance understanding of SSWU and its physiological effects. First, SSWU depended on leaf hydration status, although there was no significant effect of Ψ_{leaf} on K_{surf}. Second, leaf hydraulic conductance (K_{leaf}) lost through dehydration was recovered by shoot absorption of liquid water. The recovery of K_{leaf} via SSWU depended on leaf water potential and retraced the same path as

K_{leaf} loss in response to dehydration. Given the prevalence of SSWU across diverse plant species and ecosystems (Dawson and Goldsmith, 2018), our results support recent assertions (Schreel and Steppe, 2019) on the importance of leaf wetting events in the maintenance of leaf gas exchange and plant productivity, which may affect plant fitness under changing climatic scenarios.

7. Acknowledgements

The authors thank the Australian Research Council for financial support, granted to M.C.B, L.S. and R.S.O (DP180102969). T.I.F was supported by the Becas Chile PhD scholarship program granted by CONICYT. We thank Catherine Bone and Nigel Brothers for exceptional field support and accommodation at the Daintree River, and John R. Evans for thoughtful comments on the manuscript.

CHAPTER 3: FOLIAR WATER UPTAKE ENABLES EMBOLISM REMOVAL IN EXCISED TWIGS OF *AVICENNIA MARINA*

1. Abstract

- Embolism refilling is thought to require relaxation of xylem tension, potentially excluding canopies of tall trees and plants growing in arid or saline soils. We tested whether foliar water uptake could enable embolism refilling in dehydrated twigs of the grey mangrove (*Avicennia marina*).
- Four dehydrated twigs were imaged by lab-based micro-computed tomography before and after wetting leaves.
- Emboli were observed in dehydrated stems and leaves. Embolism decreased with increasing distance from the cut end of stems, but not in leaves, suggesting that stem emboli were caused by cutting. Foliar wetting caused a significant reduction in the number of emboli in stems and a significant reduction in the area of emboli in leaves after 18.8 ± 1.7 h.
- Propagation of stem emboli into leaves may have been restricted by a vascular constriction in the stem-end of the petiole; this constriction may facilitate leaf xylem relaxation during top-down rehydration. Embolism refilling may have occurred due to capillarity or solute loading into embolised vessels. The results show that excised twigs of *A. marina* are able to recover from embolism by absorption of atmospheric water.

2. Introduction

Water transport through plants depends on the continuity of liquid water in xylem conduits, which can be disrupted by gas emboli. Transpiration from leaves causes tension in the xylem, which makes water metastable and can lead to embolism (Venturas et al., 2017). Embolism strongly reduces plant hydraulic conductivity and is thought to be the main cause of drought-induced tree mortality (Choat et al., 2018); however, there has been contention about the occurrence of embolism repair (Holbrook and Zwieniecki, 1999, Cochard and Delzon, 2013). Most of the debate has centred on whether and how plants would be able to repair embolism when water in the xylem is under tension. Short stature plants are known to resorb gas bubbles in the xylem by means of positive root pressure (Sperry, 1986, Yang et al., 2012), while taller plants may repair embolism by actively loading solutes into embolised vessels from surrounding living cells, creating an osmotic gradient for water movement (Zwieniecki and Holbrook, 2009, Brodersen et al., 2010, Brodersen and McElrone, 2013). In the absence of xylem tension, capillary forces can enable refilling of embolised conduits (Rolland et al., 2015). Some authors have found that plants repair embolism by absorbing atmospheric water, but the evidence is scarce and the extent of repair is limited (Mayr et al., 2014b, Earles et al., 2016).

Atmospheric water sources may be important for plants living in water-limited environments, which seldom experience xylem relaxation. Tension in the xylem can be caused by drought, gravity or salinity, and thus tall trees (Earles et al., 2016) and halophytic plants (Schreel et al., 2019) represent two groups which may benefit from foliar water uptake (FWU), and for which a plausible mechanism of embolism recovery is unclear. In a previous study, we reported that FWU enabled the mangrove *Avicennia marina* to restore leaf hydraulic conductance (K_{leaf}) lost during dehydration and characterised the kinetics of the process (Fuenzalida et al., 2019). The mechanisms involved in K_{leaf} recovery may involve changes in the hydraulic conductance outside the xylem tissue or embolism repair. Here we tested if this recovery involves embolism repair by using lab-based micro-computed tomography (micro-CT) on living excised twigs of the same species.

3. Materials and methods

Stem air discharge

Vulnerability of stem xylem to dehydration-induced embolism was characterised using the pneumatic method (Pereira et al., 2016). In August 2018, sun-exposed branches (c. 1 m long) were collected from seven adult trees of *Avicennia marina* ssp. *eucalyptifolia* (Zipp. ex Moldenke) J. Everett growing along the Daintree River, Queensland, Australia (16° 17’ 20’’ S, 145° 24’ 59’’ E). Branches were transported in black plastic bags to a field laboratory within an hour of collection. Maximum vessel length was determined by submerging the apical end of branches under water and pressurising the cut end of the stem using the pressurised end of a diaphragm vacuum pump (Air Cadet Pro, Cole-Parmer Instrument Company, USA). Starting from the tip of the branch, we cut segments c. 1 cm in length until bubbles were observable at the tip and recorded the length at which bubbling occurred using a measuring tape. The mean ± SE maximum vessel length was 43.5 ± 3 cm (n = 5).

Branches (one per each of seven trees) longer than the determined maximum vessel length were rehydrated by recutting the stem under a decanted 1:20 mixture of seawater and rainwater, misting the leaves with rainwater and covering the branches with black plastic bags. The salinity of the rehydration solution was based on reported xylem sap concentrations in *A. marina* (Ball, 1988, Stuart et al., 2007b). After overnight rehydration, the cut end of each branch was recut and fit into a silicone tube, fastened with two cable ties and sealed at the branch-tube interface using silicone glue (Aquarium SikaSeal, Sika Australia Pty Ltd, NSW, Australia). The open end of the tube was connected to a fitting (Luer-lock, Cole-Palmer, Vernon Hills, IL, USA) and secured with a cable tie. An illustration of the fitting method is provided in Fig. 3.S1.

Previous to air discharge measurements, branches were placed in black plastic bags for > 30 min to allow water potential equilibration within the sample, and cable ties were fastened using pliers. Air discharge from stems was estimated by connecting the fitted end of branches to a 4.8 mL air reservoir at an absolute pressure of c. 40 kPa for 150 s and by reading the change in pressure using a pressure transducer (PX140 series, Omega, CT, USA) connected to a micro controller (Arduino Uno, Arduino Inc., Ivrea, Italy). This measurement was performed 10-12 times for each branch at water potentials between -0.27 and -10.26 MPa, which were determined in two leaves per branch per measurement using a pressure chamber (1505D, PMS Instruments, OR, USA). The percentage of the maximum air discharged (PAD) was determined according to the methods described by Pereira et al. (2016).

We compared the measurements from stem air discharge obtained in this study to those of leaf hydraulic conductance (K_{leaf}) measured in samples from the same cohort of trees, as reported in Fuenzalida et al. (2019). As pneumatic and K_{leaf} measurements are not directly comparable, we present results as percent maximum *inferred* conductance. To do this, we normalised leaf hydraulic conductance relative to its estimated maximum (*i.e.*, the function higher asymptote) and expressed K_{leaf} as a percentage. The inferred stem hydraulic conductance was obtained as 100-PAD. We fit data from both methods with an equation of the form

$$\%\ maximum\ inferred\ conductance = \frac{100}{1 + e^{a(\Psi - \Psi_{50})}}$$

where a is the function rate constant, Ψ is the stem or leaf water potential and Ψ_{50} is the stem or leaf water potential at 50% of the maximum inferred conductance (Pammenter and Van der Willigen, 1998).

micro-CT experiment

Plant material

In August 2019, branches were collected from two adult trees of *Avicennia marina* ssp. *eucalyptifolia* on two different occasions (N = 4). Samples were collected in the evening from the same location as described for the pneumatic (and K_{leaf}) measurements, and transported in black plastic bags to the field laboratory within an hour. Leaf water potential was measured on one leaf per branch with a Scholander pressure chamber (1505D, PMS Instruments, OR, USA), and averaged −4.17 ± 0.11 MPa (mean ± SE). These values were close to the typical midday water potentials measured on site during the collection trip (−3.95 ± 0.1 MPa; mean ± SE of 4 plants averaged over three days). Branches were then re-bagged and transported to Canberra within a day.

One day after arrival, two branches (one per tree) were taken to the ANU CTLab. Branches were cut into individual twigs 10-15 cm long bearing 3 to 4 leaf pairs and the cut end was sealed with petroleum jelly to prevent water uptake via the vasculature. The leafy part of the twig was wrapped in paper towel and the twig was placed inside a 12 mm diameter glass tube for imaging. Use of this subspecies of *Avicennia marina* was essential to be able to fit twigs into such a small tube. (Other subspecies of *A. marina* have stiff leaves that break upon bending, making it impossible to fit them in a tube of this diameter, as required for maximising micro-CT resolution.) Two of the imaged twigs were imaged twice in the dry state to verify that the samples were static before imaging (Fig. 3.S2). After imaging in the dry state, tap water was provided to the paper towel until dripping. A small volume of water collected in the bottom of tubes but was > 5 cm from the cut ends of twigs in all samples.

Imaging and processing

The four samples (one per tree) were imaged using a laboratory-based microfocus X-ray source at the ANU CTLab (Hamamatsu L10711-03 micro-focus X-ray tube). Scans were performed using a source voltage of 80 kV and a current of 14 μA, which allowed repetitive scans to be performed without causing visible damage to the samples. Samples were imaged at 4 h intervals during 12-24 h along a region of interest (ROI) c. 40 mm long, usually containing one or two leaf pairs. Each data acquisition took 4.7 ± 0.3 h and involved c. 14,000 projections with an effective angular spacing of 0.1°; exposure times used were 0.6 and 0.75 s. Reconstructed tomograms had dimensions of 6500 × 2700 × 2700 voxels or 26 × 11 × 11 mm with a voxel size of c. 4 μm. Details about the reconstruction process can be found in Kingston et al. (2018).

Optical microscopy

A sample from the same group of samples used for micro-CT imagine was sectioned using a sledge microtome (GSL1, Schenkung Dapples, Switzerland) at different points along the stem, petioles and leaves. Samples 20-30 μm thick were stained by submerging in aqueous 0.05% (v/v) toluidine blue and mounted on a microscope slide. Micrographs were obtained using a microscope (DM6000, Leica, Germany) and photographed using a digital camera (SPOT Flex 64 MP, Diagnostic Instruments, USA). In the case of stems, images were stitched together using the Adobe Photoshop ‘Photomerge’ tool. Micrographs were selected based on quality and comparability to the anatomical features of interest obtained from micro-CT reconstructions. Vessel size distributions were obtained by manually drawing over the perimeter of each vessel and analysed using a threshold function in ImageJ (NIH, USA). The estimated hydraulic conductivity for each section of interest was calculated by summation of the fourth power of the vessel radii in each section, according to the Hagen-Poiseuille equation.

Analyses

Reconstructed tomograms were averaged over 32 Z-slices using the self-developed software WebMango and converted into 16-bit TIF images. Averaging of Z-slices reduced image noise, allowing clearer distinction of emboli (Fig. 3.S3). Greyscale level adjustments were automated using Adobe Photoshop image processor to enhance contrast and visualise embolised vessels. We manually removed the tissues surrounding the vascular bundles and, in the case of the stems, the area corresponding to the pith. These procedures enabled us to quantify the area occupied by air within the vasculature, excluding the large airspaces occupied by the aerenchyma tissue surrounding the vascular bundle. When emboli were not observable and samples were static, the number and area of emboli was recorded as zero. Images were then imported into ImageJ, converted to 8-bit and analysed by particle area using a threshold function.

Due to movement during rehydration, changes in the occurrence of emboli with time after wetting could not be quantified in three of the four samples. However, movement decreased with time and thus we quantified the occurrence of embolism in the wet state after the samples reached a static position. Time intervals between scans differed across samples; thus, we chose a comparable time point across all samples after 18.8 ± 1.7 h (mean ± SD) of wetting. In the samples in the dry state and after 18.8 h of wetting, we recorded the number of emboli and the total embolised area along the ROI and along 2-5 leaves per sample. Leaves used for quantitative analyses were chosen according to image quality, selecting only samples that were static and in which embolism could be clearly quantified. Leaf measurements were made at discrete points based on comparable anatomical features at the stem-end of the petiole, the leaf-end of the petiole and the leaf lamina. For analysing the effects of wetting on embolism, we used linear mixed-effects models considering hydration state (dry or wet), position within the leaf and their interaction as fixed factors; plant individual was used as a random factor in all analyses. Analyses were performed in R using the *lme4*, *lmerTest* and *nls* packages.

4. Results

Stem and leaf hydraulic vulnerability

The inferred stem hydraulic conductance decreased significantly during dehydration (Fig. 3.1). Minimum and maximum volumes of air discharged from stems were 55.2 ± 14.6 µL and 700.7 ± 81.9 µL (mean ± SE), respectively. As branches dehydrated, the water potential difference between two leaves within a branch was < 0.2 MPa for water potentials down to c. -4 MPa; further dehydration introduced larger water potential disequilibria (c. 0.5 MPa difference),

indicative of loss of hydraulic conductivity. The water potential at 50% maximum air discharge (Ψ_{50}) was estimated to be -5.54 ± 0.07 MPa (Fig. 3.1).

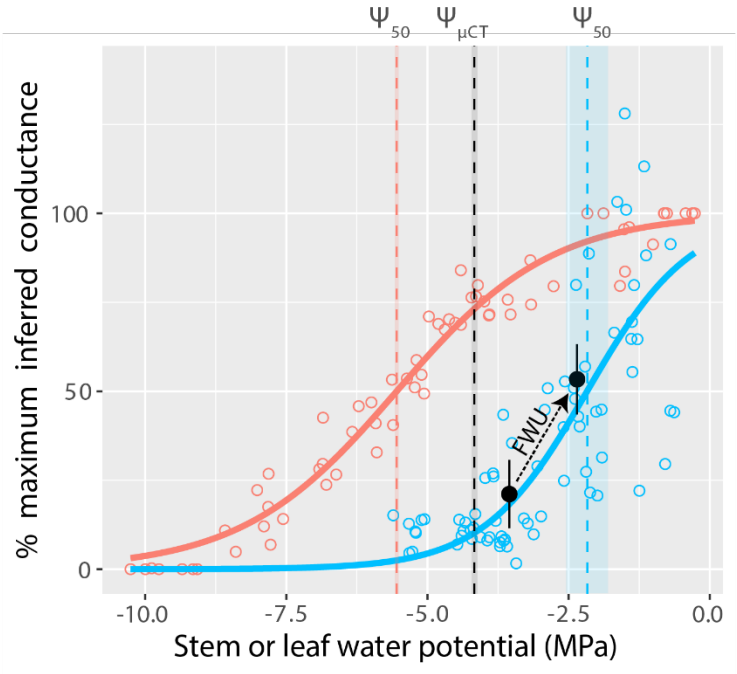

Figure 3.1. Decline in stem inferred hydraulic conductance of *Avicennia marina* ssp. *eucalyptifolia* (red symbols) placed in the context of the decline in leaf hydraulic conductance reported in Fuenzalida et al. (2019) (blue symbols). Black points correspond to the mean leaf water potential and hydraulic conductance before and after FWU (Fuenzalida et al., 2019). Vertical coloured lines depict the water potential at which 50% of the inferred conductance has been lost. The black vertical dashed line indicates the average leaf water potential from the branches used for micro-CT imaging in this study. Shaded areas correspond to standard error. N = 7 for pneumatic measurements; N = 8 for K_{leaf} measurements.

Embolism

Micro-computed tomograms revealed emboli in the xylem of all dehydrated samples (Fig. 3.2). Vessel diameters determined via optical microscopy ranged from 3 to 30 µm, with the smallest vessels occuring in the stem-petiole junction and the biggest vessels occuring in stems. Thus, most vessels were within the resolution range of micro-CT imaging (4 µm voxels) (Fig. 3.2 E). After wetting, emboli refilled with water within 13-43 h (Fig. 3.3). The majority of emboli in the ROI occurred proximal to the cut end of the stem, and stem emboli decreased significantly in number ($F_{39.6}$ = 35.69, P < 0.001) and area ($F_{38.6}$ = 28.54, P < 0.001) towards the apical end of the ROI (Fig. 3.4 A, D). In contrast, the number of leaf emboli and the embolised area were not correlated with height along the ROI ($F_{44.5}$ = 2.65, P = 0.11; $F_{43.2}$ = 2.07, P = 0.16) (Fig. 3.4

B, E). There were fewer emboli ($t_{43.2}$ = 2.74, P = 0.02) and a smaller embolised area ($t_{42.8}$ = 3.05, P = 0.01) in the stem-petiole junction than in the leaf (Fig. 3.4 C, F).

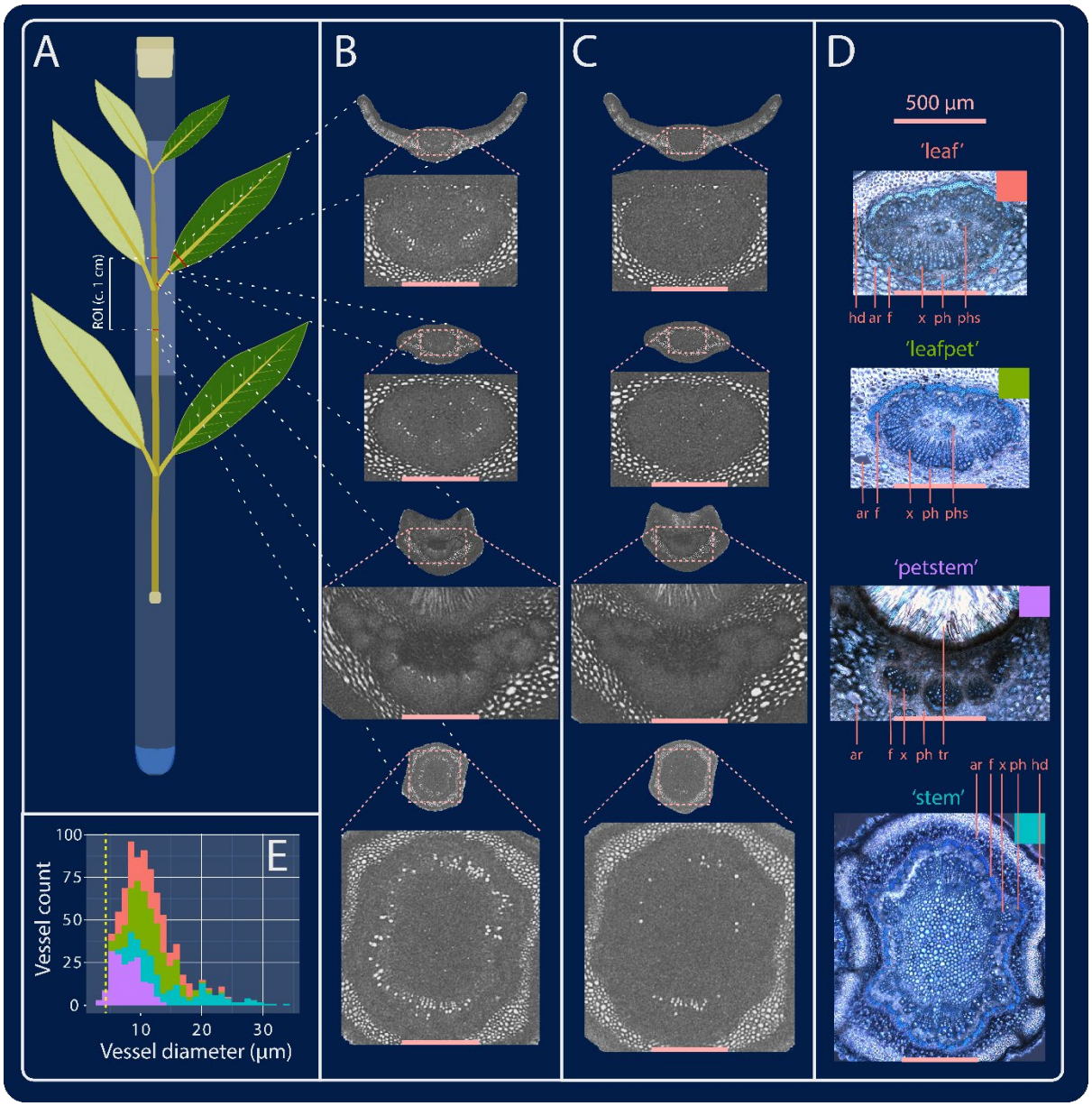

Figure 3.2. Exemplary diagram and images of the experimental setup and main results. A: An excised twig bearing three leaf pairs suspended inside a tube is shown (not to scale). The cut end of the twig was sealed with petrolleum jelly, the entire leafy part covered with a paper towel (depicted by the light shaded area of the tube) and the top of the tube sealed with a rubber bung; red lines show the approximate location of slices within of the region of interest (ROI), which was c. 4 cm long. (Leaves are illustrated protruding out of the tube, but actual samples were completely enclosed inside the glass container.) B: Color-inverted slices from micro-CT imaging under the dry condition for four representative sections of the tissues studied. Dark regions correspond to regions with high electron density (*i.e.*, high water

content); white areas correspond to regions filled with air. C: Same slices as in panel B after 18.8 h of wetting. Note the emboli inside the vascular bundle of all organs in the dry state, and the swelling of the tissues and decrease in embolism after wetting. D: Vascular bundles from a similar sample stained with toluidine blue; hd = hypodermis, ar = aerenchyma, f = fibres, x = xylem, ph = phloem, phs = phloem strand, tr = trichomes. E: Stacked histogram of vessel size distribution for each organ of the sample is shown in panel D (colour coded according to the box in the top right of optical images); the red dashed line corresponds to the resolution from micro-CT imaging (4 µm/voxel). All pink bars are 500 µm. N = 1.

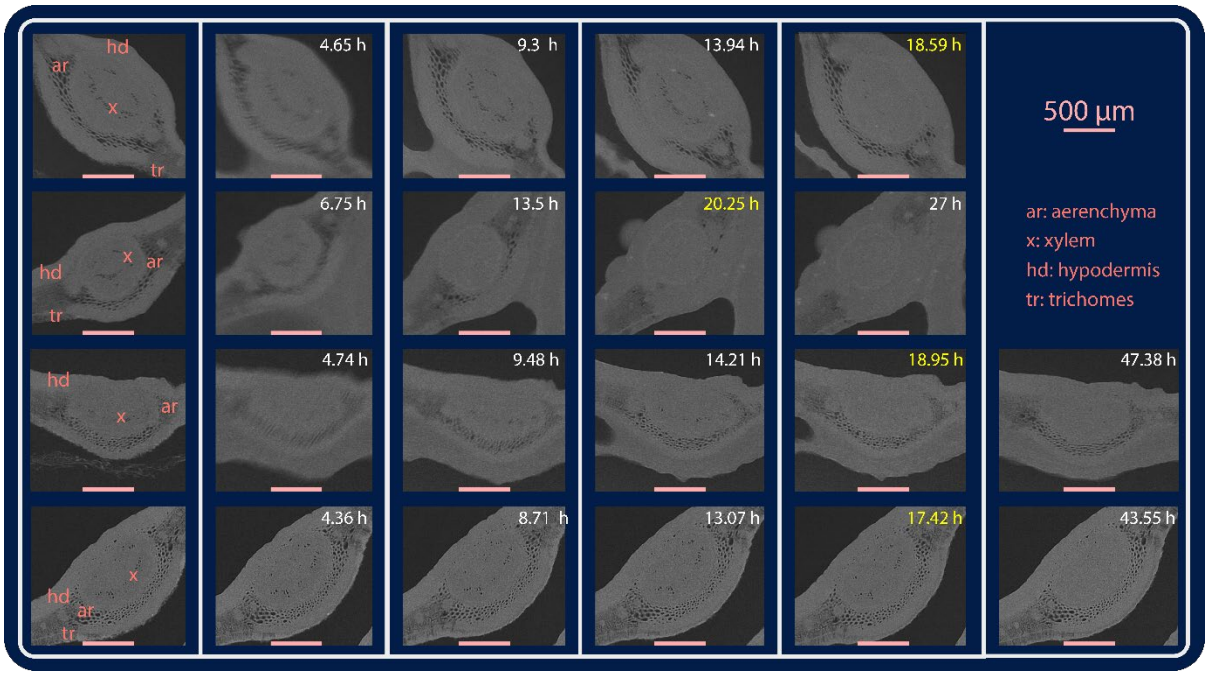

Figure 3.3. Time course of embolism recovery during rehydration via foliar water uptake. Rows show an exemplary leaf from each sample. Note the movement and swelling of leaf tissues followed by nearly complete emolism recovery in all samples within 48 h, as well as refilling of cisternae within the aerenchyma tissue (Nguyen et al., 2017b). Yellow text denotes times that were used for statistical analyses. All pink bars are 500 µm. N = 4.

After 18.8 h since wetting, we observed a mixed reduction in the number and area of emboli across the organs. In stems, wetting significantly reduced the number ($F_{35.94}$ = 5.11, P = 0.03), but not the area of embolised vessels ($F_{36.83}$ = 2.65, P = 0.11). There was no interaction between the position along the ROI and wetting in the number ($F_{35.94}$ = 1.94, P = 0.17) or the area of embolised vessels ($F_{36.93}$ = 1.08, P = 0.31).

Embolism in the leaf midrib also showed a mixed response after 18.8 h of wetting (Fig. 3.4 C, F). Wetting caused no significant decrease in the number ($F_{41.25}$ = 1.55, P = 0.22) but a significant decrease in the area ($F_{41.15}$ = 5.6, P = 0.02) of emboli in leaves. The effect of wetting

was consistent along the midrib, with no interaction between position and wetting on the number ($F_{41.25}$ = 0.11, P = 0.9) or area ($F_{41.15}$ = 0.36, P = 0.7) of embolised vessels. On average, the effects of wetting after 18.8 h resulted in the number of emboli in the midrib decreasing from 16.8 ± 6.68 to 12 ± 7.65; the corresponding embolised area decreased from 2,292 ± 995 μm^2 to 1,202 ± 788 μm^2 (mean ± SE). Partial refilling of cisternae was also observed in aerenchyma tissue (Fig. 3.3).

We observed a weakly significant change in emboli diameter in stems ($F_{34.05}$ = 3.78, P = 0.06) and leaves ($F_{34.46}$ = 3.8, P = 0.06) after 18.8 h since wetting (Fig. 3.5).

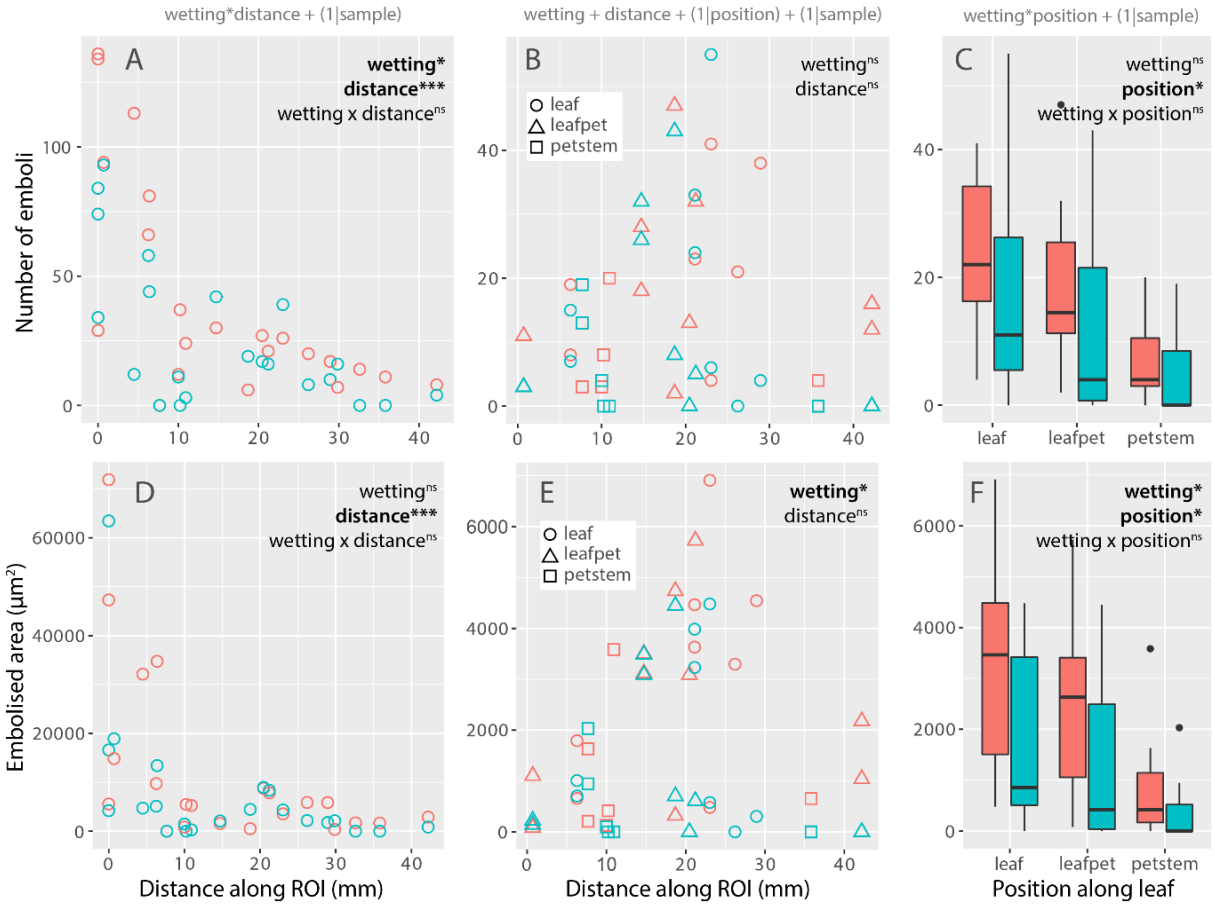

Figure 3.4. Embolism occurrence and recovery in response to wetting across and within organs. A: Number of stem emboli along the region of interest (ROI) before and after wetting. B: Number of leaf emboli along the ROI before and after wetting. C: Number of emboli from the leaf to the stem-end of the petiole before and after wetting. D: Stem embolised area along the ROI before and after wetting. E: Leaf embolised area along the ROI before and after wetting. F: Embolised area from the leaf to the stem-end of the petiole before and after wetting. See Fig. 3.1 for a representative image of the anatomical features distinguishing the position along the leaf. Red and blue symbols depict quantities before and after wetting, respectively.

Models written above each column correspond to the *lmer* syntax used for the statistical analyses. ***P < 0.001, ** P < 0.01, *P < 0.05, ^{+}P < 0.1, ^{ns}P > 0.1. N = 4.

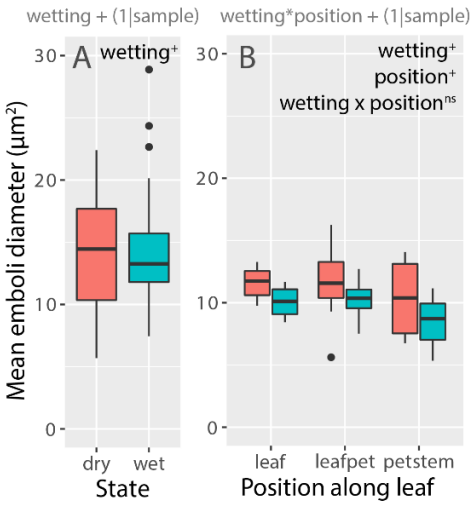

Figure 3.5. Effect of wetting on emboli diameter within organs. Emboli diameter in stems (A) and leaves (B) before and after wetting. Models written above each plot correspond to the *lmer* syntax used for the statistical analyses. ^{+}P < 0.1, ^{ns}P > 0.1. N = 4.

5. Discussion

How and whether plants living under constant xylem tension are able to recover from embolism is an unresolved debate. Our results showed that rehydration through foliar water uptake can lead to the refilling of xylem emboli in rehydrating stems and leaves of excised *Avicennia marina* twigs. Embolism refilling may be involved in hydraulic recovery driven by FWU (Fuenzalida et al., 2019).

Response of hydraulic conductivity to dehydration

Leaf and stem inferred hydraulic conductivity decreased with dehydration and presented a 3 MPa difference between the Ψ_{50} values (Fig. 3.1). While the methods used for estimating the inferred leaf and stem hydraulic conductance are not directly comparable, direct observation of emboli via micro-CT revealed an opposite trend, where embolism occurrence was higher in stems (Fig. 3.4). Two reasons may explain this pattern: (1) loss of leaf hydraulic conductance is likely dominated by changes in conductivity outside of the xylem tissue, and not by embolism (Scoffoni et al., 2017a); and (2) stem emboli may have been caused by cutting (Wheeler et al., 2013), not due to natural embolism. Indeed, we observed a decrease in the number and area of embolised vessels with increasing distance from the bottom of the ROI (Fig. 3.4 A, D). Thus, the levels of embolism observed in stems should not be regarded as representative of natural embolism. In contrast, embolism in leaves was not correlated with position along the

ROI (Fig. 3.4 B, E); therefore, we cannot attribute leaf emboli to open vessels. Instead, embolism in leaves was likely caused by dehydration.

Recovery in response to wetting

Wetting promoted embolism repair in all organs. However, the reduction in embolism was not always significant after 18.8 h of rehydration (Fig. 3.4). Nearly complete embolism repair was observed in leaves after 48 h (Fig. 3.3). These findings contribute to the understanding the mechanisms driving embolism recovery. It is unclear whether this refilling can occur under natural conditions.

The observed embolism recovery took several hours; however, the conditions required for micro-CT imagining are not representative of what plants experience in the field. Prolonged exposure to darkness and saturated atmospheres, absorption of X-ray radiation, tissue excision and handling may introduce substantial differences when compared to plants growing *in situ*. In particular, if water is absorbed by leaf tissues, the use of excised tissues may allow the expulsion of air emboli via the cut end of the samples (despite plugging with petroleum jelly), which is unlikely to occur in an intact tree. In spite of these limitations, most micro-CT studies working with excised tissues have found limited evidence of embolism repair, even after soaking. For example, Earles et al. (2016) reported a c. 4% reduction of embolism in excised *Sequoia sempervirens* stems soaked for 16 h; Tomasella et al. (2022) found no reduction in embolism after soaking stems of *Fraxinus ornus* and *Olea europaea* for 2-4 h. Similarly, Schreel et al. (2022) found no evidence of embolism recovery via FWU in *Fagus sylvatica*. Such results contrast with the extent of embolism recovery observed in excised twigs of *Avicennia marina*.

Foliar water uptake is a slow process relative to water uptake through the vasculature (Guzmán-Delgado et al., 2018, Fuenzalida et al., 2019), and this may pose a limit to the conditions under which embolism repair takes place. Images presented in this study were taken 18.8 h after wetting and at saturating humidity, yet we still observed samples that were swelling after 9 h of rehydration; embolism repair took more than 18 h in some samples (Fig. 3.3). The results contrast with those obtained in Fuenzalida et al. (2019), where FWU ceased or reached a negligible rate after c. 5 h of intermittent spraying. Conditions in the present experiment were different to those, as samples imaged via micro-CT were only sprayed once and, presumably, salts in the leaf surface were less diluted than in Fuenzalida et al. (2019). The reduced effect of dilution could have slowed the process. (We did not measure the leaf surface salinity in samples used for micro-CT, so differences in salt accumulation may have driven the differences.) In *Avicennia marina*, hollow trichomes with thick cell walls in the abaxial leaf surface absorb and fill with water readily after being wet (Nguyen et al., 2017b).

Presumably, water then has to move symplastically, as trichomes sit on top of a living basal cell (Fitzgerald et al., 1992, Nguyen et al., 2017b); a similar mechanism has been recently described in detail in *Tillandsia* (Raux et al., 2020). For a salt-secreting halophyte like *Avicennia marina*, symplastic water absorption via specialised structures (Tan et al., 2013) may be required to prevent uptake of salts previously secreted to the leaf surface and the associated metabolic cost. This idea implies that salt-secreting mangroves may respond differently to the variety of wetting events experienced in natural settings, such as rain or dew, according to the effects that such events have on the dilution of leaf surface water. Indeed, (Coopman et al., 2021) showed that reverse sap-flow rates in *Avicennia marina* increase with increasing relative humidity above the point of deliquescence, indicating that dilution of leaf surface water influences the rate of FWU. While these observations may be relevant to the interpretation of FWU in natural settings, they remain speculative regarding the rehydration of micro-CT samples, for which we did not determine the kinetics and specific pathways of water uptake. Aside from the anatomically natural pathways for uptake, it is possible that water absorption occurred through observed tissue injuries caused by arthropods or by handling of the samples. However, the timing of rehydration during micro-CT imaging contrasts with field observations (Coopman et al., 2021) and greenhouse experiments (Schreel et al., 2019) indicating that *Avicennia marina* equilibrates to water potentials equivalent to those of the substrate within 2-4 hours of exposure to atmospheric water. Thus, micro-CT conditions may introduce significant differences when compared to the process as observed in natural settings.

The mechanism by which xylem vessels refilled with water is unknown. Possible mechanisms include capillary refilling or active loading of solutes into embolised vessels. However, capillary refilling is unlikely to occur if the xylem water is under tension. The pressure developed across a water-air meniscus is described by the Young-Laplace equation. Assuming a contact angle of 0° (*i.e.*, a perfectly hydrophilic surface), the equation takes the form $P = -2\gamma/r$, where γ is the surface tension of water (0.072 N m^{-1}) and r is the radius of the meniscus. For a typical *Avicennia marina* vessel with r = 5 µm, the xylem pressure at which a bubble will tend to grow is P = −28.8 kPa, so capillary refilling would require nearly complete xylem relaxation. This idea is consistent with the observation that one of the samples exhibited noticeable refilling of aerenchyma cisternae (Fig. 3.3), which have been described to fill with water at water potentials > −100 kPa (Nguyen et al., 2017b). (Also based on the Young-Laplace equation, the critical pressure for the refilling of such voids scales with 1/r, and for a typical cisternae r = 25 µm, so P = −5.76 kPa.) However, capillary refilling may not explain differential refilling of embolised vessels (Fig. 3.3) and is not consistent with the weak observation that emboli diameter decreased with wetting (Fig. 3.5). The latter implies that

vessels with a larger-than-average diameter were preferentially refilled. A possible mechanism by which xylem vessels could be refilled is the active loading of solute into embolised vessels. While we do not have direct or consistent evidence supporting this phenomenon, we observed an increase in electron density within the petiole vascular bundle in two of the four samples (Fig. 3.S4). The observed increases in electron density were only observed several hours after wetting; it is possible that this effect was caused by active accumulation of inorganic ions within vessels, which may provide the concentration gradient required for refilling. However, these observations remain anecdotal, and further work is required to determine if loading of inorganic salts acts as a refilling mechanism in *Avicennia marina*.

We found no evidence of embolism spreading from stems to leaves (Fig. 3.4 B, E). This may be caused by the vascular constriction that occurs between the stem and the petiole (Fig. 3.2), as originally suggested by Zimmermann and Sperry (1983), although in this case the propagation of emboli was constrained in the opposite direction (from stems to leaves). Using the data from the sample shown in Fig. 3.2E, the anatomically estimated hydraulic conductivity (by the Hagen-Poiseuille equation) in the leaf-petiole junction is 3.7 times higher than at the stem-petiole junction. This vascular constriction may restrict embolism propagation between organs. As mentioned above, the levels of stem embolism observed in this study are unlikely to be representative of native embolism, and it is possible that stem embolism will not take place at these levels of dehydration in intact plants (see stem air discharge in Fig. 3.1). Thus, the vascular constriction at the stem-petiole junction may prevent embolism spreading from leaves into stems (Zimmermann and Sperry, 1983), and may allow plants to transiently decouple leaf from stem water potential due to a considerable flow resistance at the junction. However, this differential rehydration process would require the rate of FWU to be higher than the rate of leaf water export via the petiole. The latter seems unlikely, as the hydraulic resistance across the leaf surface has been conservatively estimated as > 12 times greater than that within the mesophyll over a wide range of hydration, casting doubt on the possibility of differential rehydration of leaves and stems. However, local xylem relaxation could be possible in discrete leaf regions which remain hydraulically isolated from the rest of the leaf. The possible role of nodal vascular constrictions in promoting xylem relaxation and embolism recovery via FWU warrants further study.

6. Conclusion

The results showed that FWU enabled embolism repair in detached twigs of the mangrove *Avicennia marina* ssp. *eucalyptifolia*. While we observed emboli in all organs, only leaf embolism depicted a natural phenomenon, as stem embolism was likely caused by open vessels. Propagation of emboli from stems into leaves was possibly restricted by a vascular

constriction at the stem-petiole junction. Results suggest preferential refilling of larger-than-average diameter embolised vessels, which may have been facilitated by solute loading. While foliar wetting reduced embolism, extrapolating these results to natural conditions requires further study on intact plants to account for differences introduced by the experimental conditions. Our findings support a role of atmospheric water sources in maintaining tree hydraulic function, suggesting that FWU may be necessary, rather than negligible (Schreel and Steppe, 2020).

7. Acknowledgments

We thank Nigel Brothers and Catherine Bone for outstanding field support in the Daintree River and to Levi Beeching for technical support during the experiment. TIF was funded by the Becas Chile PhD scholarship granted by ANID, scholarship 72180256. The Australian Research Council funded this research via grant DP180102969, awarded to MCB.

CHAPTER 4: MEASUREMENT OF PLANT WATER STATUS VIA STATIC UNIAXIAL COMPRESSION OF THE LEAF LAMINA

1. Abstract

Turgor pressure is an essential, but difficult to measure indicator of plant water status. Turgor has been quantified by localised compression of cells or tissues, but a simple method to perform these measurements is lacking. We hypothesized that changes in leaf turgidity can be monitored by uniaxially compressing the leaf lamina and measuring the mechanical stress under a constrained thickness (stress relaxation), and that changes in leaf water content can be monitored by measuring the leaf thickness under a constant mechanical stress. Using a simple, custom-built leaf squeeze-flow rheometer, we performed different compression tests on leaves from thirteen plant species. The mechanical stress measured during stress relaxation was correlated with leaf bulk turgor pressure ($R^2 > 0.95$) and thus with balancing pressure ($R^2 > 0.94$); the leaf thickness measured under constant mechanical stress was correlated with relative water content ($R^2 > 0.74$). The coefficients of these relationships were related to the leaf bulk osmotic pressure at the turgor-loss point. An idealised average-cell model suggests that, under isothermal conditions, the bulk stationary bulk modulus during compression is largely determined by the bulk osmotic pressure. Our study presents an inexpensive, accessible and automatable method to monitor plant water status non-invasively.

Symbols and abbreviations

CS: constant stress; SR: stress relaxation; pSR: passive stress relaxation; cSR controlled stress relaxation; $-\sigma$: applied compressive stress, h_c: compressed leaf thickness, BP: balancing pressure; Ψ: water potential; Π: osmotic pressure; P: turgor pressure; E: bulk elastic modulus; RWC: relative water content; V: cell water volume; v: cell volumetric strain; TLP: turgor-loss point; Φ: leaf water volume relative to TLP.

2. Introduction

Plants suffer environmental changes over daily and seasonal scales, which cause large variations in the rates of photosynthesis (Munné-Bosch et al., 1999, Chaves et al., 2002) and growth (Zweifel et al., 2021). Such variations are often mediated by changes in the hydrostatic pressure of cells, called turgor pressure (Lockhart, 1965, Rodriguez-Dominguez et al., 2016). Turgor gives some structure and rigidity to soft plant tissues, such as leaves, flowers and growing stems and roots, and causes the swelling and shrinking movements that occur with changing water content (Skotheim and Mahadevan, 2005). In this sense, turgor is fundamental for organisms that do not control the osmolality of the extracellular environment, providing a buffer against sudden changes in water availability that would otherwise lyse the cell membrane (Wolfe et al., 1986). Aside from its structural role, turgor supports growth by driving plastic expansion of the cell wall (Lockhart, 1965), affects organ development through complex mechanical feedback loops (Green, 1962, Dumais et al., 2006, Hamant et al., 2008), and

causes stomata to open (Franks et al., 1998) regulating gas exchange between leaves and the atmosphere. Turgor is thus essential to plant life, and is also a valuable indicator of plant water status. However, turgor measurements are not routine.

Three main approaches to measure turgor pressure exist. First, turgor can be measured directly, by probing and measuring the hydrostatic pressure inside a single cell (Green and Stanton, 1967, Hüsken et al., 1978). This technique also enables quantification of the volumetric elastic moduli and the membrane hydraulic conductivity; however, the method is relatively complex and requires careful manipulation, making it largely impractical in field settings. In a second approach, *bulk* turgor (*i.e.*, that of an 'average' cell within a tissue) can be inferred from the relation between water content and water potential (Ψ) (Tyree and Hammel, 1972). When leaves are wilted (*i.e.*, turgor is nearly zero), and if the solute concentration in the xylem is small, the balancing pressure (BP ~ –Ψ) required to push water out of a cut leaf increases in proportion to the intracellular concentration of solute (Scholander et al., 1965). By measuring the BP and water volume during slow dehydration, an estimate of the bulk osmotic pressure[1] (Π) at all levels of hydration can be obtained, whereby the bulk turgor pressure can be derived as P = Π − BP. This widely used technique is simple and accurate, but cannot be performed on tissue attached to the plant, is time-consuming and laborious, and cannot be easily automated.

A third approach to measure turgor pressure is via localised compression of cells or tissues. Various techniques can be employed for this purpose; they have been reviewed by Geitmann (2006), Beauzamy et al. (2014) and Bidhendi and Geitmann (2019). The main principle behind these measurements is that the mechanical properties can be derived and used to infer water status by measuring the force and the deformation applied. While simple in principle, these techniques are commonly applied at the nm-µm scale and require costly instrumentation such as micro-indenters or atomic-force microscopes. Additionally, they often need to employ optical microscopy to determine the contact area between the sample and the indenter, which is necessary to obtain the stress. Similar principles can be applied to tissues at a larger (µm-mm) scale (Ferrier and Dainty, 1977), where the cost of instrumentation can be reduced significantly. Such measurements could be useful for plant ecophysiologists and agronomists, who will mostly be interested in bulk properties. Thus, the goal of this study is to test if these principles can be scaled up to produce a practical and affordable method to monitor plant water status.

[1] The pressure required to stop water diffusion through a semipermeable membrane separating a solution from pure water, equal to minus one times the osmotic potential. We use osmotic pressure throughout.

Leaf squeeze-flow rheometry

There are various names given to techniques that compress samples between parallel plates, such as ‘simple unconfined compression’, ‘uniaxial compression’ and ‘squeeze-flow’ (Engmann et al., 2005). The disciplines that coined these terms fall broadly within the fields of material science and rheology. Rheology is the science that studies the flow of matter under load, with particular emphasis on viscoelastic and plastic materials, which exhibit time-dependent deformation. At the tissue scale, the rheology of fruits and vegetables has been linked to turgor pressure (Lin and Pitt, 1986, De Belie et al., 2000, Jackman et al., 1992), and the uniaxial compression of single and multilayered tissues has been employed to estimate the elastic and hydraulic properties of cells (Ferrier and Dainty, 1977, Ferrier and Dainty, 1978). In the method devised by Ferrier and Dainty (1977), a layer of cells is compressed with a constant mechanical stress (called a creep experiment in rheology), and the change in thickness is monitored over time. By assuming that water permeation across the membrane is the rate-determinant process of the change in thickness, this method can be used to estimate the membrane hydraulic conductivity. However, the method has received little attention, and has not, to our knowledge, been used for continuous monitoring of leaf water status. Thus, we aimed to expand the application of the method by Ferrier and Dainty (1977) to monitor leaf water status, and to standardise the experimental procedures using basic concepts from material science.

Two standard experimental paradigms in rheology are creep and stress relaxation. In a creep (or, from herein, ‘constant stress’) experiment, a sample is loaded with a constant stress (the force per unit area), and the resulting deformation is monitored over time. In a stress relaxation experiment, the sample is constrained to a given deformation, and the change in stress is monitored over time. We hypothesized that constant stress (CS) and stress relaxation (SR) could be used as measurement paradigms to monitor leaf water content and leaf bulk turgor pressure, respectively. The concepts here are somewhat different from standard rheology, because the mass of the leaf tissue studied is usually not conserved. Our working premises were simple: to monitor changes in bulk turgor pressure, the normal stress applied to the compressed leaf may be measured under a constrained leaf thickness; to monitor leaf water content, the thickness of the leaf may be measured under a constant load. An illustration of our working hypotheses is shown in Fig. 4.1 for two different measurements during a change in leaf hydration. In this paper, the imposed mechanical stress is always compressive. By convention, tensile stresses are positive, so the applied compressive stress $-\sigma$ (not to be confused with the osmotic reflection coefficient) is used throughout.

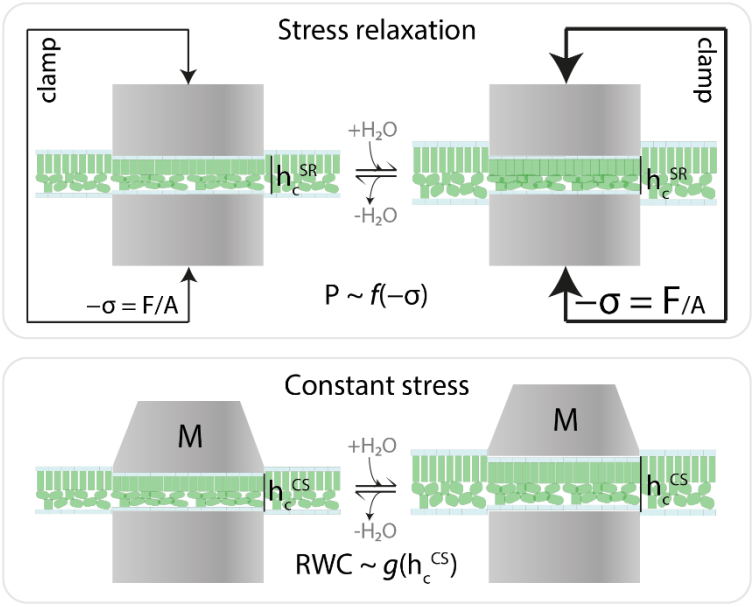

Figure 4.1. Illustration of our working hypotheses. In a stress relaxation experiment (top row), the leaf is compressed with a clamp to a constrained leaf thickness (h_c^{SR}); as the leaf changes water status (depicted by the rehydration/dehydration arrows), we hypothesise that leaf bulk turgor pressure (P) can be approximated as a function *f* of the applied compressive stress (−σ = F/A). (The size of the arrows represents the magnitude of the clamping force under changing water status, which under constrained thickness changes due to the reaction force that the leaf exerts on the clamp.) In a constant stress experiment (bottom row), the leaf is compressed between two parallel plates under constant force, here represented by a weight of mass M; as the leaf changes water status, we hypothesise that leaf relative water content (RWC) can be approximated as a function *g* of the compressed leaf thickness h_c^{CS}.

3. Methods

Leaf squeeze-flow rheometer

Experiments were conducted using an affordable (~US$300) custom-made leaf squeeze-flow rheometer (Fig. 4.2). Variations on the instrument design occurred during this study; in this section we describe the version shown in Fig. 4.2 (differences are mentioned where appropriate). A load cell (FX29, TE Connectivity, Switzerland) was mounted between two microscope slides held together by two rubber bands and placed between the anvil and spindle of a 500 µm pitch analog micrometer (103-129, Mitutoyo, Japan). Leaf samples were loaded between the stationary micrometer anvil (diameter = 6.4 mm), which delimits the compression area of the sample, and the upper microscope slide to minimise shear stress caused by the spindle rotation. A microcontroller (Arduino MEGA 2560, Keyestudio, China) performed force readings from the load cell and operated a two-phase 400 steps/revolution NEMA17 stepper motor using a stepper motor driver (TB6600, China). The motor was coupled

to the micrometer knob using a rigid shaft and mounted on a sliding linear guide to allow motor translation. The motor was operated at a microstep setting of 1/32 of a step, giving a theoretical minimum translation step of *c*. 39 nm. Translation of the spindle was calculated by counting number of steps taken by the motor. A digital temperature sensor (BME280, Core Electronics, Australia) was directly attached to the micrometer handle and insulated using a closed-cell polyurethane foam to monitor the temperature of the frame. An infrared digital temperature sensor (SEN0206, DF Robot, China) was mounted next to the micrometer anvil to track the temperature of the adaxial leaf surface (Fig. 4.2).

The instrument was programmed to perform constant stress (CS) and stress relaxation (SR) experiments. For CS experiments, the motor was instructed to move in response to the pressure reading difference from the set point (*i.e.*, negative feedback) to maintain constant applied force. The motor step size was varied according to the predicted mechanical compliance of the empty system (Fig. 4.2E) as a function of the instantaneous error between the set point and the pressure reading. This control system can be described as a form of proportional 'bang-bang' control.

The instrument has a certain level of mechanical compliance (*c*. 1.3 μm N^{-1}, Fig. 4.2E), which implies that, when performing an SR experiment, the instrument dimensions change as a function of load. To correct this deflection, the motor was instructed to move in proportion to the estimated deflection of the instrument, or not to move at all; we distinguish these tests as *controlled* stress relaxation (cSR), and *passive* stress relaxation (pSR), respectively. Controlled stress relaxation is a common procedure in mechanical testing systems, enabling the sample thickness to remain close to constant (ASTM E328-13). Briefly, cSR was achieved by calculating the predicted mechanical compliance (Fig. 4.2E) as a function of the change in pressure between consecutive readings during SR, and by correcting this deflection by taking discrete steps. As positioning corrections were always a multiple of the minimum step size (*c*. 39 nm), corrections introduced an error given by the remainder between the step size and the estimated system deflection. This positioning error was added over time and corrected in the next control cycle, providing effective control over the sample thickness.

Controlled stress relaxation is desirable to obtain reproducible measurements independent of the instrument's mechanical compliance, although it can be difficult to achieve and may introduce noise to the data. The present instrument can only perform cSR tests when the direction of stress relaxation does not change. Changing direction involves taking 'dead steps' due to the instrument backlash, and this issue is not corrected for in the present version of the instrument; in most cases, positioning corrections are much smaller than the instrument backlash, so cSR is difficult to achieve. Comparatively, pSR has practical advantages as it is

easier to implement (it can be applied without a motor), allows increased precision and sensitivity, and is independent of mechanical backlash. As we discuss in the Supplementary discussion, each of these tests has a distinct heuristic value.

Plant material

Experiments were conducted using a diverse set of species grown ornamentally within the ANU Campus in Canberra, Australia. Experiments were performed at the end of winter and during early spring of 2021; thus, we focused this study on evergreen species. A total of twelve angiosperms and one conifer from ten different families were chosen (Table S1). As our goal was to test the applicability of uniaxial compression for the measurement of plant water status, replication within a single species was kept at a minimum to test the technique in as many species as possible. For experiments in which we used excised tissue, branches were collected between 08:00 and 10:00 h using secateurs, placed in a black plastic bag and brought to the lab within five minutes. In the lab, the branches were recut under water and allowed to rehydrate for *c*. 15 min before the preparation of each experiment. From the mechanical stress readings obtained via passive SR, we verified that plants had achieved a steady hydration state at the start of each experiment. This water potential was slightly negative, with a mean ± SE value of −0.3 ± 0.06 MPa across 15 branches. All experiments were conducted under laboratory conditions (T ~ 22 °C, RH ~ 50%).

Exemplary constant stress and stress relaxation experiments

To illustrate the ability of the instrument to perform the intended techniques and assess the equilibration kinetics of leaf squeeze-flow rheometry, we performed CS and SR tests on the lamina (avoiding the midvein and, when possible, secondary veins) of attached leaves in two species, *Salvia officinalis* and *Populus nigra*. In preliminary experiments, we determined that many leaves could be compressed with stresses up to 800 kPa without visual signs of damage. Leaves from branches collected and treated as described above were pre-compressed under a constant stress of 100 kPa for 5 min to ensure good contact between the leaf surfaces and the compression plates[2]. After equilibration at 100 kPa, leaves were subject to: (i) a CS routine at 500 kPa for 5 min followed by recovery at 100 kPa; (ii) a cSR routine after a 25 µm step followed by recovery after a -25 µm step; and (iii) a pSR routine after a 25 µm step followed by recovery after a -25 µm step. The step size for SR was chosen as it represented a relatively small uniaxial strain (*e.g.*, a 5% decrease in thickness for a 500 µm thick leaf); the stress value for CS was chosen as it represented an intermediate value

[2] In preliminary experiments, we determined this pressure was enough to flatten the leaf lamina without causing visible damage to the tissue. In our system, this pressure is equivalent to a measuring force of 3.2 N; in comparison, the measuring force provided by the ratchet stop of the micrometer is 5-10 N.

between the pre-compressive stress and the preliminary upper value of 800 kPa. In all tests, the compression rate during each step was 195 μm s^{-1} and the control loop was operated at 5 Hz.

Dead leaf tests

The hypothesis that the imposed stress is related to bulk leaf turgor pressure assumes that a significant component of the load is borne by an increased turgor pressure in cells within the compressed region. To verify the role of living tissue in supporting the load, we subjected leaves (N = 3) from a sclerophyllous species (*Quillaja saponaria*) to a cSR procedure before and after killing the leaf. The choice to perform the test in a sclerophyllous species was made to assess the case where significant resistance to deformation may be offered by the leaf structure in the absence of turgor. Leaves were pre-compressed under CS at 100 kPa and then compressed with a 25 μm step at a rate of 195 μm s^{-1}, followed by relaxation and recovery in periods of 2 min. After recovery, leaves were submerged under water at 80 °C for 30 s; the temperature used for this treatment was chosen according to Yang et al. (2017). Immediately after the 30 s elapsed, leaves were blotted dry and the same routine was repeated. Data from the cSR experiment were analysed according to Peleg (1979) to quantify the 'liquidity' of the sample and the stress relaxation time constant before and after heating. We use the term 'liquidity' to quantify the relative stress attained at equilibrium, where a minimum value of 0 means no relaxation (*i.e.*, an ideal elastic solid) and a maximum value of 1 means full relaxation (*i.e.*, an ideal liquid) (Peleg, 1979).

Simultaneous constant stress and passive stress relaxation experiments

Our main hypotheses were that CS can be used to monitor leaf water content, and that SR can be used to quantify changes in leaf bulk turgor pressure. Preliminary experiments indicated that pSR was a strong predictor of changes in leaf water potential. Thus, capitalising on the simplicity of this method, we first approached the hypotheses by performing simultaneous CS and pSR experiments.

To perform CS tests, a leaf from a branch rehydrated as described in the *Plant Material* section was compressed in an instrument similar to the one shown in Fig. 4.2, with the difference that the motor had a planetary gearbox (1:139) and a different load cell (FS2050-1500, TE Connectivity, Switzerland). The gearbox provided increased torque and precision in unidirectional movement, although it increased backlash, reducing the effective resolution of the system due to 'dead steps' taken when the motor changed direction. Backlash in this system was *c*. 4 μm. CS tests were conducted at a pressure of 400 kPa using a microcontroller (Arduino UNO R3, Keyestudio, China) operated with the control loop at 2 Hz. For the pSR test, a different leaf from the same branch was compressed using a digital micrometer

(SHAHE, China) and the force was measured using an amplified load cell (FX29, TE Connectivity, Switzerland) and a 16-bit analog-to-digital converter (ADS1115, Tenstar Robot, China) connected to the microcontroller. Data were logged into a Secure Digital card. Samples used for pSR experiments were compressed manually to a pressure of *c*. 800 kPa and left to equilibrate for *c*. 10 min, after which the branch was cut in air to start dehydrating. Branches were dehydrated until the pressure during pSR reached *c*. 200 kPa, when the branches were recut under water and allowed to rehydrate until they approached equilibrium.

During the experiment we monitored the balancing pressure and the leaf relative water content in three leaves per time point per branch. Excised leaves were placed inside a plastic bag we had previously breathed in and measured within 5 min. The balancing pressure (BP) was measured using a pressure chamber (1505D, PMS Instruments, USA). The leaf relative water content was measured by weighing three leaves and by rehydrating them for 24 h inside a 50 mL plastic tube with the tip of the petiole submerged under water. After, rehydration, leaves were blotted dry with a paper towel, weighed again, and oven-dried at 80 °C to obtain the dry weight. Relative water content was calculated according to Weatherley (1950), as

$$RWC = \frac{fresh\ mass - dry\ mass}{saturated\ mass - dry\ mass} \times 100\% \qquad Eqn.1$$

To test the hypothesis that RWC can be approximated as a function of the leaf thickness, we normalised the dimensional compressed leaf thickness during CS (h_c^{CS}) relative to its estimated maximum. The maximum h_c^{CS} was determined as the y-intercept of the regression between h_c^{CS} and BP considering data where this relation was linear (*i.e.*, near 'full hydration'). The relative compressed leaf thickness during CS (H_c^{CS}) was obtained as

$$H_c^{CS} = \frac{h_c^{CS}}{h_c^{CS}(BP = 0)} \times 100\% \qquad Eqn.2$$

Pressure-volume curves

Leaves from each branch used for the CS and pSR experiment were used to build pressure-volume curves. Before cutting the branch in air to start dehydration, three leaves were excised and placed inside a plastic bag we had previously breathed in. Leaves were then subject to alternate measurements of balancing pressure and fresh mass until the leaves looked wilted. Leaves were oven-dried for 48 h at 80 °C to obtain the dry weight.

Leaf pressure-volume curves were analysed by plotting the inverse of the balancing pressure (1/BP) against the leaf fresh mass (Tyree and Hammel, 1972). The linear portion of the data was determined by fitting the three data points with lowest fresh mass with a linear regression, and by adding points with increasing fresh mass until the R^2 value was close to

maximal and adding extra data points resulted in consistently positive residuals (*i.e.*, until the curve started trending upwards). The TLP was determined as the highest measured fresh mass within the fitted data. The leaf water volume was normalised relative to the volume at the turgor-loss point as

$$\Phi = \frac{fresh\ mass - dry\ mass}{fresh\ mass_{TLP} - dry\ mass} \qquad Eqn.3$$

Following determination of Φ, 1/BP was plotted against Φ and the osmotic pressure at the turgor-loss point (Π_{TLP}) was obtained as the inverse of the regression function evaluated at Φ = 1. The leaf apoplastic water fraction (af) was obtained as the x-intercept between Φ and 1/BP. Using the linear regressions obtained via this method, an estimate of the osmotic pressure Π at all levels of hydration was obtained, whereby the bulk leaf turgor pressure was derived as P = Π – BP. The leaf bulk elastic modulus (E) was obtained by linear regression, in the positive turgor range, as E = ΔP/ΔΦ.

Data from leaf pressure-volume curves were used to test the hypothesis that P can be estimated from stress relaxation. To do this, a linear regression equation was used to obtain P as a function of BP; these regressions (all with $R^2 > 0.99$) were then used to estimate the bulk turgor pressure from the BP measured in the samples used for pSR.

In vivo measurements

Avicennia marina subsp. *australasica* plants were grown from propagules collected in November 2019 along the Clyde River estuary, NSW, Australia. Propagules were germinated in sand saturated with a 50% seawater solution. After depletion of cotyledonary reserves, plants were transplanted into 10 L plastic buckets with a 50% seawater solution and fertilised occasionally with a liquid seaweed fertiliser (Seasol, Seasol International, Australia). At the time of the experiment, each bucket contained six plants bearing *c*. 10 mature leaf pairs. Water was not added during the experiment. A full-spectrum LED light source (TS1000, Mars Hydro, China) installed *c*. 50 cm above the canopy provided a 14/10 h light/darkness cycle. CS and pSR tests were conducted as described for the simultaneous CS and pSR experiments using the instrument shown in Fig. 4.2, with the difference that CS tests were conducted at 100 kPa.

Data analyses

Data were curated in MS Excel and analysed in R version 4.0.5. All data presented are calculated from raw measured values, except for those measured in *Avicennia marina*, which were filtered using a third-degree polynomial moving average with a 1-min window (Savitzky and Golay, 1964) using the 'sgolayfilt' function of the 'signal' package. Regressions were performed using the built-in 'lm' function and the 'nlme' package and assessed via visual

inspection of residual distributions. Figures were built using the ‘ggplot’ package and stylised in Adobe Illustrator (Adobe Systems, USA).

4. Results

Instrument performance

The custom-built leaf squeeze-flow rheometer performed well in calibration tests. We found good agreement between the stepper motor instruction and the micrometer reading (Fig. 4.2C). The observed error (RMSE = 1.1 µm) was associated with the system backlash, which was *c*. 2 µm (Fig. 4.S1). When conducting CS tests on an empty sample (Fig. 4.2A, D), the system operated as instructed (Fig. 2B), although stress overshoot and undershoot were observed immediately after changing the input stress in each step (Fig. 2A). The system deflection under load was predicted well by a third-order polynomial function, displaying no hysteresis (Fig. 2E), which allowed accurate estimation of the system dimensions for any given stress. The instrument was found to be temperature-sensitive (Fig. 2F). A thermal cycle between 5 °C and 40 °C indicated that the system deflection increased approximately logarithmically with temperature, being most sensitive (*c*. 30 nm K^{-1}) at low temperatures.

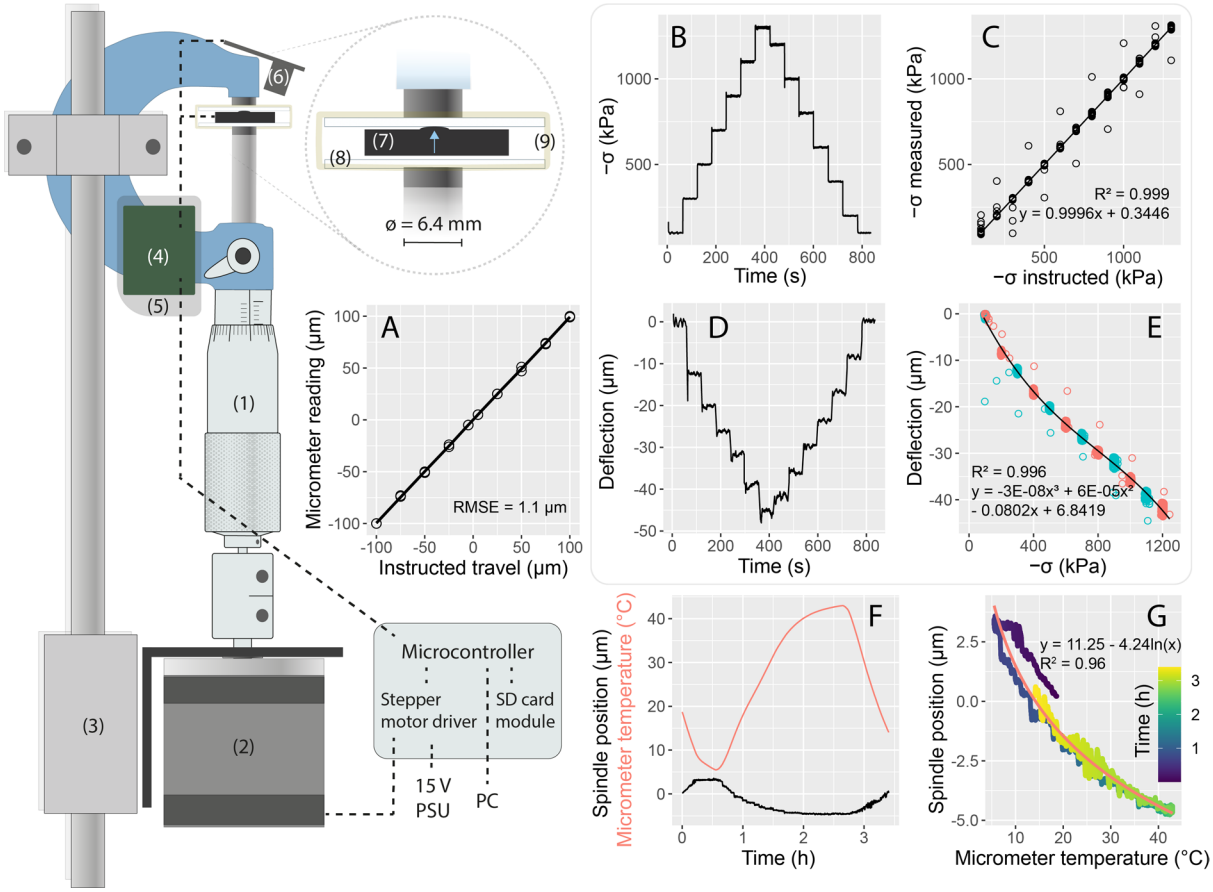

Figure 4.2. Component diagram and calibration of the leaf squeeze-flow rheometer. Components: (1) analog micrometer; (2) NEMA17 stepper motor; (3) linear guide; (4) micrometer temperature sensor; (5) foam insulation pad; (6) infrared leaf and ambient temperature sensor; (7) button compression load cell; (8) microscope glass slide; (9) rubber band. Leaf samples were compressed between the upper microscope slide and the micrometer anvil. Force, displacement and temperature data were logged to a SD card. Dashed lines denote simplified connections between components. A: Relation between the instructed distance to travel and the micrometer reading. B: Compressive stress applied (−σ = F/A) during a stairs CS test on an empty system (compressing the upper microscope slide against the micrometer anvil) with 200 kPa steps. C: Relation between the stress instructed and the stress measured by the load cell during the stairs CS test shown in B. D: System deflection during the CS test depicted in B. E: System deflection under load during the CS test shown in B; red and blue symbols denote measurements during increasing and decreasing load. F: Curves illustrating temperature sensitivity of the empty instrument during a thermal cycle while performing a CS test at 100 kPa: red is the temperature imposed and black the displacement recorded simultaneously. G: Relation between the micrometer temperature and the spindle position during the thermal cycle shown in F.

Exemplary curves and dead leaf compression test

Leaves from two species (*Populus nigra* and *Salvia officinalis*) pre-compressed under a stress of 100 kPa provided example time-dependent responses to leaf uniaxial compression. The stress relaxation half times (Peleg, 1979) were c. 6 s for *Populus* and c. 10 s for *Salvia*. (Fig. 3C-F). In CS tests (Fig. 3A, B), *Salvia* leaves compressed to a lower relative thickness than *Populus* leaves; similarly, cSR (Fig. 3C, D) and pSR (Fig. 3E, F) showed that the equilibrium stress reached after a 25 µm compression step was higher in the case of *Populus*. *Salvia* leaves were visibly damaged after the CS test; other tests resulted in no visible damage to the compressed tissues. The technique consistently revealed mechanical differences between the species. While pSR and cSR yielded similar results, cSR produced noisier data in the case of poplar (Fig. 3C, E). In the cSR procedure, the sample thickness was constant to about ± 0.5 µm.

Compressing leaves from the sclerophyllous species *Quillaja saponaria* revealed changes in the leaf stress relaxation kinetics following heat damage (Fig. 3I). After submerging tissues under 80 °C water for 30 s, the 'liquidity' of the samples increased from 0.199 ± 0.026 to 0.711 ± 0.041 (mean ± SE) (t = -10.54; P = 0.0005) (Fig. 3J); the time half-time of stress relaxation decreased from 6.32 ± 0.84 s to 2.41 ± 0.66 s (t = 3.65; P = 0.022) (Fig. 3K).

Constant stress and stress relaxation as guiding principles to monitor leaf water status

The leaf thickness under CS (h_c^{CS}) and the compressive stress applied during passive stress relaxation ($-\sigma^{pSR}$) were measured during a dehydration-rehydration cycle. Cutting in air induced a decline in h_c^{CS} and $-\sigma^{pSR}$, which was largely reversed by cutting the stems under water. Stress relaxation curves during dehydration were varied in shape and can be described as S-shaped or J-shaped. The time required for a 50% decrease in $-\sigma^{pSR}$ since the time of cutting in air varied widely between species, with a mean ± SE of 2.1 ± 0.7 h. In all species, the recovered $-\sigma^{pSR}$ was lower than the initial $-\sigma^{pSR}$; a similar pattern was observed for h_c^{CS}, with the exception of *Corymbia citriodora* (Fig. 4 B6). Variations to typical rehydration kinetics curves were observed, *e.g.*, in a *Callistemon viminalis* branch which exhibited an unusual rehydration pattern (Fig. 5A). The relation between h_c^{CS} and $-\sigma^{pSR}$ was non-linear; in most cases, the slope of $-h_c^{CS}/\sigma^{pSR}$ increased during dehydration and also during rehydration. The latter steepening of the curves resulted in hysteresis loops which displayed wide variation in terms of area and recovery.

Passive stress relaxation provided a good estimator of balancing pressure (BP) and the relation was, in most cases, approximately linear (Figs. 4 & 5, Fig. S2). The mean ± SD R^2 value for the linear regressions between $-\sigma^{pSR}$ and BP was 0.98 ± 0.01 (N = 15 branches from 9 species); the mean ± SD RMSE was 0.123 ± 0.06 MPa. The leaf relative thickness

measured during CS (H_c^{CS}) was positively related to the leaf relative water content (RWC). The mean ± SD R^2 value for the linear regressions between H_c^{CS} and RWC was 0.87 ± 0.08 (N = 5 branches from 5 species). In some species, however, the relation between H_c^{CS} and RWC was clearly non-linear (e.g., in *Fraxinus griffithii*, Fig. 4 D2). Overall, the technique was less accurate in estimating RWC than BP.

Relation to leaf pressure-volume parameters

The parameters extracted from the relation between the applied stress ($-\sigma^{pSR}$) and BP during passive stress relaxation (Figs. 4 & 5) and those obtained between leaf relative thickness (H_c^{CS}) and RWC (Fig. 4) were related to leaf pressure-volume parameters. In the case of the regression parameters between $-\sigma^{pSR}$ and BP, the intercept and slope were correlated with the bulk osmotic pressure at the turgor-loss point (Fig. 6A, B) and the leaf bulk elastic modulus (Fig. 6C, D); no significant relation was found between these parameters and the leaf apoplastic fraction (Fig. 6E, F). In the case of the regression parameters between H_c^{CS} and RWC, the intercept and slope were related to the bulk osmotic pressure at the turgor-loss point (Fig. 6G, H). No significant relation between the intercept and slope between H_c^{CS} and RWC and the leaf bulk elastic modulus or the leaf apoplastic water fraction was found (Fig. 6 I-L). We note that the results for the relationships between H_c^{CS} and RWC may be weaker due to a smaller sample size.

Balancing pressure measurements shown in Figs. 4 and 5 were used to estimate the leaf bulk turgor pressure (P) during dehydration using data from leaf pressure-volume curves. As expected from the shown relation between BP and $-\sigma^{pSR}$, linear regression showed that $-\sigma^{pSR}$ was strongly correlated with leaf bulk turgor pressure (Fig. 7), with an $R^2 > 0.95$ across 15 branches from 9 different species.

In vivo measurements

Measurements performed on a living potted mangrove (*Avicennia marina* subsp. *australasica*) revealed that the technique was capable of measuring small changes in water status induced by light (Fig. 8). Thickness and pressure decreased during the day and increased during the night. Immediately after light exposure, the plant exhibited sudden increases in pressure followed by a sharp decline. Over the four days, we observed a *c*. 7 µm decrease in leaf thickness and a *c*. 20 kPa decrease in the applied stress. Diurnal variations in h_c^{CS} were in the order of < 5 µm; daily variations in $-\sigma^{pSR}$ were < 35 kPa. These changes were not well resolved by raw measurements, but implementation of a Savitzky-Golay filter with a 1-min window produced data with acceptable resolution. Dimensional changes due to variations in the micrometer temperature were negligible in this experiment (*c*. 75 nm expansion/contraction during light and dark periods, according to the relation shown in Fig. 2G).

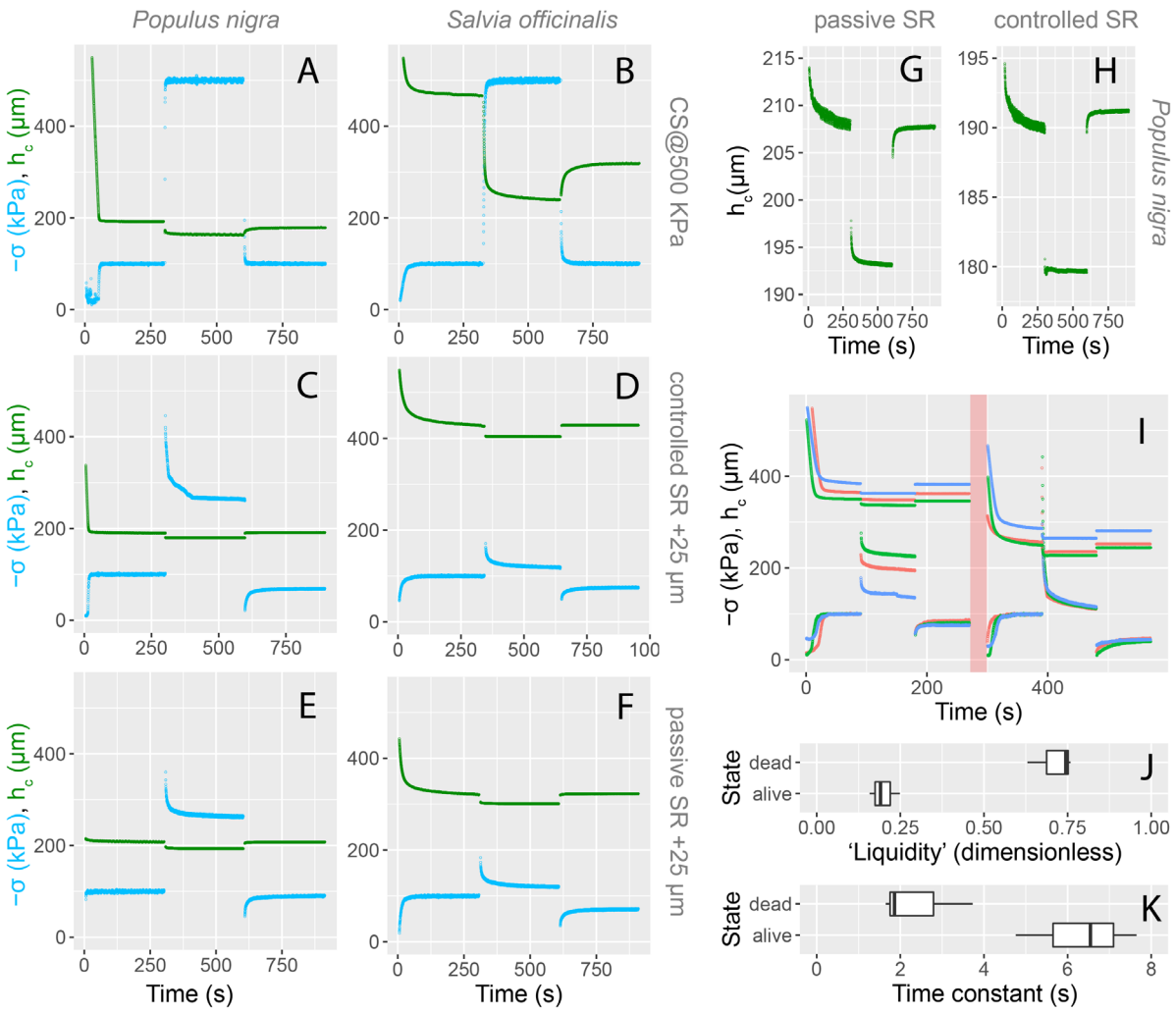

Figure 4.3. A-F: Examples of constant stress (CS) and stress relaxation (SR) tests. Leaves were pre-compressed under a stress of 100 kPa to ensure good contact between the leaf surfaces and the compression plates. Leaves were then subject to: constant stress at 500 kPa (A, B); controlled stress relaxation (*i.e.*, with the spindle position adjusted to maintain constant sample thickness) following a ± 25 µm step at 195 µm s^{-1} (C, D); and passive stress relaxation (*i.e.*, with the spindle position fixed) following a ± 25 µm step at 195 µm s^{-1} (E, F). Green curves correspond to the sample thickness; blue curves correspond to the applied compressive stress. These tests were performed on living leaves attached to a branch with the cut end maintained under water, so the water status of the (uncompressed) tissue is assumed constant. N = 1. G, H: sample thickness obtained during the passive and controlled stress relaxation tests shown in panels C and E. I: Controlled stress relaxation tests on three *Quillaja saponaria* leaves before and after immersion under water at 80 °C for 30 s (red shaded area); colours denote different samples. Samples were subjected to constant stress at 100 kPa followed by stress relaxation and recovery after a ± 25 µm step at 195 µm s^{-1}. Upper curves correspond to the sample thickness and lower curves correspond to the applied compressive stress. Note the difference in the leaf thickness and relaxation kinetics before and after killing

the tissue. J: Fitted coefficients using the method by Peleg (1979) to quantify the 'liquidity' of the samples, where a value of zero means no relaxation (*i.e.*, an elastic solid) and a value of one means complete relaxation (*i.e.*, a liquid); P = 0.0005 (Student's t-test). K: Stress relaxation half-time according to the method by Peleg (1979); P = 0.022 (Student's t-test). N = 3.

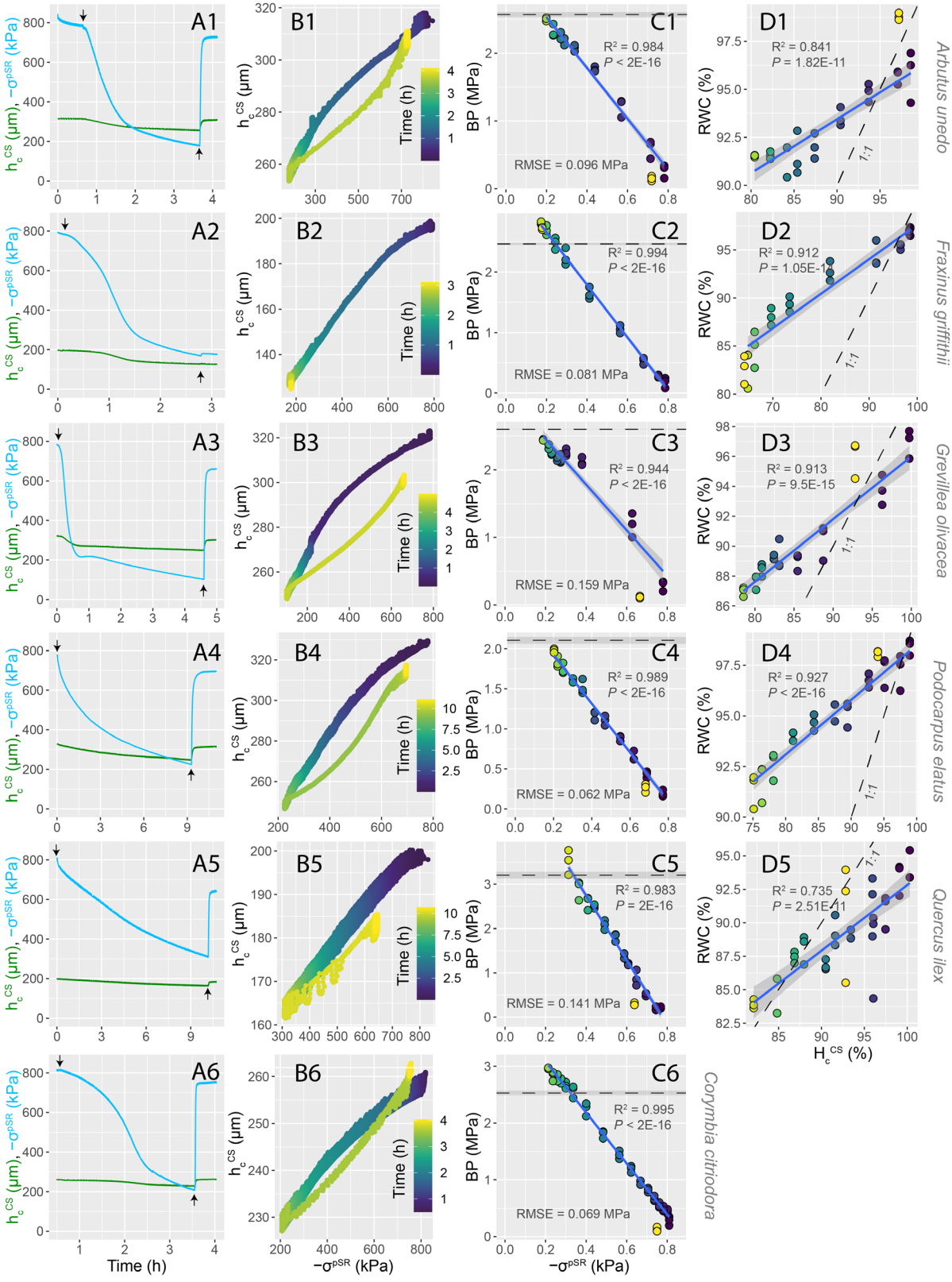

Figure 4.4. Simultaneous constant stress (CS) and passive stress relaxation (pSR) experiments performed on a single branch per species under changing water status. A1-A6: Leaf thickness measured during CS at 400 kPa (h_c^{CS}, green lines) and stress applied during passive SR ($-\sigma^{pSR}$, blue lines) for different species during a dehydration-rehydration cycle.

Down and up arrows indicate the time at which branches were cut in air and under water to start dehydration and rehydration, respectively. B1-B6: Relation between the thickness measured during CS and the stress measured during passive SR. C1-C6: Relation between the balancing pressure measured in three leaves per branch per time point and the stress measured during passive SR. The horizontal dashed lines indicate the osmotic pressure at the turgor-loss point (Π_{TLP}); shaded areas correspond to standard error. D1-D5: Relation between the leaf relative water content (RWC) measured in three leaves per time point and the relative leaf thickness measured during CS (H_c^{CS}); dashed lines correspond to the 1:1 line. Regressions in columns C and D only consider points obtained during dehydration. Colour scales for time shown in column B also apply to panels in columns C and D within the same row. N = 1.

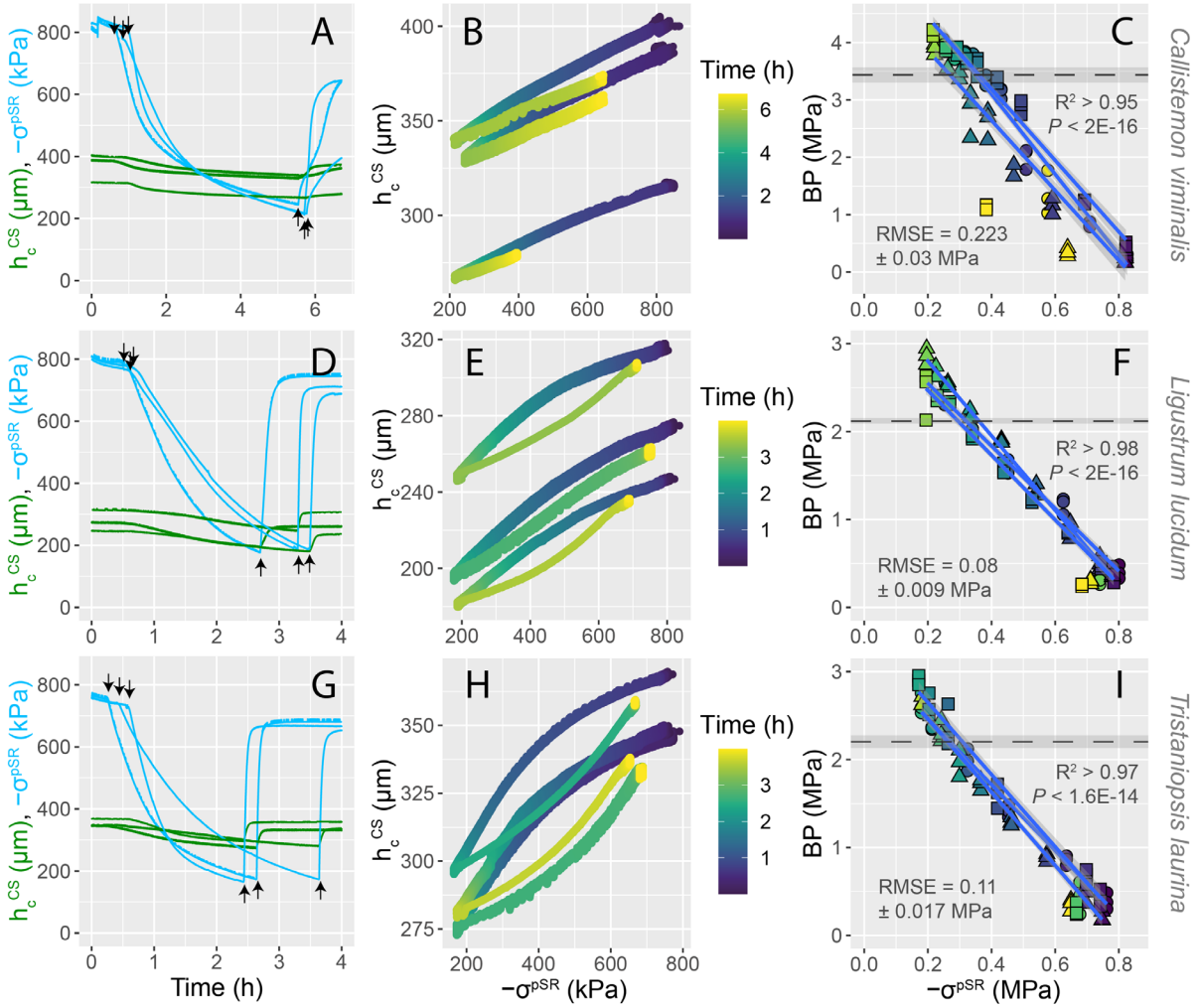

Figure 4.5. Simultaneous constant stress and passive stress relaxation experiments performed on three branches per species under changing water status. A, D, G: Leaf thickness measured during CS at 400 kPa (h_c^{CS}, green lines) and stress applied during passive SR ($-\sigma^{pSR}$, blue lines) for different species during a dehydration-rehydration cycle. Down and up

arrows indicate the time at which branches were cut in air and under water to start dehydration and rehydration, respectively. B, E, H: Relation between the thickness measured during CS and the stress measured during passive SR. C, F, I: Relation between the balancing pressure measured in three leaves per branch per time point and the stress measured during passive SR. The horizontal dashed lines indicate the osmotic pressure at the turgor-loss point (Π_{TLP}); shaded areas correspond to standard error. Regressions only consider points obtained during dehydration. Colour scales for time shown in B, E and H also apply to panels C, F and I, respectively. N = 3.

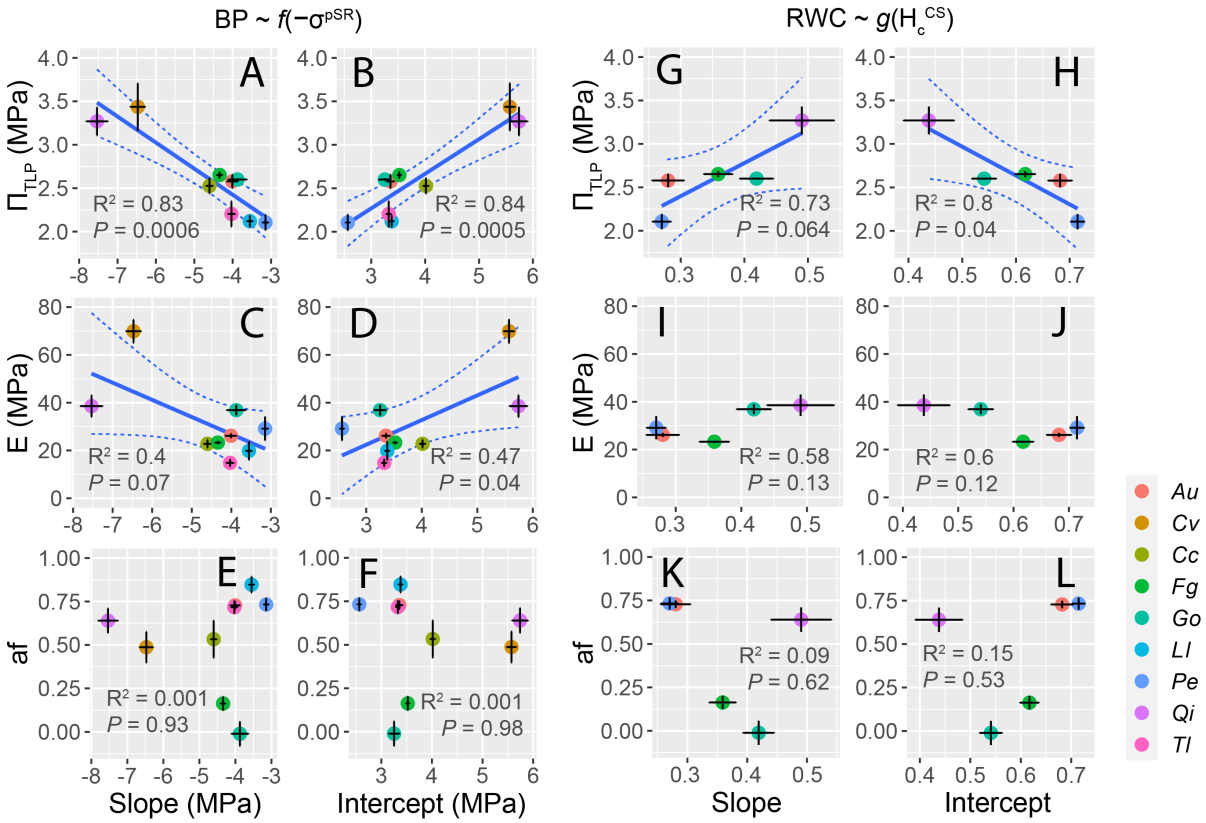

Figure 4.6. Relation between pressure-volume parameters and the linear regression coefficients from the experiments shown in Figs. 4 and 5. A-F: Relation between the regression coefficients of the stress applied during passive stress relaxation ($-\sigma^{pSR}$) and leaf pressure-volume parameters. G-L: Relation between the regression coefficients of the leaf relative thickness measured during CS (H_c^{CS}) and leaf pressure-volume parameters. Colours denote different species as per the legend. *Au* = *Arbutus unedo*; *Cv* = *Callistemon viminalis*; *Cc* = *Corymbia citriodora*; *Fg* = *Fraxinus griffithii*; *Go* = *Grevillea olivacea*; *Ll* = *Ligustrum lucidum*; *Pe* = *Podocarpus elatus*; *Qi* = *Quercus ilex*; *Tl* = *Tristaniopsis laurina*. Π_{TLP} = leaf bulk osmotic pressure at the turgor-loss point; E = leaf bulk elastic modulus; af = leaf apoplastic water fraction.

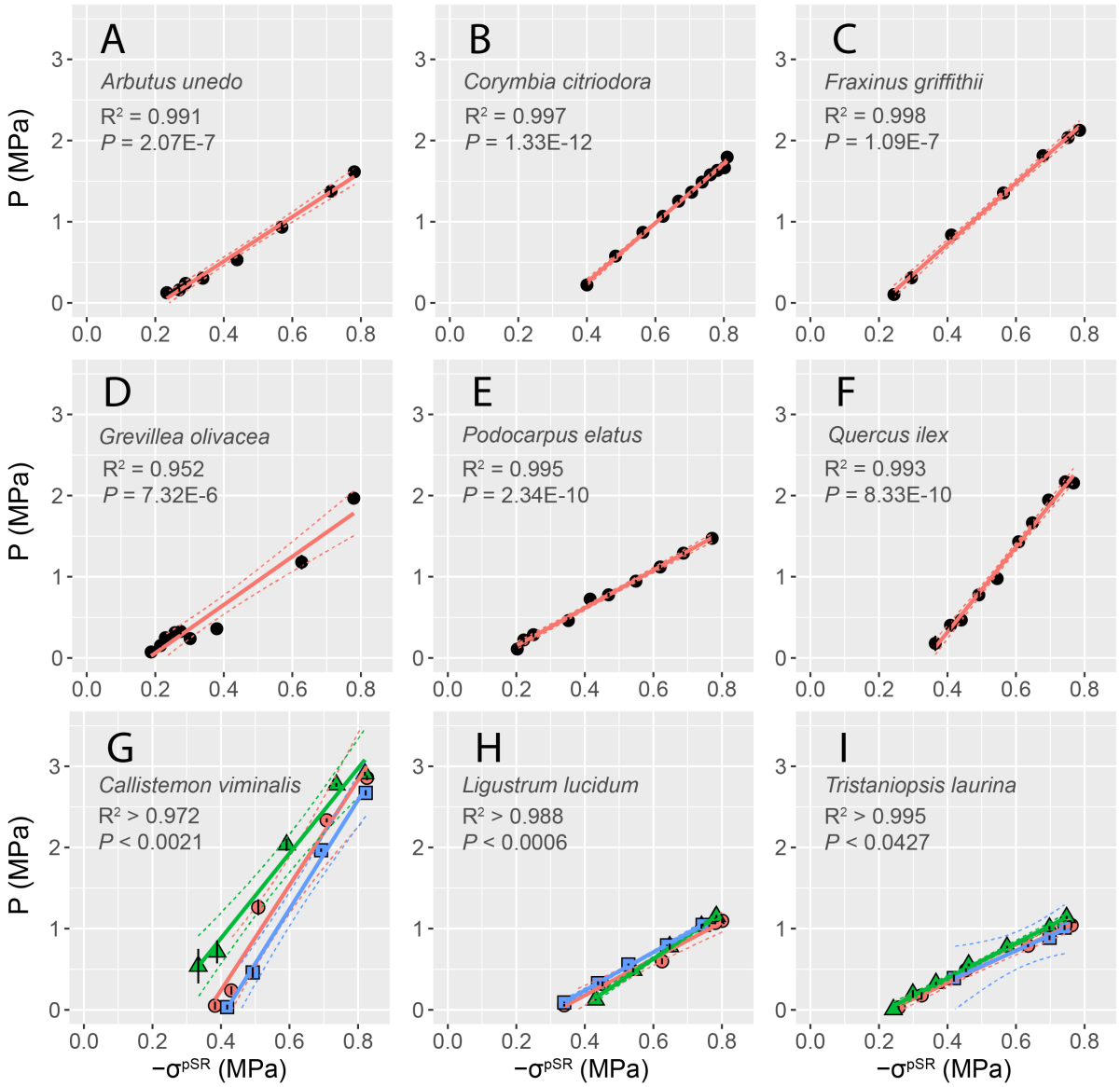

Figure 4.7. Relation between the stress applied during passive stress relaxation ($-\sigma^{pSR}$) and the bulk turgor pressure (P) estimated from leaf pressure-volume curves. Colours and symbols in panels G-I denote different plants.

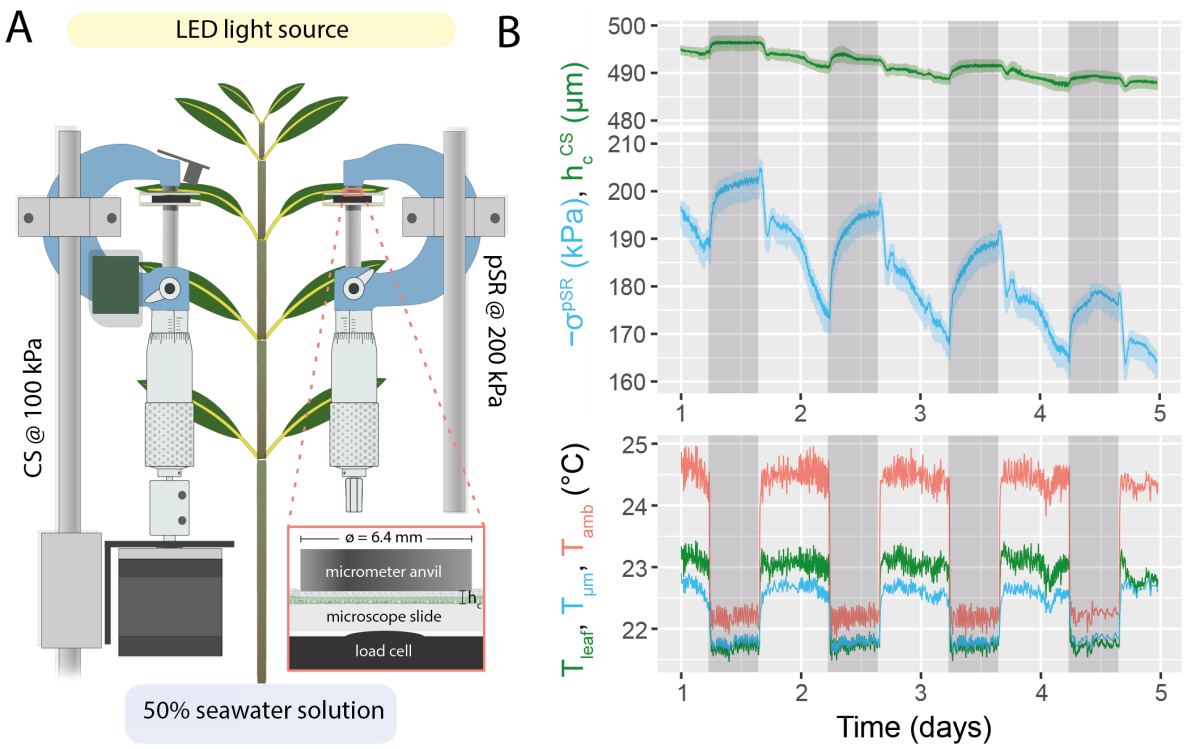

Figure 4.8. Simultaneous constant stress (CS) and passive stress relaxation (pSR) experiments performed on a living potted plant (*Avicennia marina* subsp. *australasica*) under laboratory conditions. A: Simplified view of the experimental setup (electrical connections are omitted for simplicity). A motorised micrometer was used for running a CS test at 100 kPa and a manual micrometer was used to perform a passive SR test at *c*. 200 kPa. The plant was maintained inside a tub with a 50% seawater solution and was irradiated using a full-spectrum LED light source. The red rectangular area shows a magnified view of an idealised uniaxially compressed *Avicennia* leaf (to scale). B: Results from the simultaneous CS and passive SR experiment. Shaded grey bars indicate periods of darkness. These measurements were filtered using a third-degree polynomial moving average (Savitzky and Golay, 1964) with a 1 min window; shaded coloured bands correspond to the raw measurements. Temperature-induced variations in the system thickness calculated from Fig. 2G are negligible in this experiment (*c*. 75 nm variation between during day and night). The small and steady decline in thickness and mechanical stress may be due to an increase in salinity of the hydroponic solution. T_{leaf} = adaxial leaf surface temperature; $T_{\mu m}$ = micrometer frame temperature; T_{amb} = temperature of the infrared sensor directly above the leaf. N = 1.

5. Discussion

Leaf squeeze-flow rheometry was applied as an empirical method to monitor plant water status. The stress measured during passive stress relaxation was related to leaf bulk turgor pressure ($R^2 > 0.95$) and balancing pressure ($R^2 > 0.94$). The relative leaf thickness measured

during constant stress was related, although sometimes non-linearly, to leaf relative water content ($R^2 > 0.74$). Squeeze-flow rheometry enabled precise non-destructive monitoring of plant water status with high temporal resolution at low cost, opening new opportunities for the measurement of plant hydration dynamics.

Instrument performance

The leaf squeeze-flow rheometer performed adequately; given its cost and simplicity, it may be useful to plant scientists interested in studying water in plants. For the purposes of replication and improvement, a discussion about the instrument performance is given in the Supplement.

Effects of uniaxial compression on the components of cell water status

In this study we emphasized the study of leaf squeeze-flow rheometry under changing water status when the compressed region was in hydrostatic equilibrium with the surrounding tissue. However, results from example curves comparing two species with distinct leaves, poplar (*Populus nigra*) and sage (*Salvia officinalis*), revealed rheological differences between the species during CS and SR. In poplar, we observed nearly complete recovery of the original thickness or pressure after undergoing CS and stress relaxation tests; by contrast, sage leaves displayed large irreversible losses of thickness, particularly during the CS test. Although we did not investigate the physical basis of CS and SR, these differences may be determined by the permeation of water through the cell membrane, diffusion or flow of water through the leaf apoplast, loss of intracellular solute due to compression, and/or plastic yield of the tissue. These phenomena, with an emphasis on membrane permeation, have been studied by Ferrier and Dainty (1977), who provided a theoretical framework for the estimation of the bulk modulus and the membrane hydraulic conductivity using uniaxial compression of a single cell layer and simple models of wall geometry and mechanics. However, the theory presented by Ferrier and Dainty (1977) did not incorporate the effects of uniaxial compression on the volume-averaged components of cell water status, which we describe below.

Leaves with flat laminae can be described as a cellular composite in the form of a sandwich beam (Gibson et al., 1988). Tissue on the sunny side of the leaf is packed with cylindrical cells with their long axis perpendicular to the epidermis, forming a layer known as the ‘palisade’ parenchyma; the shady side of the leaf can be described as an open-cell foam and is aptly called ‘spongy’ parenchyma (Borsuk et al., 2022). Most leaf tissues are porous, so uniaxial compression can presumably deform cells by changing their shape, *i.e.*, by making them wider and shorter. An idealised average-cell view of the time-dependent changes in water status that occur with uniaxial compression is shown in Fig. 9 (here we illustrate the case of stress relaxation, but a similar behaviour would be expected during CS). This simplified

view excludes non-ideal osmotic behaviour and plastic yield, so may only be applied to cells experiencing small strains.

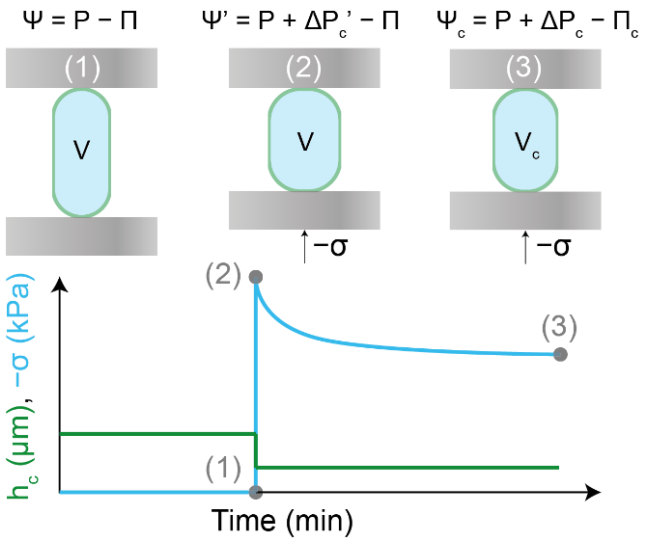

Figure 4.9. Idealised average-cell view of the changes in leaf water status brought by leaf uniaxial compression during stress relaxation. An uncompressed cell (1) is quickly compressed between two parallel plates, inducing immediate cell deformation with no change in the cell volume V, transiently raising the cell hydrostatic pressure to $P + \Delta P_c'$ (2)[3]. The plates are then maintained at a fixed position. In a timescale of minutes, relaxation of tension in the cell wall and water movement out of the cell cause the cell hydrostatic pressure to drop to $P + \Delta P_c$. Equilibrium (3) is reached when the new hydrostatic pressure is balanced by the increased osmotic pressure Π_c.

Under the mechanical stresses we worked with, water is effectively incompressible. Therefore, immediately after loading, we expect the volume of the cells to remain unchanged (Nilsson et al., 1958, Ferrier and Dainty, 1977), and the change in shape to induce an increased tension in the cell walls, increasing the intracellular hydrostatic pressure to $(P + \Delta P_c')$, where the last term indicates the maximum change in intracellular hydrostatic pressure caused by compression. In this state, the water potential of the compressed cells is $\Psi_c' = (P + \Delta P_c') - \Pi$, while outside the compressed region it is simply $\Psi = P - \Pi$. Water within the compressed region may equilibrate with water outside the compressed region, and two processes may be involved in this relaxation. First, water from inside the cell has to move

[3] In response to sudden compression, cells within porous tissues conserve volume by increasing width while reducing height. Assuming that the compressed sample is conserved in area because of friction against the pad, cells in non-porous tissues do not have the possibility of changing width, so their geometry is expected to change little during compression. The average cell would, however, conserve volume by increasing width while reducing height, as sketched.

across the cell membrane into the cell wall; and second, water has to diffuse or flow via the apoplastic space to the tissue outside the compressed region. If the membrane represents the only resistance to water movement, then the water potential in the compressed apoplast may be assumed equal to Ψ (*i.e.*, the apoplast remains in equilibrium with the tissue outside). (Using this approximation, Ferrier and Dainty (1977) estimated the hydraulic conductivity of the membrane of onion cells.) Conversely, if the apoplast represents the only resistance to water movement, then the water potential in the apoplast within the compressed region is likely to approach zero as free water accumulates in the apoplastic space, before dissipating along a pressure gradient. Probably, both of these resistances to water movement play a role in determining the kinetics of stress relaxation (Ferrier and Dainty, 1978), so the water potential outside the cells during the equilibration process is unknown. Therefore, here we restrict the discussion to the initial and final states.

If the volume of the compressed tissue is negligible in relation to the volume of the tissue studied (*e.g.*, the whole leaf, branch or plant), the water potential of the uncompressed tissue may be assumed constant. Thus, if the compressed region equilibrates with water outside the compressed region, then water redistribution is expected to lower $\Delta P_c'$ and raise the osmotic pressure in cells within the compressed region, until they reach equilibrium values ΔP_c and Π_c. This can be written as

$$\Psi_c = P + \Delta P_c - \Pi_c = \Psi = P - \Pi$$

which gives $\Delta P_c = \Pi_c - \Pi$. Making the approximation that the intracellular osmotically inactive volume is negligible and the cell osmotic behaviour is ideal (with unity reflection coefficient), then a cell having n osmoles of solute and an original volume V shrinks to V_c, where $\Pi V = nRT = \Pi_c V_c$. Defining the volumetric strain as $v = (V_c - V)/V$ (which is negative for compression) and combining these equations gives

$$\Delta P_c = \Pi_c - \Pi = \frac{nRT}{V_c} - \frac{nRT}{V} = nRT\frac{V - V_c}{VV_c} = -\frac{nRT}{V_c}v = -\Pi_c v$$

From the Boyle-Van't Hoff relation and from the definition of the volumetric strain, it follows that $\Pi_c = \Pi/(1+v)$ (Philip, 1958), so

$$\Delta P_c = \frac{\Pi v}{1+v} \qquad Eqn.\,4$$

In Eqn. 4, ΔP_c and v are not readily measurable, and the relation between $-\sigma$ and ΔP_c is not simple. While we do not know how the imposed stress relates to the change in turgor, it may be reasonable to make the approximation that they are proportional (Ferrier and Dainty, 1978), given the strong linear relationships found between $-\sigma^{pSR}$ and P (Fig. 7). Thus,

$$-\sigma \propto \frac{\Pi v}{1+v} \qquad Eqn.5$$

For small strains, $\Pi_c \approx \Pi$, so the compressed cell may be approximated as linear-elastic. In this approximation, the osmotic pressure corresponds to the so-called 'stationary' bulk modulus (Zimmermann and Hüsken, 1980, Tyerman, 1982), which differs from the 'instantaneous' bulk modulus described by Ferrier and Dainty (1977).

The relationships shown above provide insight into the behaviour of uniaxially compressed cells, but cannot be directly applied to leaves, where compressive behaviour is complicated by variations in tissue porosity, anisotropy, and the turgor dependence of the bulk modulus. In theory, if one could relate v to the leaf uniaxial strain, the behaviour of the cells could be inferred from measurements performed at the leaf level, and a bulk value for Π may be obtained non-invasively. Further work is needed for this endeavour, for which the mechanical behaviour of porous cellular materials may provide an approachable starting point (Gibson, 2005, Borsuk et al., 2022).

Constant stress and stress relaxation as measurement paradigms to monitor leaf water status

Constant stress and stress relaxation are routine tests used in rheology to study the deformation and flow kinetics of viscoelastic specimens. In plant science, Ferrier and Dainty (1977) have used CS experiments to estimate mechanical and hydraulic properties of uniaxially compressed tissues. However, CS and SR seem to have not been applied for continuous monitoring of plant water status. Given their simplicity and precision, CS and SR might become useful measurement paradigms to monitor the hydration dynamics of living plants.

Experimental evidence indicated that the applied stress measured during passive stress relaxation ($-\sigma^{pSR}$) can be used as an indicator of changes in leaf bulk turgor pressure (P). This indicator, which quantifies the effect of leaf bulk turgor on uniaxial stress, can be interpreted as the 'turgidity' of the leaf, or the sensorial perception of the leaf bulk turgor pressure. With this, however, it must be remembered that $-\sigma^{pSR}$ is not a direct measurement of P. Possibly due to complex changes in cell wall geometry and stresses, the slopes of P vs $-\sigma^{pSR}$ were greater than unity by a factor of several (Fig. 7). This is roughly in agreement with estimations from Ferrier and Dainty (1978), who estimated the ratio between the applied stress and the change in turgor caused by compression to be around 1-4.3. The relation between $-\sigma^{pSR}$ and BP was also approximately linear (Figs. 4 & 5) and their relation varied according to Π_{TLP} (Fig. 6).

Although the predictive power of $-\sigma^{pSR}$ was high, residual distributions indicated that its relation to BP is not always linear over the range studied (Fig S2). In some species, such as *Callistemon viminalis* and *Corymbia citriodora*, we observed a slight change in slope around the TLP, whereas in *Ligustrum lucidum*, *Tristianopsis laurina* and *Fraxinus griffithii* the relation was approximately linear beyond the TLP. In other species, we did not reach dehydration levels beyond the TLP. Departures from linearity may be caused by steeper changes in the leaf osmotic pressure once the tissues become flaccid. Other departures from linearity in the relation between BP and $-\sigma^{pSR}$ may be associated to a lack of hydrostatic equilibrium across the membrane. For example, in *Grevillea olivacea*, most turgor was lost within the first 30 min since cutting in air, during which the observed BP was higher than predicted by $-\sigma^{pSR}$ (Fig. 4 C3). The latter may suggest the water potential outside the cells to be decreasing at a higher rate than the reduction in cell turgor. Thus, the proportional relation between $-\sigma^{pSR}$ and BP may be restricted to cases where equilibrium across the cell membrane is met.

As leaf thickness is not constant during pSR, the relation between $-\sigma^{pSR}$ and BP is to some extent dependent on the mechanical compliance of the instrument (Fig. 2E). Thus, our results are restricted to instruments with comparable mechanical compliance (*c*. 1.3 μm N^{-1}), and it remains to show the relation between $-\sigma^{cSR}$ and BP. While we are unable to perform cSR tests under changing water status in our custom-built squeeze-flow rheometer, researchers with access to universal testing machines or dynamic mechanical analysers could test this relationship in a matter of hours. Thus, while pSR has advantages due to the simplicity of the instrument and reduced noise in the data, cSR may provide greater replicability as the results should be independent of the instrument's mechanical compliance.

The relation between H_c^{CS} and RWC sometimes exhibited substantially non-linear behaviour over the range studied. In the five species studied, the slope was smaller than unity by a factor of a few, indicating a steeper decrease in H_c^{CS} than in RWC. Non-linearity was possibly caused by changes in leaf structure, porosity and and/or leaf area during dehydration. At the levels of mechanical stresses we worked with, compressed leaves likely dehydrate with the epidermis firmly adhered to the compression plate, so the compressed region probably does not shrink in area during dehydration. In principle, decreases in RWC with no change in H_c^{CS}, as observed in *Fraxinus griffithii* (Fig. 3 D2), could result from leaf area shrinkage outside the squeezed region. Additionally, the steeper decline in H_c^{CS} than in RWC suggests a decrease in the compressed leaf porosity during dehydration. Possibly, the latter is due to an increased ability of the cell walls to bend with decreasing turgor, which leads to progressive filling of the intercellular space during dehydration. Thus, while H_c^{CS} may be correlated with leaf water content, care must be taken before assuming the linearity of this relation and the ranges over which it may be valid. The values of the intercepts and slopes between H_c^{CS} and

RWC should be considered cautiously, as we did not determine the time required to achieve full hydration and thus RWC may have been underestimated (Arndt et al., 2015). The lower predictive power of H_c^{CS} to estimate RWC is probably related to a smaller sample size and to the imprecise nature of RWC.

In this study we focused on turgid leaves, and it remains to show the relationships between $-\sigma^{pSR}$ and BP, and those between H_c^{CS} and RWC where turgor is zero or negative (Ding et al., 2014). For flaccid tissues, it is likely that the slopes would change due to a lower bulk modulus and due to steeper changes in the leaf bulk osmotic pressure with changing hydration. Thus, careful attention should be given to the linearity of these relationships beyond the turgid range. Also, non-recoverable losses of thickness and uniaxial stress in samples undergoing dehydration-rehydration cycles suggest that the leaf properties changed during our experiments. The reasons for this loss of turgidity may include plastic damage due to compression or rehydration, changes in the cell wall properties and/or loss of intracellular solute during rehydration (Meinzer et al., 1986, Meinzer et al., 2014). Future work should determine the relative contributions of these factors to ensure the technique is applied within the elastic range.

Relation to existing techniques for measuring plant water status

To the best of our knowledge, constant stress and stress relaxation have not been explicitly recognised as complementary paradigms to monitor plant water status, although similar methods have been employed. Many systems used to measure the thickness of stems or leaves operate using a displacement transducer with a relatively soft spring (Liming, 1957, Zweifel and Zeugin, 2008, Búrquez, 1987, Bravdo and Sharon, 1997), so the applied force changes only slightly with changing thickness. Thus, such systems may be regarded as a form of CS experiment. Conversely, some dendrometers are relatively stiff clamps and monitor the deformation of stems and fruits using a strain gage (Link et al., 1998), akin to a pSR experiment. Additionally, other methods employ magnetic clamps to measure the leaf thickness (Afzal et al., 2017) or pressure (Westhoff et al., 2009). Using magnets introduces further complications, because the attraction force between the magnets increases strongly and non-linearly with decreasing distance (Vokoun et al., 2009). Following Newton's third law of motion, the force measured over a static leaf should be equal to the force applied by the sensor. When using magnetic sensors, daily minima in leaf hydration have been observed to correspond to daily maxima in the 'leaf patch pressure' (Westhoff et al., 2009, Zimmermann et al., 2010), which may be due to leaf shrinkage and thus higher attraction force between the magnets. This may explain why the pressure output of magnetic clamps is inversely and non-linearly related to turgor pressure (Westhoff et al., 2009, Rüger et al., 2010, Ehrenberger et al., 2012a, Ehrenberger et al., 2012b); however, it does not explain why magnetic clamps

show an inversion of the pressure output under severe dehydration (Rodriguez-Dominguez et al., 2012, Marino et al., 2021). The output of magnetic clamps contrasts with the output obtained during pSR, where the changes in $-\sigma^{pSR}$ were directly and linearly related to P (Fig. 7). From these findings, we conclude that CS and SR are suitable measurement paradigms to monitor the leaf thickness and turgidity, respectively.

Hysteresis between leaf thickness and turgidity

Constant stress and passive stress relaxation experiments revealed non-linear relations between h_c^{CS} and $-\sigma^{pSR}$ with variations in the area and shape of the hysteresis loop (Figs. 4 & 5). While we did not investigate the source of this behaviour, it is possible that these hydration hysteresis loops are caused by capillary effects and/or hysteresis in the stress-strain relations of cell wall materials and geometry. In the case of elastic hysteresis, energy may be dissipated by friction between cellulose microfibrils in a mechanism analogous to the deformation of rubbers (Joule, 1859); this possibility has been previously discussed by Tyerman (1982). Aside from elastic hysteresis, capillary sorption hysteresis may play a role in the hydration of cell wall interstices, such as those described for wood (Barkas, 1942, Fredriksson and Thybring, 2019) and, more generally, for porous materials (Albers, 2014). Complex interactions between elastic and capillary hysteresis may also take place, as in high molecular weight polymers (Urquhart, 1929, Smith, 1947). Further research is needed to interpret the significance and mechanisms behind leaf hydration hysteresis loops.

The relation between h_c^{CS} and $-\sigma^{pSR}$ and their hysteresis loop are relevant to the methods used to measure plant water transport. Commonly, plant ecophysiologists have studied plant hydration dynamics using invasive techniques that yield noisy data, carrying large uncertainty in the estimations of tissue conductance (Sack et al., 2002, Brodribb and Holbrook, 2003). Two main limitations of such methods are the use of excised tissues (which introduces inter-leaf variability and leads to potential artifacts in the measurements) and the lack of continuous measurements of leaf water potential. The last issue stems from the available techniques used to measure water potential: (i) the pressure bomb cannot be used quickly enough to track tissue rehydration with high temporal resolution; and (ii) thermocouple psychrometry has equilibration times which can be longer than the rehydration process. Recently, Bourbia et al. (2021) have addressed the issue by continuously estimating water potential from optical measurements of petiole width; however, this method assumes a unvarying relation between petiole dimensions and water potential. In the case of uniaxially compressed leaves, we showed that this relation is most often not linear and is highly dependent on the direction of the hydration process. The lack of hysteresis during dehydration-rehydration cycles is sometimes assumed to estimate leaf hydraulic conductance (Brodribb and Holbrook, 2003), but previous research (Kamiya et al., 1963, Tyerman, 1982) and our

present work indicate that hysteresis is present in dehydration-rehydration cycles of plant tissue. Thus, our results highlight long-standing issues and assumptions in the study of plant hydration dynamics and suggest an accessible method to approach them.

In vivo measurements

A trial on a single potted *Avicennia marina* plant indicated that the technique is suitable to monitor changes in plant water status *in vivo*. These results conformed to expectations of plant water status under changing light, suggesting that leaf squeeze-flow rheometry may be a valuable tool to monitor leaf thickness and turgidity non-invasively over a range of time-scales. The technique provides improved temporal resolution relative to the pressure chamber or thermocouple psychrometry, and so could be used complementarily. However, temperature effects on the instrument dimensions currently limit the applicability of leaf squeeze-flow rheometry under field settings. It is not clear whether the leaf thickness and turgidity declined due to an increase in the salinity of the hydroponic solution. Future efforts may develop the technique to be suitable for field conditions.

6. Conclusions

Leaf squeeze-flow rheometry was applied as a technique to study plant hydration dynamics. The measurement paradigms of constant stress and stress relaxation were found to be useful empirical means of monitoring changes in leaf relative water content and turgidity during dehydration-rehydration cycles, establishing a simple method to track leaf water status non-invasively. Our results and an idealised average-cell model of leaf uniaxial compression suggest that the leaf stiffness during compression is strongly dependent on the leaf bulk osmotic pressure. However, the main limitation to the use of this model is that the porosity inside the compressed leaf is unknown, so we are unable to relate the deformation of the lamina to the deformation of the average cell. Further work will be needed to establish a working model for the effects of uniaxial compression on the components of water status in porous tissues. While here we focused on static uniaxial compression under hydrostatic equilibrium, the study of non-equilibrium states during compression, as well as dynamic mechanical analyses such as oscillatory sweep tests, may provide further insights into plant water movement and broaden the applications of leaf squeeze-flow rheometry. Our findings may stimulate the development of sophisticated actuated plant sensors with potential applications in productive and natural systems.

7. Acknowledgements

We thank John Passioura for experimental support and advice and for comments on the manuscript; Jacques Dumais for a discussion on the effects of leaf uniaxial compression on cell water status; Javier Merrill and Patrick Meir for comments on the manuscript; and Aria Carroll for assistance in the experiments. We also thank Steve Tyerman for pointing us to the work by Ferrier & Dainty, and Wieland Fricke and Tim Brodribb for constructive reviews. TIF was funded by the Becas Chile program by ANID, Scholarship 72180256. This research was funded using TIF's personal funds and supported by the Australian Research Council Discovery Project, Grant DP180102969.

CHAPTER 5: GENERAL DISCUSSION

The present work investigated two distinct topics relevant to the study of plant hydration dynamics. Chapters 2 and 3 characterised the role of FWU on plant hydraulic function, and Chapter 4 presented a method to monitor plant water status using leaf uniaxial compression. These findings contribute new evidence regarding the functional roles of atmospheric water inputs on plant life, and establish simple measurement paradigms from rheology for monitoring plant water status. The implications of these findings and their relevance in reference to the available scientific literature are discussed below.

1. Role of atmospheric water sources in plant hydraulic function

The ability of leaves to absorb atmospheric water is widespread amongst plants (Berry et al., 2018). Such widespread prevalence has sparked interest in the topic of foliar water uptake, which has received increased scientific attention over the last decade. However, the functional roles of FWU remain elusive, and it is unclear whether the widespread ability of plant leaves to access atmospheric water is adaptive or incidental. For example, Binks et al. (2020) have expressed the view that FWU may be equivalent to stomatal conductance, suggesting that stomatal pores may serve as a prevalent pathway for water uptake. By contrast, particular species have specific adaptations for the absorption of atmospheric water. Common examples of species adapted to FWU are epiphytic or aerophytic bromeliads in the genus *Tillandsia*, whose leaves are covered by specialised trichomes acting as a unidirectional water valve (Raux et al., 2020). While some plants (like *Tillandsia*) rely exclusively on atmospheric water absorption, the presence of specialised water uptake pathways in trees, which also have an edaphic water source, suggests that FWU may have functional roles beyond its (generally small) contribution to water balance.

The species studied in this work, *Avicennia marina* (Forssk.) Vierh., is adapted for FWU. *Avicennia marina* inhabits tidal inundated saline environments and so has, in principle, infinite access to water. Despite this availability, *A*. *marina* can be considered conservative regarding water use (Ball, 1988), which can be attributed to the need for salt exclusion at the roots and subsequent accumulation of salts in the rhizosphere (Passioura et al., 1992). As secreted salts also accumulate on the leaf surface, *A. marina* is able to absorb water from unsaturated atmospheres by deliquescence (Coopman et al., 2021). The pathways for FWU in *Avicennia* are not fully resolved, but evidence indicates that water can be absorbed via specialised trichomes in the abaxial surface (Nguyen et al., 2017b) and via salt glands (Tan et al., 2013). In support of a functional role for FWU, Steppe et al. (2018) and Schreel et al. (2019) found a role for FWU in turgor-driven shoot growth of *Avicennia marina*, and Coopman et al. (2021) showed that branch rehydration driven by FWU could enhance hydraulic safety

margins of *A. marina* grown under arid conditions. However, it remains unclear how FWU affects water transport in this species.

Current controversies in the literature about plant hydration dynamics regard the loss and recovery of shoot hydraulic function during dehydration-rehydration cycles. Two main gaps can be recognised in this broad topic: first, which transport phenomena (bulk flow or diffusion) and pathways (apoplastic or symplastic) determine the loss and recovery of water transport capacity (Scoffoni et al., 2017a); and second, whether and how embolism refilling is possible when water in the xylem remains under tension (Holbrook and Zwieniecki, 1999). The last question remains physically challenging to explain and is a matter of speculation (Zwieniecki and Holbrook, 2009). Some researchers have hypothesised and tested whether FWU plays a role in embolism repair (Earles et al., 2016, Mayr et al., 2014b, Schreel et al., 2022), but results are so far inconclusive, and the kinetics of FWU and its effect on plant hydraulic conductance remain poorly resolved (Guzmán-Delgado et al., 2018).

Results presented in the present work are relevant to interpreting the role of FWU in the life of *Avicennia marina* and to the abovementioned gaps in knowledge. In Chapter 2, results showed that FWU can lead to reversible recovery of leaf hydraulic conductance (K_{leaf}). While K_{leaf} recovery retraced the same path observed during dehydration-dependent loss in K_{leaf}, a reduced ability for FWU in severely dehydrated branches halted K_{leaf} recovery. Results from FWU kinetics experiments suggested that most of the resistance to water movement during FWU was located on the leaf surface, whose permeability to water may be affected by dehydration. Thus, putative mechanisms for loss of K_{surf} during dehydration are mechanistically distinct from the loss of K_{leaf}, which likely involved loss of conductance outside the xylem (Scoffoni et al., 2017b) and xylem embolism.

In Chapter 3, the presence of xylem emboli in four dehydrated excised twigs of *A. marina* was confirmed by micro-CT imaging. While stem emboli were attributed to a cutting artifact, embolism in leaves was likely caused by dehydration. Water provision to the shoot surface of these twigs promoted embolism refilling in all organs, suggesting that FWU may play a functional role in embolism refilling in *A. marina*. The water absorption process was apparently slower than in the experiments presented in Chapter 2 and in field settings (Coopman et al., 2021, Schreel et al., 2019), and the conditions used for micro-CT imaging were not representative of the natural environment. Interestingly, two of the four rehydrating samples displayed an increased electron density in the outer vessels within the petiole vascular bundle, suggesting that salts may have accumulated in this tissue during xylem refilling. This observation, although anecdotal, is consistent with the idea that plants may actively load solute into embolised vessels to promote embolism refilling (Zwieniecki and

Holbrook, 2009), and deserves further attention; use of energy-dispersive-X-ray analysis coupled with cryo-SEM imaging may be a well-suited technique for this purpose. The results substantiate the view that FWU is a functionally important water source for *A*. *marina*, but extrapolating this view to natural conditions requires field validation. It is unclear how these findings may be relevant to different taxa.

Some of the results presented in Chapters 2 and 3 were inconclusive and should be interpreted with caution. In Chapter 2, a non-significant decline in K_{surf} was observed during dehydration, despite a significant decline of FWU. In this regard, it is worth noting that the method used was noisy and provided a limited ability to resolve changes in water status over time. Simplistic (although common) assumptions were involved in these calculations, such as the use of capacitance values obtained from dehydrating leaves during the rehydration process. The method used for estimating K_{leaf} (Brodribb, 2003) was also built on simplistic assumptions, such as a logarithmic increase in water potential over time, hydrostatic equilibrium across the plasma membrane and the applicability of capacitance values obtained during dehydration for determining the leaf rehydration kinetics. All of these assumptions are challenged by some of the data presented in Chapter 4. In Chapter 3, the experimental design used and the available techniques to monitor plant water status did not allow non-destructive tracking of water potential over time, so it is unclear whether refilling occurred under xylem tension.

2. Use of static uniaxial compression for measurement of plant water status

The measurement of plant water status is a fundamental research goal in plant science for optimising irrigation in agriculture and for modelling the vast water fluxes that are mediated by plants. However, common techniques employed for measurement of bulk tissue water status have changed little over the last 50 years. Perhaps, this apparent lack of advance has been caused by disjunct efforts separated by a matter of scale. Plant ecophysiologists rely heavily on the use of the pressure-bomb technique (Scholander et al., 1965, Tyree and Hammel, 1972) and thermocouple psychrometry (Boyer, 1968) to measure plant water potential, and on the use of mass measurements for determination of plant water content (Weatherley, 1950). In contrast, plant cell biologists and plant biomechanists often employ delicate techniques such as the pressure-probe (Hüsken et al., 1978), ball tonometry (Lintilhac et al., 2000), nanoindentation (Burri et al., 2019) or atomic-force microscopy (Beauzamy et al., 2015) to measure cell mechanical properties. In between these approaches separated by scale lies an interestingly practical gap thus far unfulfilled: is it feasible to use small-scale measurement principles to infer bulk changes in the water status of larger tissues?

In Chapter 4, two measurement paradigms of rheology, constant stress (CS) and stress relaxation (SR), were shown to be practical and effective means of measuring plant water status non-invasively. While the problem of uniaxially compressing leaves is mechanically complex, the technique presented is simple, and the value of CS and SR to monitor plant water status has not, to my knowledge, been recognised in the literature. The applied uniaxial stress measured during passive SR ($-\sigma^{pSR}$) was used to estimate leaf turgor pressure (P), and the leaf thickness measured during CS (H_c^{CS}) was used to estimate leaf relative water content (RWC). Although the relation between $-\sigma^{pSR}$ and P was approximately linear, the relation between H_c^{CS} and RWC sometimes exhibited departures from linearity, which may be explained by changes in porosity or leaf area during dehydration. In both cases, the slopes departed from unity, and the main determinant of regression parameters between squeeze-flow and pressure-volume data was the leaf osmotic pressure at the turgor-loss point (Π_{TLP}). This result might have practical value in the sense that, if the relation between the regression parameters and Π_{TLP} across different species is known, it may be possible to estimate P and RWC without a using pressure chamber. As plant ecophysiologists have adopted the use of osmometry as a quick method to estimate the osmotic pressure of plant tissues (Bartlett et al., 2012), this approach may become valuable to reduce calibration efforts.

Leaf squeeze-flow rheometry makes it possible to study plant hydration dynamics with improved temporal resolution and thus opens the possibility to answer questions that have so far remained unapproachable due to practical or methodological reasons. In particular, the technique may be useful to study the time-dependent processes of leaf deformation and their relation to water diffusion through the plasma membrane and the leaf apoplast. However, questions regarding the actual deformation of individual cells during leaf uniaxial compression remain open. Due to the porous nature of leaves, it is likely that dimensional changes in leaf thickness are partially explained by changes in airspace volume during compression, which remain hard to predict or measure. In this regard, the simplified single-cell model introduced in Chapter 4 presents a first and incipient approach to the constitutive relations relevant to leaf squeeze-flow rheometry. Further efforts incorporating knowledge from plant biology, biophysics and rheology will be needed to develop a realistic model of leaf uniaxial compression.

The approach to leaf squeeze-flow rheometry presented in Chapter 4 opens the possibility to apply measurement paradigms from rheology to plant hydration dynamics in general, which might find practical use in field settings. The ability to automate the technique makes it feasible to incorporate into agricultural robotics and opens a wide opportunity to develop actuated plant sensors. While the current implementation is only applicable to environments at constant or nearly constant temperature, future engineering developments

may widen the impact of leaf squeeze-flow rheometry. The application of different measurement paradigms (such as oscillatory sweep tests) and the application of constant stress and stress relaxation to other plant organs, such as stems or flowers, may be attempted in the near future.

References

AFZAL, A., DUIKER, S. W. & WATSON, J. E. 2017. Leaf thickness to predict plant water status. *Biosystems Engineering,* 156**,** 148-156.

ALBERS, B. 2014. Modeling the hysteretic behavior of the capillary pressure in partially saturated porous media: a review. *Acta Mechanica,* 225**,** 2163-2189.

ALLEN, C. D., MACALADY, A. K., CHENCHOUNI, H., BACHELET, D., MCDOWELL, N., VENNETIER, M., KITZBERGER, T., RIGLING, A., BRESHEARS, D. D. & HOGG, E. T. 2010. A global overview of drought and heat-induced tree mortality reveals emerging climate change risks for forests. *Forest ecology and management,* 259**,** 660-684.

ANGELES, G., BOND, B., BOYER, J. S., BRODRIBB, T., BROOKS, J. R., BURNS, M. J., CAVENDER-BARES, J., CLEARWATER, M., COCHARD, H. & COMSTOCK, J. 2004. The cohesion-tension theory. *New Phytologist,* 163**,** 451-452.

ARNDT, S. K., IRAWAN, A. & SANDERS, G. J. 2015. Apoplastic water fraction and rehydration techniques introduce significant errors in measurements of relative water content and osmotic potential in plant leaves. *Physiologia Plantarum,* 155**,** 355-368.

BALL, M. 1988a. Salinity Tolerance in the Mangroves Aegiceras corniculatum and Avicennia marina. I. Water Use in Relation to Growth, Carbon Partitioning, and Salt Balance. *Functional Plant Biology,* 15**,** 447-464.

BALL, M. C. 1988b. Salinity tolerance in the mangroves Aegiceras corniculatum and Avicennia marina. I. Water use in relation to growth, carbon partitioning, and salt balance. *Functional Plant Biology,* 15**,** 447-464.

BANKS, J. 1806. *A short account of the cause of the disease in corn, called by farmers the blight, the mildew, and the rust*, J. Harding.

BARKAS, W. W. 1942. Wood water relationships—VII. Swelling pressure and sorption hysteresis in gels. *Transactions of the Faraday Society,* 38**,** 194-209.

BARTLETT, M. K., SCOFFONI, C., ARDY, R., ZHANG, Y., SUN, S., CAO, K. & SACK, L. 2012. Rapid determination of comparative drought tolerance traits: using an osmometer to predict turgor loss point. *Methods in Ecology and Evolution,* 3**,** 880-888.

BEAUZAMY, L., DERR, J. & BOUDAOUD, A. 2015. Quantifying Hydrostatic Pressure in Plant Cells by Using Indentation with an Atomic Force Microscope. *Biophysical Journal,* 108**,** 2448-2456.

BEAUZAMY, L., NAKAYAMA, N. & BOUDAOUD, A. 2014. Flowers under pressure: ins and outs of turgor regulation in development. *Annals of Botany,* 114**,** 1517-1533.

BERRY, Z. C., EMERY, N. C., GOTSCH, S. G. & GOLDSMITH, G. R. 2018. Foliar water uptake: processes, pathways, and integration into plant water budgets. *Plant, Cell & Environment*.

BIDHENDI, A. J. & GEITMANN, A. 2019. Methods to quantify primary plant cell wall mechanics. *Journal of Experimental Botany,* 70**,** 3615-3648.

BINKS, O., COUGHLIN, I., MENCUCCINI, M. & MEIR, P. 2020. Equivalence of foliar water uptake and stomatal conductance? *Plant, Cell & Environment,* 43**,** 524-528.

BLACKMAN, C. J., BRODRIBB, T. J. & JORDAN, G. J. 2009. Leaf hydraulics and drought stress: response, recovery and survivorship in four woody temperate plant species. *Plant, Cell & Environment,* 32**,** 1584-95.

BORSUK, A. M., RODDY, A. B., THÉROUX-RANCOURT, G. & BRODERSEN, C. R. 2022. Structural organization of the spongy mesophyll. *New Phytologist,* n/a.

BOURBIA, I., PRITZKOW, C. & BRODRIBB, T. J. 2021. Herb and conifer roots show similar high sensitivity to water deficit. *Plant Physiology,* 186**,** 1908-1918.

BOYER, J. S. 1968. Relationship of Water Potential to Growth of Leaves 1. *Plant Physiology,* 43**,** 1056-1062.

BRAVDO, B. & SHARON, Y. A fully-automated orchard irrigation system based on continuous monitoring of turgor potential with a leaf sensor. III International Symposium on Sensors in Horticulture 562, 1997. 55-61.

BRODERSEN, C. R. & MCELRONE, A. J. 2013. Maintenance of xylem Network Transport Capacity: A Review of Embolism Repair in Vascular Plants. *Front Plant Sci,* 4**,** 108.

BRODERSEN, C. R., MCELRONE, A. J., CHOAT, B., MATTHEWS, M. A. & SHACKEL, K. A. 2010. The dynamics of embolism repair in xylem: in vivo visualizations using high resolution computed tomography. *Plant Physiology*, pp. 110.162396.

BRODRIBB, T. & HOLBROOK, N. M. 2004. Diurnal depression of leaf hydraulic conductance in a tropical tree species. *Plant, Cell & Environment,* 27, 820-827.

BRODRIBB, T. J. 2003. Stomatal Closure during Leaf Dehydration, Correlation with Other Leaf Physiological Traits. *Plant Physiology,* 132, 2166-2173.

BRODRIBB, T. J. & COCHARD, H. 2009. Hydraulic failure defines the recovery and point of death in water-stressed conifers. *Plant Physiology,* 149, 575-84.

BRODRIBB, T. J. & HOLBROOK, N. M. 2003. Stomatal closure during leaf dehydration, correlation with other leaf physiological traits. *Plant Physiology,* 132, 2166-2173.

BRODRIBB, T. J., POWERS, J., COCHARD, H. & CHOAT, B. 2020. Hanging by a thread? Forests and drought. *Science,* 368, 261.

BRODRIBB, T. J., SKELTON, R. P., MCADAM, S. A., BIENAIME, D., LUCANI, C. J. & MARMOTTANT, P. 2016. Visual quantification of embolism reveals leaf vulnerability to hydraulic failure. *New Phytologist,* 209, 1403-9.

BROWN, H. R. 2013. The Theory of the Rise of Sap in Trees: Some Historical and Conceptual Remarks. *Physics in Perspective,* 15, 320-358.

BUCCI, S., SCHOLZ, F., GOLDSTEIN, G., MEINZER, F. & STERNBERG, L. D. S. 2003. Dynamic changes in hydraulic conductivity in petioles of two savanna tree species: factors and mechanisms contributing to the refilling of embolized vessels. *Plant, Cell & Environment,* 26, 1633-1645.

BÚRQUEZ, A. 1987. Leaf Thickness and Water Deficit in Plants: A Tool for Field Studies. *Journal of Experimental Botany,* 38, 109-114.

BURRI, J. T., VOGLER, H., MUNGLANI, G., LÄUBLI, N. F., GROSSNIKLAUS, U. & NELSON, B. J. 2019. A Microrobotic System for Simultaneous Measurement of Turgor Pressure and Cell-Wall Elasticity of Individual Growing Plant Cells. *IEEE Robotics and Automation Letters,* 4, 641-646.

CHAVES, M. M., PEREIRA, J. S., MAROCO, J., RODRIGUES, M. L., RICARDO, C. P. P., OSÓRIO, M. L., CARVALHO, I., FARIA, T. & PINHEIRO, C. 2002. How Plants Cope with Water Stress in the Field? Photosynthesis and Growth. *Annals of Botany,* 89, 907-916.

CHOAT, B., BRODRIBB, T. J., BRODERSEN, C. R., DUURSMA, R. A., LOPEZ, R. & MEDLYN, B. E. 2018. Triggers of tree mortality under drought. *Nature,* 558, 531-539.

COCHARD, H. & DELZON, S. 2013. Hydraulic failure and repair are not routine in trees. *Annals of Forest Science,* 70, 659-661.

COOPMAN, R. E., NGUYEN, H. T., MENCUCCINI, M., OLIVEIRA, R. S., SACK, L., LOVELOCK, C. E. & BALL, M. C. 2021. Harvesting water from unsaturated atmospheres: deliquescence of salt secreted onto leaf surfaces drives reverse sap flow in a dominant arid climate mangrove, Avicennia marina. *New Phytologist,* n/a.

CREEK, D., BLACKMAN, CHRIS J., BRODRIBB, T. J., CHOAT, B. & TISSUE, D. T. 2018. Coordination between leaf, stem, and root hydraulics and gas exchange in three arid-zone angiosperms during severe drought and recovery. *Plant, Cell & Environment,* 41, 2869-2881.

DAWSON, T. E. & GOLDSMITH, G. R. 2018. The value of wet leaves. *New Phytol*.

DE BELIE, N., HALLETT, I. C., HARKER, F. R. & DE BAERDEMAEKER, J. 2000. Influence of Ripening and Turgor on the Tensile Properties of Pears: A Microscopic Study of Cellular and Tissue Changes. *Journal of the American Society for Horticultural Science jashs,* 125, 350-356.

DING, Y., ZHANG, Y., ZHENG, Q. S. & TYREE, M. T. 2014. Pressure-volume curves: revisiting the impact of negative turgor during cell collapse by literature review and simulations of cell micromechanics. *New Phytol,* 203, 378-87.

DIXON, H. H. & JOLY, J. 1895. XII. On the ascent of sap. *Philosophical Transactions of the Royal Society of London. (B.),* 186, 563-576.

DUMAIS, J., SHAW, S. L., STEELE, C. R., LONG, S. R. & RAY, P. M. 2006. An anisotropic-viscoplastic model of plant cell morphogenesis by tip growth. *The International journal of developmental biology,* 50**,** 209-222.

DUTROCHET, H. 1826. *L'agent immédiat du mouvement vital dévoilé dans sa nature et dans son mode d'action chez les vegétaux et chez les animaux*, Baillière.

EARLES, J. M., SPERLING, O., SILVA, L. C., MCELRONE, A. J., BRODERSEN, C. R., NORTH, M. P. & ZWIENIECKI, M. A. 2016. Bark water uptake promotes localized hydraulic recovery in coastal redwood crown. *Plant, Cell & Environment,* 39**,** 320-8.

EHRENBERGER, W., RÜGER, S., FITZKE, R., VOLLENWEIDER, P., GÜNTHARDT-GOERG, M., KUSTER, T., ZIMMERMANN, U. & AREND, M. 2012a. Concomitant dendrometer and leaf patch pressure probe measurements reveal the effect of microclimate and soil moisture on diurnal stem water and leaf turgor variations in young oak trees. *Functional Plant Biology,* 39**,** 297-305.

EHRENBERGER, W., RÜGER, S., RODRÍGUEZ-DOMÍNGUEZ, C. M., DÍAZ-ESPEJO, A., FERNÁNDEZ, J. E., MORENO, J., ZIMMERMANN, D., SUKHORUKOV, V. L. & ZIMMERMANN, U. 2012b. Leaf patch clamp pressure probe measurements on olive leaves in a nearly turgorless state. *Plant Biology,* 14**,** 666-674.

EICHERT, T., KURTZ, A., STEINER, U. & GOLDBACH, H. E. 2008. Size exclusion limits and lateral heterogeneity of the stomatal foliar uptake pathway for aqueous solutes and water-suspended nanoparticles. *Physiol Plant,* 134**,** 151-60.

ELLER, C. B., LIMA, A. L. & OLIVEIRA, R. S. 2016. Cloud forest trees with higher foliar water uptake capacity and anisohydric behavior are more vulnerable to drought and climate change. *New Phytologist,* 211**,** 489-501.

ENGMANN, J., SERVAIS, C. & BURBIDGE, A. S. 2005. Squeeze flow theory and applications to rheometry: A review. *Journal of Non-Newtonian Fluid Mechanics,* 132**,** 1-27.

FERNANDEZ, V., BAHAMONDE, H. A., JAVIER PEGUERO-PINA, J., GIL-PELEGRIN, E., SANCHO-KNAPIK, D., GIL, L., GOLDBACH, H. E. & EICHERT, T. 2017. Physico-chemical properties of plant cuticles and their functional and ecological significance. *J Exp Bot,* 68**,** 5293-5306.

FERRIER, J. M. & DAINTY, J. 1977. A new method for measurement of hydraulic conductivity and elastic coefficients in higher plant cells using an external force. *Canadian Journal of Botany,* 55**,** 858-866.

FERRIER, J. M. & DAINTY, J. 1978. The external force method for measuring hydraulic conductivity and elastic coefficients in higher plant cells: application to multilayer tissue sections and further theoretical development. *Canadian Journal of Botany,* 56**,** 22-26.

FICK, A. 1855. Ueber Diffusion. *Annalen der Physik,* 170**,** 59-86.

FITZGERALD, M. A., ORLOVICH, D. A. & ALLAWAY, W. G. 1992. Evidence that abaxial leaf glands are the sites of salt secretion in leaves of the mangrove Avicennia marina (Forsk.) Vierh. *New Phytologist,* 120**,** 1-7.

FLEXAS, J., CARRIQUI, M. & NADAL, M. 2018. Gas exchange and hydraulics during drought in crops: who drives whom? *Journal of Experimental Botany,* 69**,** 3791-3795.

FRANKS, P. J., COWAN, I. R. & FARQUHAR, G. D. 1998. A study of stomatal mechanics using the cell pressure probe. *Plant, Cell & Environment,* 21**,** 94-100.

FREDRIKSSON, M. & THYBRING, E. E. 2019. On sorption hysteresis in wood: Separating hysteresis in cell wall water and capillary water in the full moisture range. *PLOS ONE,* 14**,** e0225111.

FUENZALIDA, T. I., BRYANT, C. J., OVINGTON, L. I., YOON, H.-J., OLIVEIRA, R. S., SACK, L. & BALL, M. C. 2019. Shoot surface water uptake enables leaf hydraulic recovery in Avicennia marina. *New Phytologist,* 224**,** 1504-1511.

GEITMANN, A. 2006. Experimental Approaches Used to Quantify Physical Parameters at Cellular and Subcellular Levels. *American Journal of Botany,* 93**,** 1380-1390.

GIBSON, L. J. 2005. Biomechanics of cellular solids. *Journal of Biomechanics,* 38**,** 377-399.

GIBSON, L. J., ASHBY, M. F. & EASTERLING, K. E. 1988. Structure and mechanics of the Iris leaf. *Journal of Materials Science,* 23**,** 3041-3048.

GIBSON, L. J., ASHBY, M. F., SCHAJER, G. S. & ROBERTSON, C. I. 1982. The mechanics of two-dimensional cellular materials. *Proceedings of the Royal Society of London. A. Mathematical and Physical Sciences,* 382**,** 25-42.

GREEN, P. B. 1962. Mechanism for Plant Cellular Morphogenesis. *Science,* 138**,** 1404-1405.

GREEN, P. B. & STANTON, F. W. 1967. Turgor Pressure: Direct Manometric Measurement in Single Cells of Nitella. *Science,* 155**,** 1675-1676.

GUZMAN-DELGADO, P., MASON EARLES, J. & ZWIENIECKI, M. A. 2018. Insight into the physiological role of water absorption via the leaf surface from a rehydration kinetics perspective. *Plant, Cell & Environment*.

GUZMÁN-DELGADO, P., MASON EARLES, J. & ZWIENIECKI, M. A. 2018. Insight into the physiological role of water absorption via the leaf surface from a rehydration kinetics perspective. *Plant, Cell & Environment,* 41**,** 1886-1894.

HALES, S. 1727. *Vegetable Staticks: Or, an Account of Some Statical Experiments on the Sap in Vegetables: Being an Essay Towards a Natural History of Vegetation. Also, a Specimen of an Attempt to Analyse the Air, by a Great Variety of Chymio-statical Experiments; which Were Read at Several Meetings Before the Royal Society*, W. and J. Innys, at the West End of St. Paul's.

HAMANT, O., HEISLER, M. G., JÖNSSON, H., KRUPINSKI, P., UYTTEWAAL, M., BOKOV, P., CORSON, F., SAHLIN, P., BOUDAOUD, A., MEYEROWITZ, E. M., COUDER, Y. & TRAAS, J. 2008. Developmental Patterning by Mechanical Signals in Arabidopsis. *Science,* 322**,** 1650-1655.

HAO, G. Y., HOFFMANN, W. A., SCHOLZ, F. G., BUCCI, S. J., MEINZER, F. C., FRANCO, A. C., CAO, K. F. & GOLDSTEIN, G. 2008. Stem and leaf hydraulics of congeneric tree species from adjacent tropical savanna and forest ecosystems. *Oecologia,* 155**,** 405-15.

HEDWIG, J. 1793. *Sammlung seiner zerstreuten Abhandlungen und Beobachtungen über botanisch-ökonomische Gegenstände*, SL Crusius.

HILL, J. F. 2012. Early Pioneers of Photosynthesis Research. *In:* EATON-RYE, J. J., TRIPATHY, B. C. & SHARKEY, T. D. (eds.) *Photosynthesis: Plastid Biology, Energy Conversion and Carbon Assimilation.* Dordrecht: Springer Netherlands.

HOLBROOK, N. M. & ZWIENIECKI, M. A. 1999. Embolism Repair and Xylem Tension: Do We Need a Miracle? *Plant Physiology,* 120**,** 7.

HÜSKEN, D., STEUDLE, E. & ZIMMERMANN, U. 1978. Pressure Probe Technique for Measuring Water Relations of Cells in Higher Plants 1. *Plant Physiology,* 61**,** 158-163.

JACKMAN, R. L., MARANGONI, A. G. & STANLEY, D. W. 1992. THE EFFECTS OF TURGOR PRESSURE ON PUNCTURE AND VISCOELASTIC PROPERTIES OF TOMATO TISSUE. *Journal of Texture Studies,* 23**,** 491-505.

JASECHKO, S., SHARP, Z. D., GIBSON, J. J., BIRKS, S. J., YI, Y. & FAWCETT, P. J. 2013. Terrestrial water fluxes dominated by transpiration. *Nature,* 496**,** 347-350.

JOHNSON, D. M., WOODRUFF, D. R., MCCULLOH, K. A. & MEINZER, F. C. 2009. Leaf hydraulic conductance, measured in situ, declines and recovers daily: leaf hydraulics, water potential and stomatal conductance in four temperate and three tropical tree species. *Tree Physiology,* 29**,** 879-87.

JOHNSON, K. M., JORDAN, G. J. & BRODRIBB, T. J. 2018. Wheat leaves embolized by water stress do not recover function upon rewatering. *Plant, Cell & Environment,* 41**,** 2704-2714.

JOULE, J. P. 1859. V. On some thermo-dynamic properties of solids. *Philosophical Transactions of the Royal Society of London,* 149**,** 91-131.

KAMIYA, N., TAZAWA, M. & TAKATA, T. 1963. The relation of turgor pressure to cell volume inNitella with special reference to mechanical properties of the cell wall. *Protoplasma,* 57**,** 501-521.

KINGSTON, A. M., MYERS, G. R., LATHAM, S. J., RECUR, B., LI, H. & SHEPPARD, A. P. 2018. Space-Filling X-Ray Source Trajectories for Efficient Scanning in Large-Angle Cone-Beam Computed Tomography. *IEEE Transactions on Computational Imaging,* 4**,** 447-458.

KOPPEN, W. 1936. Das geographische system der klimat. *Handbuch der klimatologie*, 46.
KRAMER, P. J. 1974. Fifty Years of Progress in Water Relations Research. *Plant Physiology,* 54, 463-471.
KRAMER, P. J. & CURRIER, H. B. 1950. Water Relations of Plant Cells and Tissues. *Annual Review of Plant Physiology,* 1, 265-284.
LIMING, F. G. 1957. Homemade Dendrometers. *Journal of Forestry,* 55, 575-577.
LIN, T.-T. & PITT, R. E. 1986. RHEOLOGY OF APPLE AND POTATO TISSUE AS AFFECTED BY CELL TURGOR PRESSURE. *Journal of Texture Studies,* 17, 291-313.
LINK, S. O., THIEDE, M. E. & BAVEL, M. G. V. 1998. An improved strain-gauge device for continuous field measurement of stem and fruit diameter. *Journal of Experimental Botany,* 49, 1583-1587.
LINTILHAC, P. M., WEI, C., TANGUAY, J. J. & OUTWATER, J. O. 2000. Ball Tonometry: A Rapid, Nondestructive Method for Measuring Cell Turgor Pressure in Thin-Walled Plant Cells. *Journal of Plant Growth Regulation,* 19, 90-97.
LO GULLO, M. A., NARDINI, A., TRIFILÒ, P. & SALLEO, S. 2003. Changes in leaf hydraulics and stomatal conductance following drought stress and irrigation in Ceratonia siliqua (Carob tree). *Physiologia Plantarum,* 117, 186-194.
LOCKHART, J. A. 1965. An analysis of irreversible plant cell elongation. *Journal of Theoretical Biology,* 8, 264-275.
MARINO, G., SCALISI, A., GUZMÁN-DELGADO, P., CARUSO, T., MARRA, F. P. & LO BIANCO, R. 2021. Detecting Mild Water Stress in Olive with Multiple Plant-Based Continuous Sensors. *Plants,* 10.
MAYR, S., SCHMID, P., LAUR, J., ROSNER, S., CHARRA-VASKOU, K., DAMON, B. & HACKE, U. G. 2014a. Uptake of water via branches helps timberline conifers refill embolized xylem in late winter. *Plant Physiology,* 164, 1731-40.
MAYR, S., SCHMID, P., LAUR, J., ROSNER, S., CHARRA-VASKOU, K., DÄMON, B. & HACKE, U. G. 2014b. Uptake of Water via Branches Helps Timberline Conifers Refill Embolized Xylem in Late Winter. *Plant Physiology,* 164, 1731.
MEINZER, F. C., RUNDEL, P. W., SHARIFI, M. R. & NILSEN, E. T. 1986. Turgor and osmotic relations of the desert shrub Larrea tridentata. *Plant, Cell & Environment,* 9, 467-475.
MEINZER, F. C., WOODRUFF, D. R., MARIAS, D. E., MCCULLOH, K. A. & SEVANTO, S. 2014. Dynamics of leaf water relations components in co-occurring iso- and anisohydric conifer species. *Plant, Cell & Environment,* 37, 2577-2586.
MEYER, B. S. 1938. The Water Relations of Plant Cells. *Botanical Review,* 4, 531-547.
MILBURN, J. A. & JOHNSON, R. 1966. The conduction of sap. *Planta,* 69, 43-52.
MOLDENHAUER, J. J. P. 1812. *Beyträge zur anatomie der pflanzen*, Gedruckt in de Königlichen schulbuchdruckerey durch CL Wäser.
MUNNÉ-BOSCH, S., NOGUÉS, S. & ALEGRE, L. 1999. Diurnal variations of photosynthesis and dew absorption by leaves in two evergreen shrubs growing in Mediterranean field conditions. *New Phytologist,* 144, 109-119.
NGUYEN, H. T., MEIR, P., SACK, L., EVANS, J. R., OLIVEIRA, R. S. & BALL, M. C. 2017a. Leaf water storage increases with salinity and aridity in the mangrove Avicennia marina: integration of leaf structure, osmotic adjustment and access to multiple water sources. *Plant, Cell & Environment,* 40, 1576-1591.
NGUYEN, H. T., MEIR, P., WOLFE, J., MENCUCCINI, M. & BALL, M. C. 2017b. Plumbing the depths: extracellular water storage in specialized leaf structures and its functional expression in a three-domain pressure -volume relationship. *Plant, Cell & Environment,* 40, 1021-1038.
NILSSON, S. B., HERTZ, C. H. & FALK, S. 1958. On the Relation between Turgor Pressure and Tissue Rigidity. II. *Physiologia Plantarum,* 11, 818-837.
OWEN, P. C. 1952. The Relation of Germination of Wheat to Water Potential1. *Journal of Experimental Botany,* 3, 188-203.

PAMMENTER, N. V. & VAN DER WILLIGEN, C. 1998. A mathematical and statistical analysis of the curves illustrating vulnerability of xylem to cavitation. *Tree Physiology,* 18**,** 589-593.
PASSIOURA, J. B., BALL, M. C. & KNIGHT, J. H. 1992. Mangroves may Salinize the Soil and in so Doing Limit Their Transpiration Rate. *Functional Ecology,* 6**,** 476-481.
PAUL, G. 1895. Leaf-absorption. *Nature,* 52**,** 569-570.
PELEG, M. 1979. CHARACTERIZATION OF THE STRESS RELAXATION CURVES OF SOLID FOODS. *Journal of Food Science,* 44**,** 277-281.
PEREIRA, L., BITTENCOURT, P. R. L., OLIVEIRA, R. S., JUNIOR, M. B. M., BARROS, F. V., RIBEIRO, R. V. & MAZZAFERA, P. 2016. Plant pneumatics: stem air flow is related to embolism – new perspectives on methods in plant hydraulics. *New Phytologist,* 211**,** 357-370.
PHILIP, J. R. 1958. The Osmotic Cell, Solute Diffusibility, and the Plant Water Economy. *Plant physiology,* 33**,** 264-271.
PHILIP, J. R. 1966. Plant Water Relations: Some Physical Aspects. *Annual Review of Plant Physiology,* 17**,** 245-268.
PIMENTEL, D., BERGER, B., FILIBERTO, D., NEWTON, M., WOLFE, B., KARABINAKIS, E., CLARK, S., POON, E., ABBETT, E. & NANDAGOPAL, S. 2004. Water Resources: Agricultural and Environmental Issues. *BioScience,* 54**,** 909-918.
RAUX, P. S., GRAVELLE, S. & DUMAIS, J. 2020. Design of a unidirectional water valve in Tillandsia. *Nature Communications,* 11**,** 396.
RODRIGUEZ-DOMINGUEZ, C. M., BUCKLEY, T. N., EGEA, G., DE CIRES, A., HERNANDEZ-SANTANA, V., MARTORELL, S. & DIAZ-ESPEJO, A. 2016. Most stomatal closure in woody species under moderate drought can be explained by stomatal responses to leaf turgor. *Plant, Cell & Environment,* 39**,** 2014-2026.
RODRIGUEZ-DOMINGUEZ, C. M., EHRENBERGER, W., SANN, C., RÜGER, S., SUKHORUKOV, V., MARTÍN-PALOMO, M. J., DIAZ-ESPEJO, A., CUEVAS, M. V., TORRES-RUIZ, J. M., PEREZ-MARTIN, A., ZIMMERMANN, U. & FERNÁNDEZ, J. E. 2012. Concomitant measurements of stem sap flow and leaf turgor pressure in olive trees using the leaf patch clamp pressure probe. *Agricultural Water Management,* 114**,** 50-58.
ROLLAND, V., BERGSTROM, D. M., LENNE, T., BRYANT, G., CHEN, H., WOLFE, J., HOLBROOK, N. M., STANTON, D. E. & BALL, M. C. 2015. Easy Come, Easy Go: Capillary Forces Enable Rapid Refilling of Embolized Primary Xylem Vessels. *Plant Physiology,* 168**,** 1636-47.
RÜGER, S., NETZER, Y., WESTHOFF, M., ZIMMERMANN, D., REUSS, R., OVADIYA, S., GESSNER, P., ZIMMERMANN, G., SCHWARTZ, A. & ZIMMERMANN, U. 2010. Remote monitoring of leaf turgor pressure of grapevines subjected to different irrigation treatments using the leaf patch clamp pressure probe. *Australian Journal of Grape and Wine Research,* 16**,** 405-412.
SACK, L., BALL, M. C., BRODERSEN, C., DAVIS, S. D., DES MARAIS, D. L., DONOVAN, L. A., GIVNISH, T. J., HACKE, U. G., HUXMAN, T., JANSEN, S., JACOBSEN, A. L., JOHNSON, D. M., KOCH, G. W., MAUREL, C., MCCULLOH, K. A., MCDOWELL, N. G., MCELRONE, A., MEINZER, F. C., MELCHER, P. J., NORTH, G., PELLEGRINI, M., POCKMAN, W. T., PRATT, R. B., SALA, A., SANTIAGO, L. S., SAVAGE, J. A., SCOFFONI, C., SEVANTO, S., SPERRY, J., TYERMAN, S. D., WAY, D. & HOLBROOK, N. M. 2016. Plant hydraulics as a central hub integrating plant and ecosystem function: meeting report for 'Emerging Frontiers in Plant Hydraulics' (Washington, DC, May 2015). *Plant, Cell & Environment,* 39**,** 2085-2094.
SACK, L. & HOLBROOK, N. M. 2006. Leaf hydraulics. *Annu. Rev. Plant Biol.,* 57**,** 361-381.
SACK, L., MELCHER, P. J., ZWIENIECKI, M. A. & HOLBROOK, N. M. 2002. The hydraulic conductance of the angiosperm leaf lamina: a comparison of three measurement methods. *Journal of Experimental Botany,* 53**,** 2177-2184.
SAVITZKY, A. & GOLAY, M. J. E. 1964. Smoothing and Differentiation of Data by Simplified Least Squares Procedures. *Analytical Chemistry,* 36**,** 1627-1639.

SCHENK, H. J., ESPINO, S., ROMO, D. M., NIMA, N., DO, A. Y. T., MICHAUD, J. M., PAPAHADJOPOULOS-STERNBERG, B., YANG, J., ZUO, Y. Y., STEPPE, K. & JANSEN, S. 2017. Xylem Surfactants Introduce a New Element to the Cohesion-Tension Theory. *Plant Physiology,* 173**,** 1177-1196.

SCHOLANDER, P. F., BRADSTREET, E. D., HEMMINGSEN, E. A. & HAMMEL, H. T. 1965. Sap Pressure in Vascular Plants. *Negative hydrostatic pressure can be measured in plants,* 148**,** 339-346.

SCHREEL, J. D. M., BRODERSEN, C., DE SCHRYVER, T., DIERICK, M., RUBINSTEIN, A., DEWETTINCK, K., BOONE, M. N., VAN HOOREBEKE, L. & STEPPE, K. 2022. Foliar water uptake does not contribute to embolism repair in beech (Fagus sylvatica L.). *Annals of Botany***,** mcac016.

SCHREEL, J. D. M. & STEPPE, K. 2019. Foliar water uptake changes the world of tree hydraulics. *npj Climate and Atmospheric Science,* 2**,** 1.

SCHREEL, J. D. M. & STEPPE, K. 2020. Foliar Water Uptake in Trees: Negligible or Necessary? *Trends in Plant Science,* 25**,** 590-603.

SCHREEL, J. D. M., VAN DE WAL, B. A. E., HERVÉ-FERNANDEZ, P., BOECKX, P. & STEPPE, K. 2019. Hydraulic redistribution of foliar absorbed water causes turgor-driven growth in mangrove seedlings. *Plant, Cell & Environment*.

SCOFFONI, C., ALBUQUERQUE, C., BRODERSEN, C., TOWNES, S. V., JOHN, G. P., BARTLETT, M. K., BUCKLEY, T. N., MCELRONE, A. J. & SACK, L. 2017a. Outside-xylem vulnerability, not xylem embolism, controls leaf hydraulic decline during dehydration. *Plant Physiology***,** pp. 01643.2016.

SCOFFONI, C., CHATELET, D. S., PASQUET-KOK, J., RAWLS, M., DONOGHUE, M. J., EDWARDS, E. J. & SACK, L. 2016. Hydraulic basis for the evolution of photosynthetic productivity. *Nat Plants,* 2**,** 16072.

SCOFFONI, C., SACK, L. & ORT, D. 2017b. The causes and consequences of leaf hydraulic decline with dehydration. *Journal of Experimental Botany,* 68**,** 4479-4496.

SKOTHEIM, J. M. & MAHADEVAN, L. 2005. Physical Limits and Design Principles for Plant and Fungal Movements. *Science,* 308**,** 1308-1310.

SMITH, S. E. 1947. The Sorption of Water Vapor by High Polymers. *Journal of the American Chemical Society,* 69**,** 646-651.

SOBRADO, M. A. 1986. Aspects of tissue water relations and seasonal changes of leaf water potential components of evergreen and deciduous species coexisting in tropical dry forests. *Oecologia,* 68**,** 413-416.

SPERRY, J. S. 1986. Relationship of Xylem Embolism to Xylem Pressure Potential, Stomatal Closure, and Shoot Morphology in the Palm <em>Rhapis excelsa</em&gt. *Plant Physiology,* 80**,** 110.

SPRAGUE, R. K. 1991. Plants as Aristotelian Substances. *Illinois Classical Studies,* 16**,** 221-229.

STEPPE, K., VANDEGEHUCHTE, M. W., VAN DE WAL, B. A., HOSTE, P., GUYOT, A., LOVELOCK, C. E. & LOCKINGTON, D. A. 2018. Direct uptake of canopy rainwater causes turgor-driven growth spurts in the mangrove Avicennia marina. *Tree Physiology,* 38**,** 979-991.

STUART, S. A., CHOAT, B., MARTIN, K. C., HOLBROOK, N. M. & BALL, M. C. 2007. The role of freezing in setting the latitudinal limits of mangrove forests. *New Phytologist,* 173**,** 576-583.

TAN, W. K., LIN, Q., LIM, T. M., KUMAR, P. & LOH, C. S. 2013. Dynamic secretion changes in the salt glands of the mangrove tree species Avicennia officinalis in response to a changing saline environment. *Plant, Cell & Environment,* 36**,** 1410-22.

TOMASELLA, M., NATALE, S., PETRUZZELLIS, F., DI BERT, S., D'AMICO, L., TROMBA, G. & NARDINI, A. 2022. No Evidence for Light-Induced Embolism Repair in Cut Stems of Drought-Resistant Mediterranean Species under Soaking. *Plants,* 11.

TURNER, N. C. 1988. Measurement of plant water status by the pressure chamber technique. *Irrigation Science,* 9**,** 289-308.

TYERMAN, S. D. 1982. Water Relations of Seagrasses: STATIONARY VOLUMETRIC ELASTIC MODULUS AND OSMOTIC PRESSURE OF THE LEAF CELLS OF HALOPHILA OVALIS, ZOSTERA CAPRICORNI, AND POSIDONIA AUSTRALIS. *Plant Physiology,* 69**,** 957-965.
TYREE, M. T. 2003. Plant hydraulics: The ascent of water. *Nature,* 423**,** 923-923.
TYREE, M. T. & DIXON, M. A. 1986. Water stress induced cavitation and embolism in some woody plants. *Physiologia Plantarum,* 66**,** 397-405.
TYREE, M. T. & HAMMEL, H. T. 1972. The Measurement of the Turgor Pressure and the Water Relations of Plants by the Pressure-bomb Technique. *Journal of Experimental Botany,* 23**,** 267-282.
TYREE, M. T. & RICHTER, H. 1981. Alternative Methods of Analysing Water Potential Isotherms: Some Cautions and Clarifications: I. THE IMPACT OF NON-IDEALITY AND OF SOME EXPERIMENTAL ERRORS. *Journal of Experimental Botany,* 32**,** 643-653.
URQUHART, A. R. 1929. 15—THE MECHANISM OF THE ADSORPTION OF WATER BY COTTON. *Journal of the Textile Institute Transactions,* 20**,** T125-T132.
VAN DEN HONERT, T. H. 1948. Water transport in plants as a catenary process. *Discussions of the Faraday Society,* 3**,** 146-153.
VENTURAS, M. D., SPERRY, J. S. & HACKE, U. G. 2017. Plant xylem hydraulics: What we understand, current research, and future challenges. *Journal of Integrative Plant Biology,* 59**,** 356-389.
VOKOUN, D., BELEGGIA, M., HELLER, L. & ŠITTNER, P. 2009. Magnetostatic interactions and forces between cylindrical permanent magnets. *Journal of Magnetism and Magnetic Materials,* 321**,** 3758-3763.
VON MOHL, H. 1856. Welche Ursachen bewirken die Erweiterung und Verengung der Spaltöffnungen. *Botanische Zeitung,* 14**,** 713-721.
WANG, X., DU, T., HUANG, J., PENG, S. & XIONG, D. 2018. Leaf hydraulic vulnerability triggers the decline in stomatal and mesophyll conductance during drought in rice. *Journal of Experimental Botany,* 69**,** 4033-4045.
WEATHERLEY, P. E. 1950. STUDIES IN THE WATER RELATIONS OF THE COTTON PLANT. *New Phytologist,* 49**,** 81-97.
WESTHOFF, M., REUSS, R., ZIMMERMANN, D., NETZER, Y., GESSNER, A., GEßNER, P., ZIMMERMANN, G., WEGNER, L. H., BAMBERG, E., SCHWARTZ, A. & ZIMMERMANN, U. 2009. A non-invasive probe for online-monitoring of turgor pressure changes under field conditions. *Plant Biology,* 11**,** 701-712.
WHEELER, J. K., HUGGETT, B. A., TOFTE, A. N., ROCKWELL, F. E. & HOLBROOK, N. M. 2013. Cutting xylem under tension or supersaturated with gas can generate PLC and the appearance of rapid recovery from embolism. *Plant, Cell & Environment,* 36**,** 1938-1949.
WILLIAMS, H. F. 1932. ABSORPTION OF WATER BY THE LEAVES OF COMMON MESOPHYTES. *Journal of the Elisha Mitchell Scientific Society,* 48**,** 83-100.
WOLFE, J., DOWGERT, M. F. & STEPONKUS, P. L. 1986. Mechanical study of the deformation and rupture of the plasma membranes of protoplasts during osmotic expansions. *The Journal of Membrane Biology,* 93**,** 63-74.
XIONG, D., FLEXAS, J., YU, T., PENG, S. & HUANG, J. 2017. Leaf anatomy mediates coordination of leaf hydraulic conductance and mesophyll conductance to CO2 in Oryza. *New Phytol,* 213**,** 572-583.
XIONG, D. & NADAL, M. 2020. Linking water relations and hydraulics with photosynthesis. *The Plant Journal,* 101**,** 800-815.
YANG, D., LI, J., DING, Y. & TYREE, M. T. 2017. Experimental evidence for negative turgor pressure in small leaf cells of Robinia pseudoacacia L versus large cells of Metasequoia glyptostroboides Hu et W.C. Cheng. 2. Hofler diagrams below the volume of zero turgor and the theoretical implication for pressure-volume curves of living cells. *Plant, Cell & Environment,* 40**,** 340-350.

YANG, S. J., ZHANG, Y. J., SUN, M., GOLDSTEIN, G. & CAO, K. F. 2012. Recovery of diurnal depression of leaf hydraulic conductance in a subtropical woody bamboo species: embolism refilling by nocturnal root pressure. *Tree Physiology,* 32**,** 414-22.

ZIMMERMANN, M. H. & SPERRY, J. S. 1983. ANATOMY OF THE PALM RHAPIS EXCELSA, IX. XYLEM STRUCTURE OF THE LEAF INSERTION. *Journal of the Arnold Arboretum,* 64**,** 599-609.

ZIMMERMANN, U. & HÜSKEN, D. 1980. Turgor pressure and cell volume relaxation inHalicystis parvula. *The Journal of Membrane Biology,* 56**,** 55-64.

ZIMMERMANN, U., RÜGER, S., SHAPIRA, O., WESTHOFF, M., WEGNER, L. H., REUSS, R., GESSNER, P., ZIMMERMANN, G., ISRAELI, Y., ZHOU, A., SCHWARTZ, A., BAMBERG, E. & ZIMMERMANN, D. 2010. Effects of environmental parameters and irrigation on the turgor pressure of banana plants measured using the non-invasive, online monitoring leaf patch clamp pressure probe. *Plant Biology,* 12**,** 424-436.

ZWEIFEL, R., STERCK, F., BRAUN, S., BUCHMANN, N., EUGSTER, W., GESSLER, A., HÄNI, M., PETERS, R. L., WALTHERT, L., WILHELM, M., ZIEMIŃSKA, K. & ETZOLD, S. 2021. Why trees grow at night. *New Phytologist,* 231**,** 2174-2185.

ZWEIFEL, R. & ZEUGIN, F. 2008. Ultrasonic acoustic emissions in drought-stressed trees – more than signals from cavitation? *New Phytologist,* 179**,** 1070-1079.

ZWIENIECKI, M. A. & HOLBROOK, N. M. 2009. Confronting Maxwell's demon: biophysics of xylem embolism repair. *Trends Plant Sci,* 14**,** 530-4.

SUPPLEMENTARY

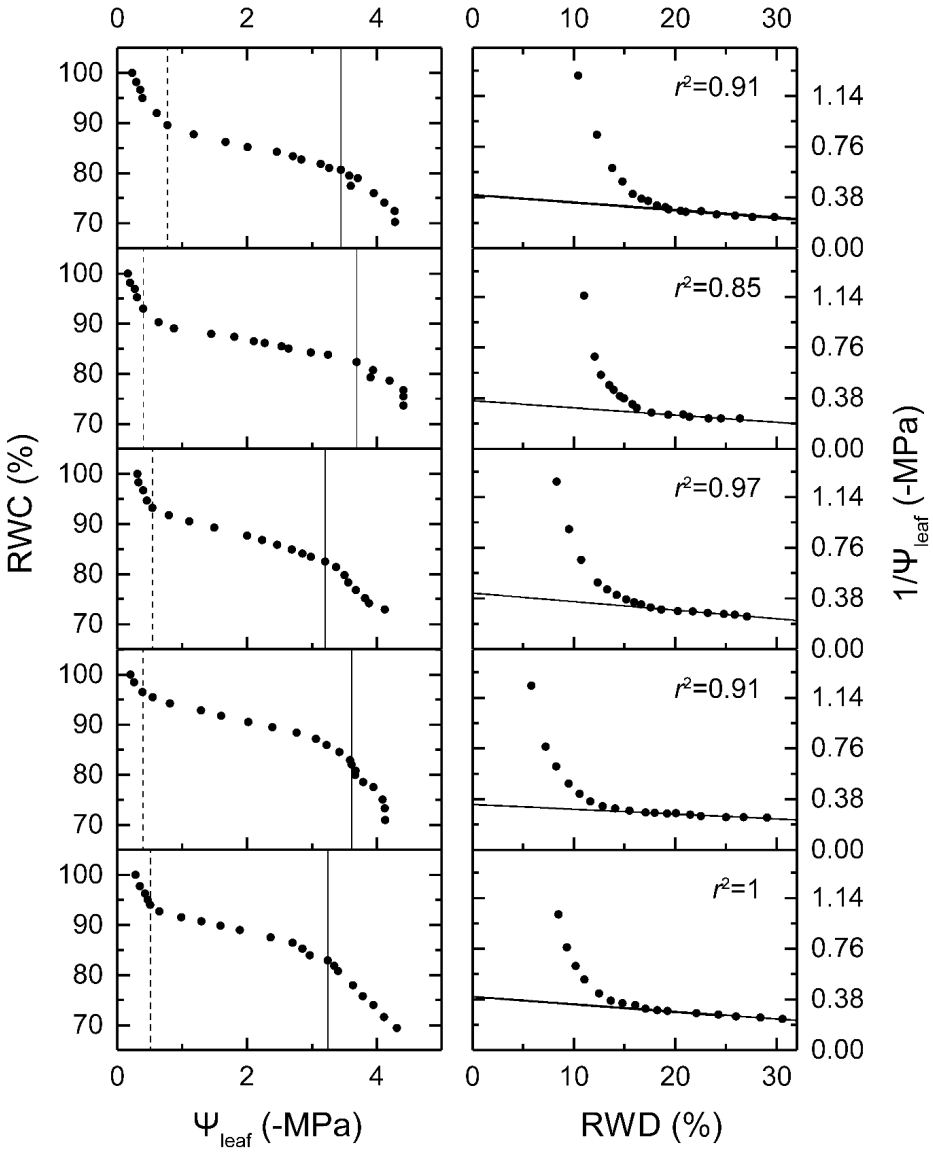

Figure. 2.S1. Left: Pressure-volume curves from 5 *Avicennia marina* subsp. *eucalyptifolia* individuals, showing a three-domain curve. Solid and dashed vertical lines indicate the Ψ_{TLP} and the Ψ_{leaf} value at full turgor (i.e. excluding apoplastic water of domain 1) for each individual curve. Right: $1/\Psi_{leaf}$ as a function of relative water deficit (RWD), used for determining the Ψ_{TLP} and the Π_{ft}.

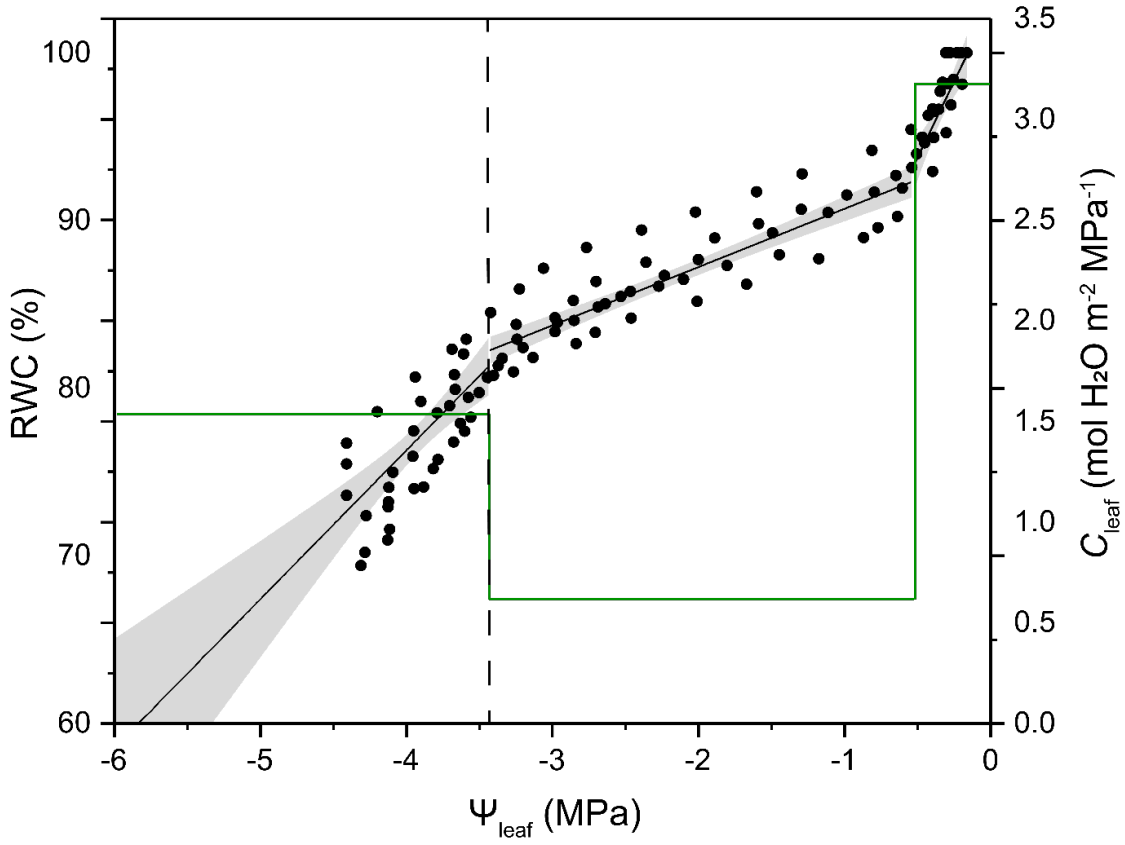

Figure 2.S2. Pressure-volume curve as fitted with linear models for each domain (black lines), and capacitance values derived from the linear fit (green). Shaded area indicates the 95% confidence interval of each model. RMSE = 1.59. n = 5.

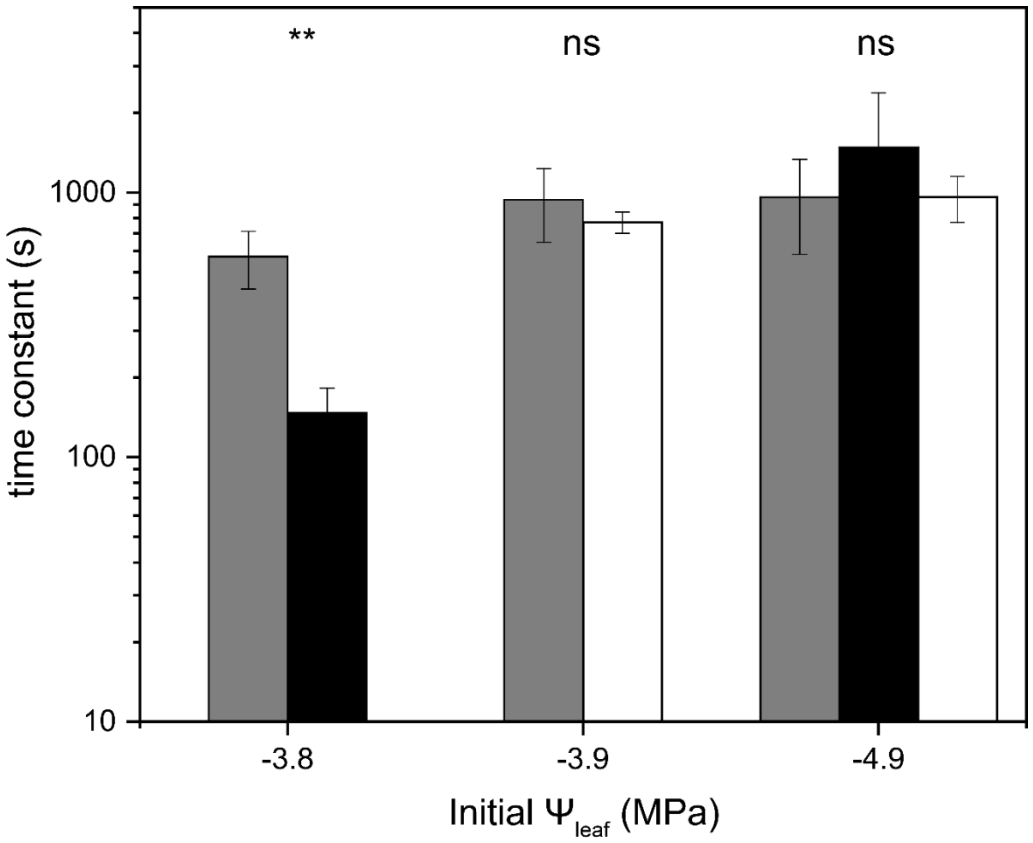

Figure 2.S3 Changes in the time constant from the exponential decay functions describing Ψ_{leaf} relaxation in *Avicennia marina* ssp. *eucalyptifolia*. Grey bars correspond to the initial (before SSWU) measurements; black bars correspond to the final (after SSWU) measurements; the white bar corresponds to control (no SSWU) measurements. Error bars correspond to SE. ** stands for $P < 0.01$; ns stands for $P > 0.05$ (paired t-tests, $n = 8$).

Table 2.S1 Analysis of Variance Table with Satterthwaite's method for the SSWU and K_{surf} dataset, considering the whole experimental period (0-12 h) or only the period in which SSWU took place (0-4.5 h). Values in which P < 0.05 are shown in bold.

Data	Dependent variable	Independent variable	Sum Sq	Mean Sq	NumDF	DenDF	*F*	*P*
0-4.5 h	SSWU	time	0.91	0.91	1	81.98	6.13	**0.02**
		Ψ_{leaf}	0.45	0.45	1	82.37	3.07	0.08
		time* Ψ_{leaf}	0.22	0.22	1	81.98	1.45	0.23
	K_{surf}	time	27751.98	27751.98	1	71.00	4.66	**0.03**
		Ψ_{leaf}	17589.87	17589.87	1	71.00	2.96	0.09
		time* Ψ_{leaf}	10261.28	10261.28	1	71.00	1.72	0.19
0-12 h	SSWU	time	0.51	0.51	1	95.99	2.69	0.10
		Ψ_{leaf}	1.40	1.40	1	96.66	7.42	**0.01**
		time* Ψ_{leaf}	0.11	0.11	1	95.99	0.60	0.44
	K_{surf}	time	14920.73	14920.73	1	85.00	2.51	0.12
		Ψ_{leaf}	11312.54	11312.54	1	85.00	1.90	0.17
		time* Ψ_{leaf}	4639.83	4639.83	1	85.00	0.78	0.38

Table 2.S2 Analysis of Variance Table with Satterthwaite's method for the SSWU and K_{surf} dataset, considering the whole experimental period (0-12 h) or only the period in which SSWU took place (0-4.5 h) using the lower and higher bounds of WCA_{sat} and PV.CI for calculations. Mean Squares column omitted for concision. Values in which P < 0.05 are shown in bold.

PV.CI	WCA_{sat}	Data	Dependent variable	Independent variable	Sum Sq	DenDF	*F*	*P*
High	High	0-4.5 h	SSWU	time	1.147	81.977	8.882	**0.004**
				Ψ_{leaf}	0.533	82.374	4.128	**0.045**
				time* Ψ_{leaf}	0.374	81.977	2.897	0.093
			K_{surf}	time	32265.319	71.000	5.966	**0.017**
				Ψ_{leaf}	25703.029	71.000	4.753	**0.033**
				time* Ψ_{leaf}	14528.439	71.000	2.687	0.106
		0-12 h	SSWU	time	0.629	95.991	3.774	0.055
				Ψ_{leaf}	1.821	96.676	10.924	**0.001**
				time* Ψ_{leaf}	0.192	95.986	1.152	0.286
			K_{surf}	time	17500.220	85.000	3.257	0.075
				Ψ_{leaf}	17133.276	85.000	3.189	0.078
				time* Ψ_{leaf}	6787.321	85.000	1.263	0.264
High	Low	0-4.5 h	SSWU	time	0.771	81.977	4.096	**0.046**
				Ψ_{leaf}	0.417	82.385	2.217	0.140
				time* Ψ_{leaf}	0.114	81.977	0.603	0.440
			K_{surf}	time	25811.676	71.000	3.548	0.064
				Ψ_{leaf}	12213.771	71.000	1.679	0.199
				time* Ψ_{leaf}	7425.999	71.000	1.021	0.316
		0-12 h	SSWU	time	0.439	95.993	1.866	0.175
				Ψ_{leaf}	1.133	96.667	4.814	**0.031**
				time* Ψ_{leaf}	0.061	95.987	0.260	0.611
			K_{surf}	time	13792.233	85.000	1.888	0.173
				Ψ_{leaf}	7484.256	85.000	1.024	0.314
				time* Ψ_{leaf}	3222.989	85.000	0.441	0.508
Low	High	0-4.5 h	SSWU	time	1.042	81.977	8.882	**0.004**
				Ψ_{leaf}	0.484	82.374	4.128	**0.045**
				time* Ψ_{leaf}	0.340	81.977	2.897	0.093
			K_{surf}	time	29327.026	71.000	5.966	**0.017**
				Ψ_{leaf}	23362.342	71.000	4.753	**0.033**

				time* Ψ_{leaf}	13205.384	71.000	2.687	0.106
		0-12 h	SSWU	time	0.572	95.991	3.774	0.055
				Ψ_{leaf}	1.655	96.676	10.924	**0.001**
				time* Ψ_{leaf}	0.174	95.986	1.152	0.286
			K_{surf}	time	15906.534	85.000	3.257	0.075
				Ψ_{leaf}	15573.007	85.000	3.189	0.078
				time* Ψ_{leaf}	6169.223	85.000	1.263	0.264
Low	Low	0-4.5 h	SSWU	time	0.701	81.977	4.096	**0.046**
				Ψ_{leaf}	0.379	82.385	2.217	0.140
				time* Ψ_{leaf}	0.103	81.977	0.603	0.440
			K_{surf}	time	23461.094	71.000	3.548	0.064
				Ψ_{leaf}	11101.504	71.000	1.679	0.199
				time* Ψ_{leaf}	6749.739	71.000	1.021	0.316
		0-12 h	SSWU	time	0.399	95.993	1.866	0.175
				Ψ_{leaf}	1.030	96.667	4.814	**0.031**
				time* Ψ_{leaf}	0.056	95.987	0.260	0.611
			K_{surf}	time	12536.221	85.000	1.888	0.173
				Ψ_{leaf}	6802.690	85.000	1.024	0.314
				time* Ψ_{leaf}	2929.482	85.000	0.441	0.508

Table 2.S3 Fitting results for the 3-parameter logistic models fitted to the two sets of K_{leaf} data compared in this study.

Parameter	Value	SE	*t*	*P*
K_{max}	14.621	2.9036	5.03548	3.06E-06
Ψ_{50}	2.5027	0.4865	5.14481	1.99E-06
a	-1.1579	0.3083	-3.75614	3.33E-04
r^2	0.6			

Table 2.S4 Fitting results for the exponential decay models fitted to the Ψ_{leaf} and leaf surface osmotic potential data used for calculating K_{surf}.

Variable/Treatment	Parameter	Value	SE	*t*	*P*	r^2
S_t	Ψ_f	0.35	0.10	3.56	0.00141	0.59
	A	0.93	0.15	6.04	1.89E-06	
	τ	2.27	0.84	2.72	0.01126	
Ψ_{leaf}=-3.2 MPa	Ψ_f	1.56	0.12	12.60	6.04E-14	0.71
	A	1.51	0.17	8.76	5.27E-10	
	τ	1.43	0.43	3.29	0.00243	
Ψ_{leaf}=-3.9 MPa	Ψ_f	1.96	0.15	13.48	1.65E-14	0.83
	A	1.90	0.17	11.46	1.11E-12	
	τ	2.38	0.49	4.83	3.49E-05	
Ψ_{leaf}=-4.9 MPa	Ψ_f	4.00	0.09	43.67	4.27E-30	0.57
	A	0.92	0.14	6.63	1.78E-07	
	τ	1.21	0.50	2.44	0.02046	

Notes 2.S1

Water potential in a rehydrating leaf relaxes as an exponential decay function of the form

$$\Psi_t = \Psi_0 \times e^{-\frac{K_{leaf}t}{C_{leaf}}}$$

where Ψ_0 is the initial water potential, Ψ_t is the water potential at time t, C_{leaf} is the leaf capacitance, and K_{surf} is the leaf hydraulic conductance. This is an analogy to Ohm's law and implies that $\Psi_t = 0$ at t = infinity, i.e., that the function asymptote is zero. Because it is not possible that $\Psi_t = 0$ when source of rehydration has a negative osmotic potential, we shall add an asymptote Ψ_{source}, then

$$\Psi_t = \Psi_{source} + \Psi_0 \times e^{-\frac{K_{leaf}t}{C_{leaf}}}$$

which is the same as

$$K_{leaf} = \frac{C_{leaf} \times Log_e\left(\frac{\Psi_0}{\Psi_t - \Psi_{source}}\right)}{t}$$

Notes 2.S2

Water movement through the petiole and into the leaf lamina occurs through the xylem and outside the xylem tissue (i.e., through the mesophyll). SSWU adds an extra resistance due to movement across surface tissues (cuticle, trichomes, etc.). While it is not clear how much of the within-xylem or outside-xylem tissue is involved in SSWU, it is likely that the resistances within the mesophyll for SSWU mostly involve outside-xylem pathways. Thus, we shall define conductance for both processes as

$$K_{leaf} = \frac{1}{r_m}$$

$$K_{surf} = \frac{1}{r_{ox} + r_c}$$

Where r_m is the resistance to water movement through the mesophyll, r_{ox} is the resistance to water movement outside the xylem, and r_c is the resistance to water movement through the cuticle (or the corresponding surface). Assuming that r_{ox} is $0.5r_m$, the partitioning of resistances can be calculated from the estimated rates of K_{leaf} and the maximum values measured for K_{surf}. At Ψ_{leaf}=-3.2 MPa, then

$$K_{leaf} = 4.51 \text{ mmol m}^{-2} \text{ s}^{-1} \text{ MPa}^{-1}$$

$$r_m = 0.222$$

$$K_{surf} = 0.204 \text{ mmol m}^{-2} \text{ s}^{-1} \text{ MPa}^{-1}$$

$$r_{ox} + r_c = 4.51$$

thus

$$\frac{r_c}{r_{ox}} = 39.63$$

Hence, at -3.2 MPa the resistance to water movement across the cuticle would be *c.* 44 times greater than through the mesophyll. Repeating the same process for -3.9 and -4.9 MPa gives:

$$K_{leaf} = 2.42 \text{ mmol m}^{-2} \text{ s}^{-1} \text{ MPa}^{-1}$$

$$r_m = 0.413$$

$$K_{surf} = 0.127 \text{ mmol m}^{-2} \text{ s}^{-1} \text{ MPa}^{-1}$$

$$r_{ox} + r_c = 7.87$$

thus

$$\frac{r_c}{r_{ox}} = 37.11$$

and

$$K_{leaf} = 0.857 \text{ mmol m}^{-2} \text{ s}^{-1} \text{ MPa}^{-1}$$

$$r_m = 1.167$$

$$K_{surf} = 0.063 \text{ mmol m}^{-2} \text{ s}^{-1} \text{ MPa}^{-1}$$

$$r_{ox} + r_c = 15.87$$

thus

$$\frac{r_c}{r_{ox}} = 26.2$$

If we consider the most conservative assumption that the resistances within and outside the xylem are involved in SSWU, the r_c/r_m ratios for the same leaf water potential values would be:

$$\frac{r_c}{r_m} = 19.3$$

$$\frac{r_c}{r_m} = 18.1$$

$$\frac{r_c}{r_m} = 12.6$$

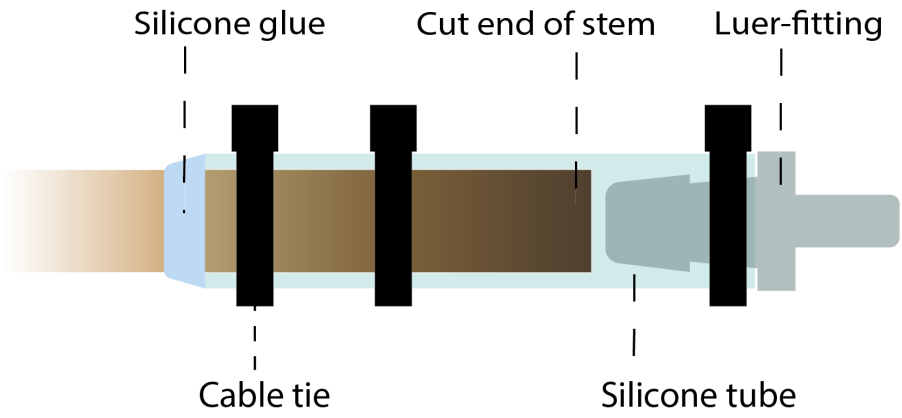

Figure 3.S1. Illustration of the fitting method used for pneumatic measurements.

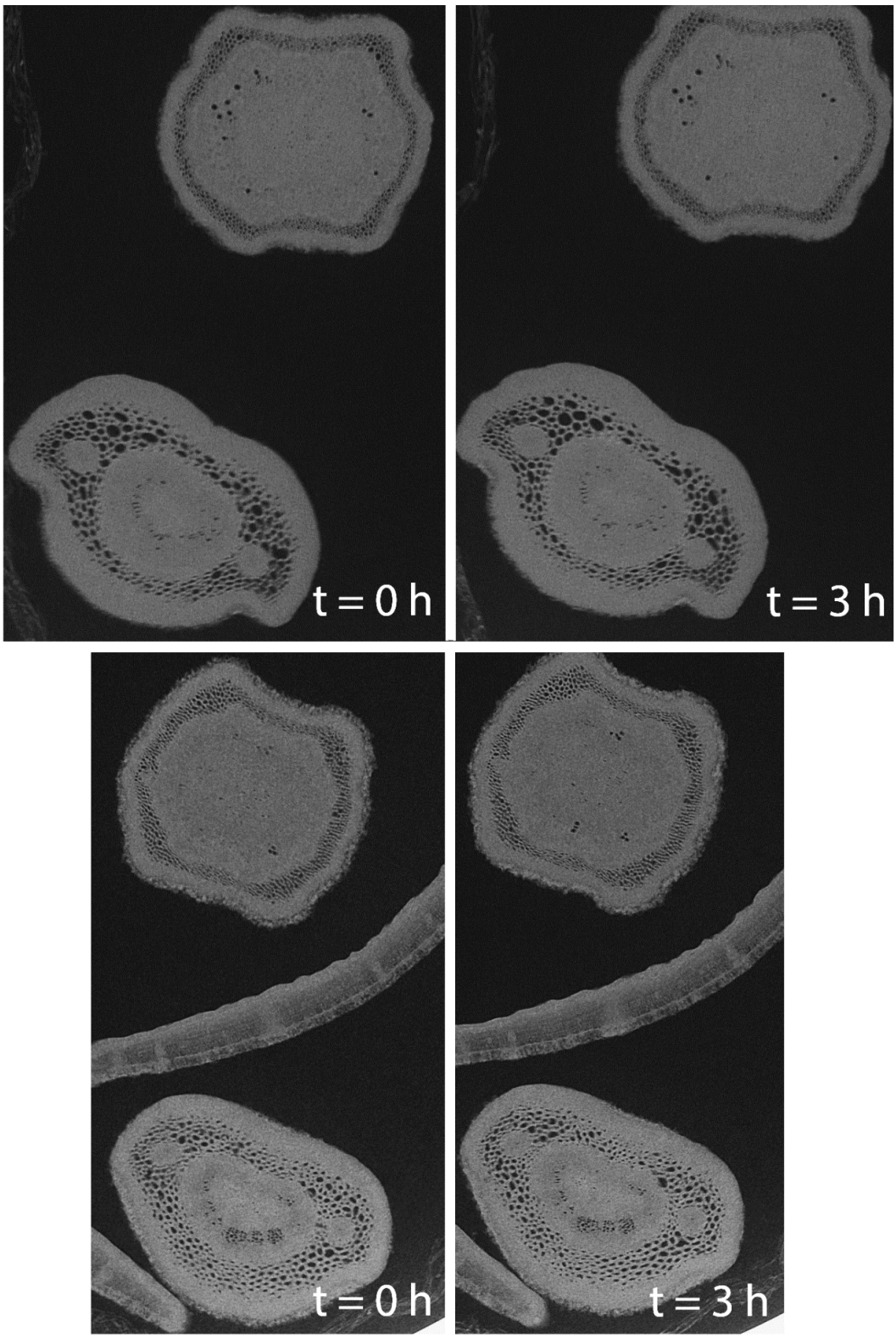

Figure 3.S2. Stems and leaves from samples imaged twice in the dry state, showing no reduction in embolism before wetting. Darker areas correspond to regions filled with air. N = 2.

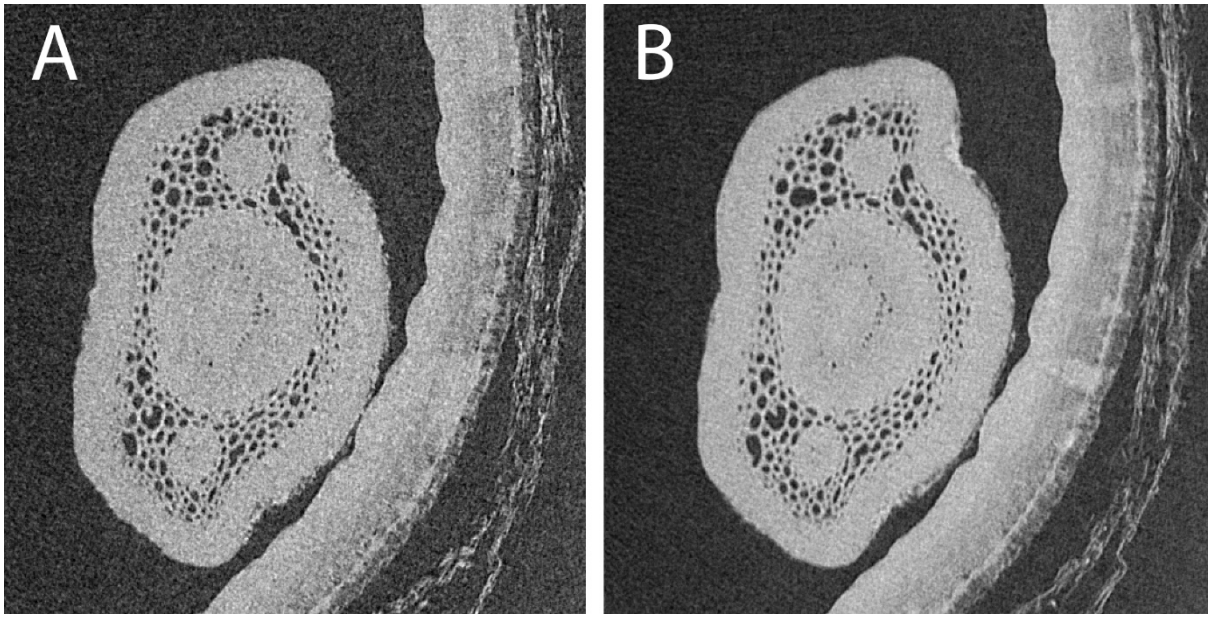

Figure 3.S3. Comparison between an unprocessed micro-CT image reconstruction (A) and the stack of 32 Z-slices (B). Note the reduction in image noise after processing, allowing cleared distinction of air-filled vessels. Darker areas correspond to regions filled with air. N = 1.

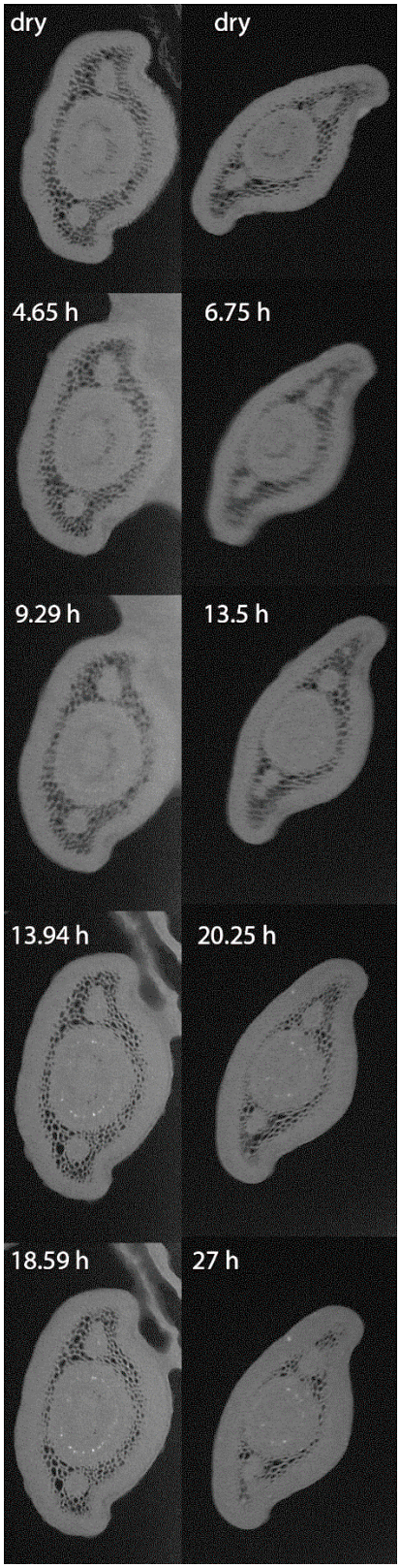

Figure 3.S4. Observed increase in electron density within the vascular bundle of two exemplary petioles from two samples. Note the bright spots located in the area around the vessels. Darker areas correspond to regions filled with air. N = 2.

Chapter 4: Supplementary discussion

Instrument performance

The custom-built squeeze-flow rheometer performed well. Using a stepper motor to operate the micrometer provided a simple method to implement precise and self-calibrated axial displacements (Fig. 2A). Mechanical backlash was the main limitation to the positioning accuracy of the system, and the main cause of the inability to perform controlled stress relaxation experiments when the direction of stress relaxation changes. The mechanical backlash may originate from gaps in the micrometer screw or the linear guide. An effective solution to this problem could be the incorporation of a linear-variable differential transformer (LVDT) and/or the use of a piezoelectric actuator, which can provide absolute positioning with sub-micron resolution. Despite this current limitation, the observed precision of the instrument compared favourably to commercially available systems to measure leaf thickness. Therefore, we found the instrument acceptable for the intended purpose.

Exemplary constant stress (CS) and stress relaxation (SR) tests (Fig. 3) showed that the instrument was capable of performing the tests intended, with two main limitations. First, controlled SR tests were performed adequately only in the cases where the direction of stress relaxation does not change. Second, the time required to achieve a constant stress during CS was dependent on the stiffness of the sample, with softer samples (e.g., *Salvia officinalis*) taking longer to reach a constant stress. Currently, the instrument only incorporates proportional control of the spindle position; use of more advanced control systems, such as proportional-integral-derivative (PID) control, can be implemented to achieve better performance during CS tests.

The instrument exhibited a temperature sensitivity of order 30 nm K^{-1} and is presently only suited for measurements at constant or nearly constant temperature. In the case of CS experiments, the estimated deflection can be simply subtracted from the actual measurements; however, during SR, the micrometer position must be adjusted to maintain a constant sample thickness. Temperature-corrected positioning control and/or use of dimensionally stable composites may be employed to correct this issue.

Loading of dead leaves

Loading living and dead leaves from the sclerophyllous species *Quillaja saponaria* showed that stress-relaxation parameters were significantly affected by heat-induced cell lysis. The marked increase in the ‘liquidity’ of the samples is consistent with expectation that much of the mechanical load in the living leaves was supported by turgor. Of course, dead leaves did not behave like an ideal liquid either, because some of the load would have been supported by the leaf structure. This effect is likely to become greater as tissue density

increases (and porosity decreases) during loading (Gibson et al., 1982). Heat-induced lysis also decreased the stress relaxation half-time. The faster equilibration of dead samples may be due to the removal of the cell membrane, which reduces the resistance to water movement out of the cells; however, it is also likely that the rheology of the leaf is affected due to release of cellular materials that may increase the viscosity of the medium. We note that the change in the SR half-time should be considered qualitatively, as dead leaves shrunk considerably after lysis and thus flow in the dead samples occurred through a smaller leaf cross-sectional area.

Table 4.S1. Species and sample sizes used for the experiments conducted in this study. Experiment numbers correspond as: (1) constant stress, passive SR and controlled SR under constant water status; (2) dead leaf test; (3) constant stress and passive SR under changing water status; (4) constant stress and passive SR on a living plant.

Species	**Family**	**Order**	**Experiment**	**Sample size**
Populus nigra L.	Salicaceae	Malpighiales	1	1
Salvia officinalis L.	Lamiaceae	Lamiales	1	1
Quillaja saponaria Molina	Quillajaceae	Fabales	2	3
Arbutus unedo L.	Ericaceae	Ericales	3	1
Callistemon viminalis (Sol ex. Gaertn.) G. Don	Myrtaceae	Myrtales	3	3
Corymbia citriodora (Hook.) K. D. Hill & L. A. S. Johnson	Myrtaceae	Myrtales	3	1
Fraxinus griffithii C. B. Clarke	Oleaceae	Lamiales	3	1
Grevillea olivacea A. S. George	Proteaceae	Proteales	3	1
Ligustrum lucidum W. T. Aiton	Oleaceae	Lamiales	3	3
Podocarpus elatus R. Br. ex Endl.	Podocarpaceae	Pinales	3	1
Quercus ilex L.	Fagaceae	Fagales	3	1
Tristaniopsis laurina (Sm.) Peter G. Wilson & J. T. Waterh.	Myrtaceae	Myrtales	3	3
Avicennia marina subsp. australasica (Walp.) J. Everett	Acanthaceae	Lamiales	4	1

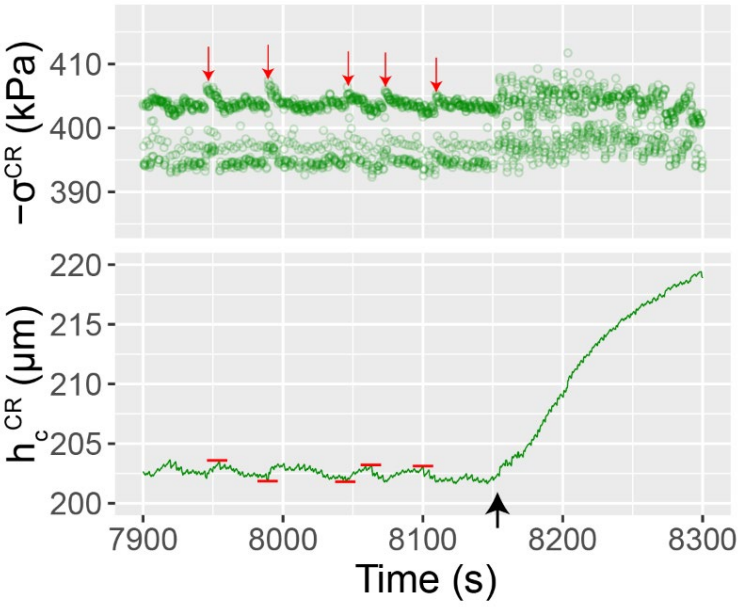

Figure 4.S1. Example of the backlash of the instrument during a constant stress test conducted at 400 kPa. Red downward arrows indicate the approximate times at which the motor took an effective compressive step during dehydration, increasing the applied stress. Red horizontal bars denote the recorded thickness at the times indicated by the arrows. Backlash corresponds to the approximate vertical distance between the red horizontal bars, which in this system is *c*. 2 μm. The black upward arrow corresponds to the time at which the dehydrating sample was recut under water. Note the change in direction of the trend in pressure, and the absence of backlash during fast rehydration.

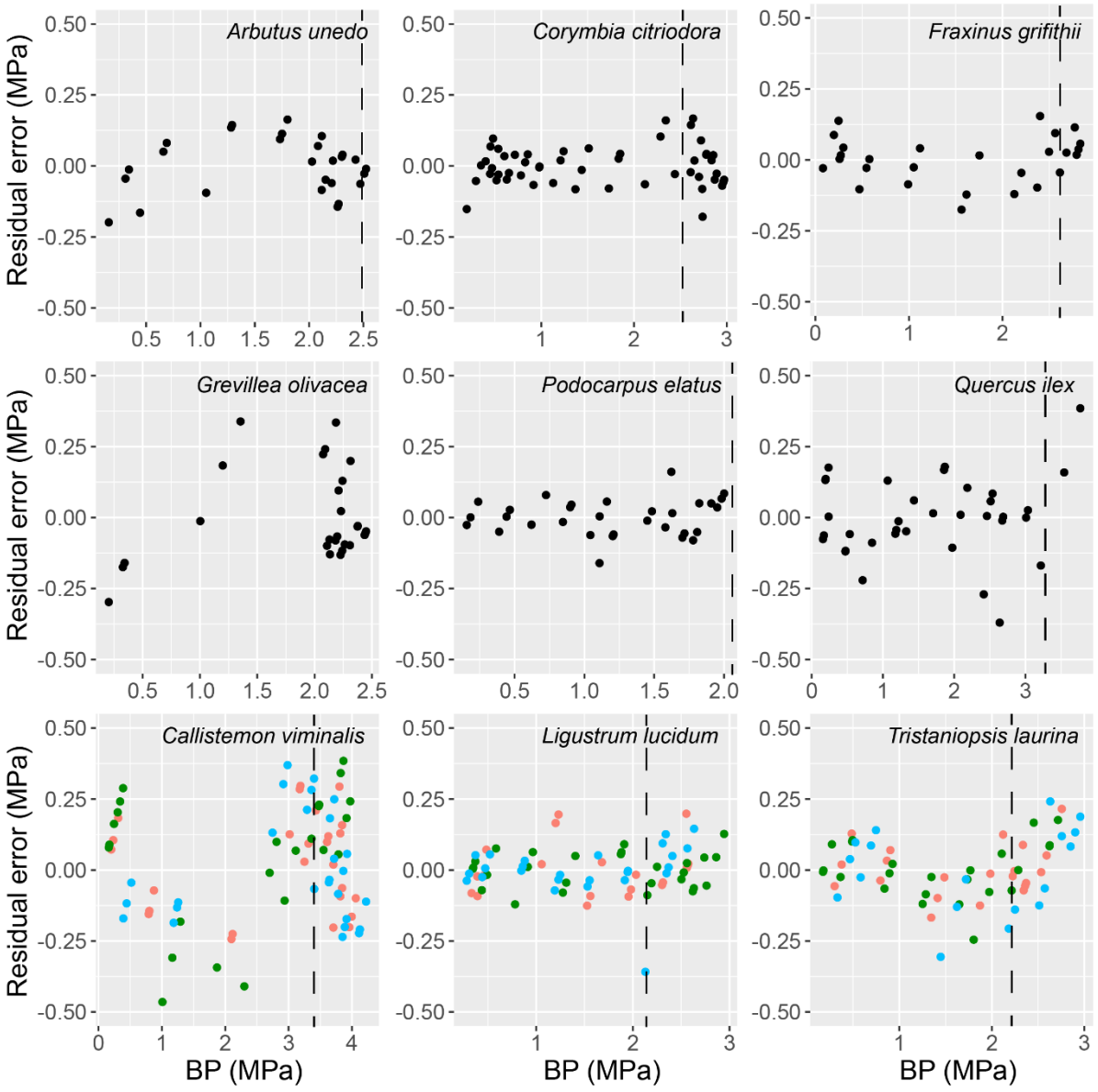

Figure 4.S2. Residual errors on the estimation of the balancing pressure (BP) from the applied compressive stress plotted against the measured values of BP. Vertical dashed lines indicate the value of osmotic pressure at the turgor-loss point. Colours denote different samples.